UNIVERSIDADE DA BEIRA INTERIOR
Ciências

Production of nanofiber-based membranes for biomolecule recovery

Bernardo Paiva Antunes

Dissertação para obtenção do Grau de Mestre em
Biotecnologia
(2º ciclo de estudos)

Orientador: Prof. Doutor Ilídio Joaquim Sobreira Correia

Covilhã, junho de 2013

UNIVERSIDADE DA BEIRA INTERIOR
Ciências

Produção de membranas à base de nanofibras para a recuperação de biomoléculas

Bernardo Paiva Antunes

Dissertação para obtenção do Grau de Mestre em
Biotecnologia
(2º ciclo de estudos)

Orientador: Prof. Doutor Ilídio Joaquim Sobreira Correia

Covilhã, junho de 2013

List of Publications

- Valente, J.F.A., V.M. Gaspar, B.P. Antunes, P. Coutinho, and I.J. Correia, *Microencapsulated chitosan-dextran sulfate nanoparticles for controled delivery of bioactive molecules and cells in bone regeneration.* Polymer, 2012. **54**(1): 5-15;

- Correia, T.R., B.P. Antunes, P.H. Castilho, J.C. Nunes, M.T. Pessoa de Amorim, I.C. Escobar, J.A. Queiroz, I.J. Correia, and A.M. Morão, *A bi-layer electrospun nanofiber membrane for plasmid DNA recovery from fermentation broths.* Separation and Purification Technology, 2013. **112**: p. 20-25.

Acknowledgments

Behind me lies a year of intense effort and hard work, which made me grow up not only in knowledge but also as a man. Nevertheless, along this path I could count on some people, whom I would like to thank:

Firstly, I would like to express my gratitude to my supervisor Professor Ilídio Correia for his guidance, patience and support during this Master Thesis. I would also like to thank him for all the conditions and knowledge provided in this area.

I would also like to show my appreciation to Eng. Ana Paula from the Optics department of Universidade da Beira Interior for the time spent on the acquisition of scanning electron microscopy images.

I thank my work group for creating a healthy working environment, and for offering me support and kindness in the toughest moments.

To my closest friends I would like to express my deepest gratitude, for being at my side in the darkest times, but as well as in the happiest.

Last but not least, to my parents, for supporting me during all these years. For your unconditional faith, guidance and love, I thank you from the bottom of my heart.

“Knowledge speaks, but wisdom listens.”

James Marshall Hendrix

Abstract

The demanding of ever-increasing quantities of highly purified biomolecules by bio-industries has triggered the development of new, more efficient, purification techniques. The application of membrane-based technologies has become very attractive in this field, for their high throughput capability, simplicity of operation and scale-up.

In this thesis it is reported the production of a bi-layer membrane by electrospinning (ES), in which a support of poly ε-caprolactone nanofibers was coated with a polyethylene oxide/sodium alginate layer, and subsequently cross-linked with calcium chloride. The membranes were characterized by SEM, ATR-FTIR, contact angle measurements, and then were applied in the recovery process of a plasmid. The results obtained show that membranes retained the suspended solids while allowing the permeation of plasmid DNA, with high recovery yields and improved RNA retention. Moreover, they also showed a very low fouling tendency.

Keywords

Bi-layer membrane, electrospinning, lysate, microfiltration, plasmid DNA

Resumo

A crescente procura de elevadas quantidades de biomoléculas altamente purificadas despoletou o desenvolvimento de novas, e mais eficientes, técnicas de purificação. A aplicação da tecnologia de membranas de microfiltração tem-se tornado muito atrativa nesta área, devido ao seu elevado rendimento, simplicidade de operação e de escalonamento.

Na presente tese é apresentada a produção de uma membrana de dupla camada por electrospinning (ES), na qual um suporte de nanofibras de poli ε-caprolactona é revestido por uma camada de óxido polietileno/alginato de sódio, e subsequentemente reticulada em cloreto de cálcio. As membranas foram posteriormente caracterizadas por SEM, ATR-FTIR, determinação do ângulo de contacto. Posteriormente, as membranas foram usadas na recuperação de plasmídeo. Os resultados obtidos demonstraram que as membranas retêm os sólidos suspensos, permitindo a passagem de ADN plasmídeo, com elevados rendimentos de recuperação e melhorias na retenção de ARN. A membrana revela baixa tendência para a colmatação.

Palavras-chave

Microfiltração, electrospinning, membrana de dupla camada, lisado, ADN plasmídeo

Resumo Alargado

A produção de fármacos em larga escala debate-se com a necessidade de recuperar biomoléculas a partir de misturas complexas (e.g. produtos de fermentação). A crescente procura de elevadas quantidades de biomoléculas altamente purificadas, por parte de indústrias como a farmacêutica, tem levado a procura de técnicas mais eficientes de purificação. O isolamento e purificação de produtos biotecnológicos podem envolver várias etapas, com diferentes princípios de separação. O processo terá de ser adaptado e otimizado ao produto que se pretende purificar, dependendo da natureza e do tamanho do mesmo. A aplicação da tecnologia de membrana (e.g. microfiltração) tem vindo a tornar-se muito atrativa nesta área, devido ao seu elevado rendimento, simplicidade de operação e de adaptação à escala industrial.

A tecnologia de membrana está principalmente associada a processos de separação (e.g. processamento de misturas biotecnológicas complexas). Esta inclui uma vasta gama de aplicações, tais como filtração estéril, clarificação, remoção de vírus, concentração de proteínas. Os processos de membrana contemplam ainda a purificação de água, e a recuperação e purificação de ácidos nucleicos.

Este trabalho tem em vista a produção de membranas através da técnica de electrospinning para a recuperação de ADN plasmídeo a partir de caldos de fermentação. A recuperação e purificação do ADN plasmídeo possui grande importância, dado o seu papel na terapia génica e na produção de vacinas.

Electrospinning trata-se de uma técnica simples e barata para a produção de nanofibras, a partir de uma vasta gama de polímeros, ou misturas de polímeros. Esta técnica oferece condições únicas para a produção de materiais à base de nanofibras (e.g. membranas), para a aplicação em várias áreas de interesse, entre as quais a filtração. As membranas produzidas por electrospinning apresentam várias vantagens para a aplicação em processos de filtração (e.g. elevado rácio área superficial/volume e poros continuamente interconectados).

Foi produzida uma membrana de dupla camada por electrospinning, na qual um suporte de nanofibras de poli ε-caprolactona é revestido por uma camada de óxido polietileno/alginato de sódio, e subsequentemente reticulada em cloreto de cálcio. A membrana produzida é comparada com membranas comerciais usadas para o mesmo tipo de processos de recuperação.

As membranas foram caracterizadas por SEM, ATR-FTIR, determinação do ângulo de contacto. A partir das imagens de SEM foi analisada a morfologia superficial das membranas, assim como a distribuição do diâmetro de fibras, no caso das membranas produzidas por

electrospinning. A determinação do ângulo de contacto das membranas permitiu concluir sobre as características de superfície das membranas.

Posteriormente, as membranas foram usadas na recuperação de plasmídeo. Os resultados obtidos demonstraram que as membranas aqui produzidas retêm os sólidos suspensos, permitindo a passagem de ADN plasmídeo, com elevados rendimentos de recuperação. A membrana produzida por electrospinning mostrou ainda melhorias na retenção de ARN, assim como baixa tendência para a colmatação, face às membranas comerciais.

Index

List of Figures

List of Tables

Chapter I:

Chapter III:

List of Acronyms

ATR-FTIR	Attenuated total reflectance-fourier transform infrared spectroscopy
ECM	Extracellular matrix
ENM	Electrospun nanofiber membrane
ES	Electrospinning
gDNA	Genomic DNA
HIC	Hydrophobic interaction chromatography
L_p	Hydraulic permeability
L_{p0}	Initial hydraulic permeability
MF	Microfiltration
MW	Molecular weight
MWCO	Molecular weight cutoff
NF	Nanofiltration
PCL	Poly ε-caprolactone
PCL ENMC	Coated PCL ENM
pDNA	Plasmid DNA
PEO	Poly(ethylene) oxide
RO	Reverse osmosis
SA	Sodium alginate
SEM	Scanning electron microscopy
UF	Ultrafiltration

Chapter I

Introduction

1. Introduction

1.1 Biomolecule purification in pharmaceutical industry

The pharmaceutical industry produces drugs on large scale to meet the needs of those who are ill. Most of the biotechnological molecules, required to drug production, are present in complex mixtures of products (e.g. fermentation broths). The recovery of these biomolecules is processed by downstream purification techniques [1].

1.1.1 Downstream Processing

This is a multistage operation that regards the isolation and purification of a biotechnological product. The complexity of this process is determined by the required purity of the product, and also by its application. Different separation principles may be required, as the products vary in terms of size and nature. As examples of these products we have, whole cells, nucleic acids, amino acids, enzymes, proteins, antibiotics, among others. Furthermore, it is of great importance to minimize the number of steps used for obtaining the desired biomolecule, so that the cost and the time of the operation can be kept as low as possible. Table 1 shows the variation of recovery costs, according to the type of solids. Hereupon, the full recovery process should be finely optimized in order to obtain the required product with high degree of purity [1, 2].

Table 1 Recovery cost variation for different types of solids (adapted from [2]).

Solids type	Density difference between solids and broth (kg m^{-3})	Cost of recovery
Cell debris	0 – 120	High
Bacterial cells	70	<
Yeast cells	90	<
Mammalian cells	70	<
Plant cells	50	<
Fungal hyphae	10	<
Microbial flocs	-	Low

The downstream processing scheme to isolate and purify target biomolecules usually features four stages [2]:

1. solid-liquid separation (or clarification)
2. concentration
3. purification
4. formulation.

In figure 1 is shown a scheme of the different stages comprised in downstream processes, pointing out purification (or isolation) methods used in those stages. Moreover, a reduction of the number of recovery stages has a high demand. Processes able to do the work of several others, will allow the saving of time and money [2].

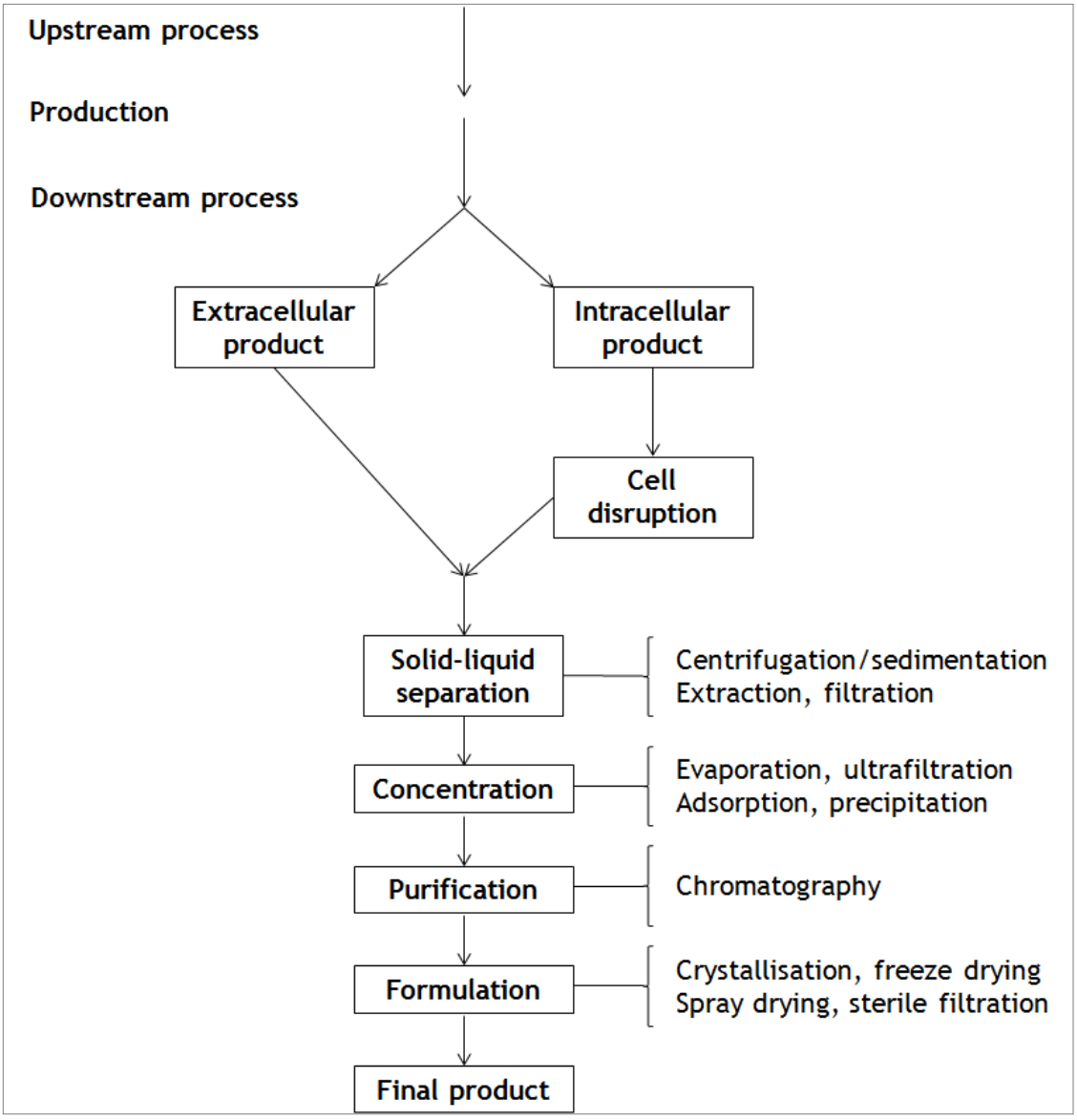

Figure 1 Scheme of the downstream process stages for the isolation and purification of biotechnological products (adapted from [2]).

1.2 Membrane science and technology

Membrane science is a broad and highly interdisciplinary field, where process engineering, material science and chemistry meet, to produce membranes that have a wide range of applications. Membranes are best known for their use in separation processes (e.g. processing of complex biotechnological mixtures), nevertheless employing biocompatible or biodegradable polymers for membrane production, allow them to be applied as culturing supports (or scaffolds) for tissue engineering purposes [3].

Membrane systems offer properties, such as, high selectivity, high surface area to volume ratio and potential for controlling the contact and mixing level between two phases. Furthermore, membranes have been used to purify biological molecules, since they can be operated at relatively low temperature and pressure, involving no phase changes or chemical additives, which minimize denaturation, deactivation and/or degradation of biological molecules [4, 5]. Moreover, membrane filtrations offer relatively simple operations and low costs, when compared with other competitive procedures, such as centrifugal separation, vacuum filtration and spray drying. Membrane processes usually achieve high efficiency in terms of separation, which has a great economical impact [6].

1.2.1 Membrane classification

Membranes used for biotechnological purposes are classified according to three factors, pore size, molecular weight cutoff (MWCO) and driving force. It is important to point out that MWCO is used to describe membrane retention capabilities, directly associated with the membrane pore dimensions [6, 7].

Membrane processes can be classified as concentration-driven, pressure-driven and electrical-driven membrane processes [8]. Herein pressure-driven membrane processes will be further characterized. Among these are microfiltration (MF), ultrafiltration (UF), nanofiltration (NF) and reverse osmosis (RO), from the least selective to the most selective, respectively [7]. Differences in terms of pore size, MWCO and applied pressure between pressure-driven membranes can be found on Table 2 and Figure 2.

Table 2 Overview of the applied pressure to membrane processes (adapted from [9]).

Membrane	MF	UF	NF	RO
Applied pressure (bar)	0.1 – 2	0.1 – 5	3 – 20	5 – 120

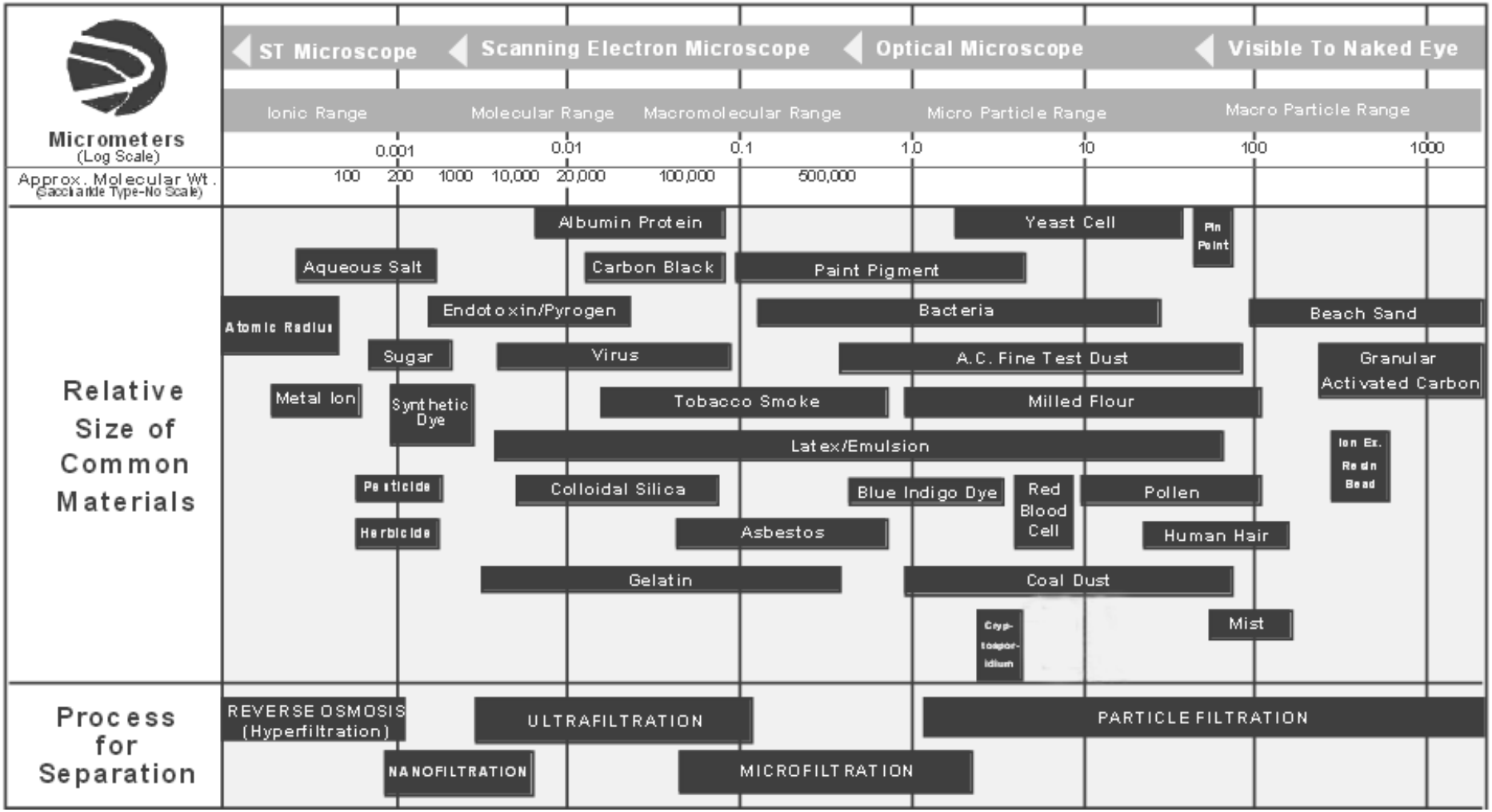

Figure 2 Pressure-driven membrane process spectrum (adapted from [7]).

1.2.2 Pressure-driven membrane applications

The application of membrane technology has been extensively reported for several applications in both upstream and downstream processes, playing a critical role in the purification of biotechnology products [5]. These applications include a wide range of processes, such as sterile filtration, clarification, initial recovery, virus removal, protein concentration, buffer exchange and protein purification [10, 11]. Furthermore, other applications are contemplated by membrane processes, such as water purification [7, 11], and nucleic acids (pDNA and RNA) recovery and purification [12, 13]. A summary of the materials, applications and commercial available membranes can be found on Table 3.

Table 3 Applications of the commercially available membranes used in pressure-driven membrane processes (adapted from [5, 10, 14]).

	Applications	Examples of commercially available membranes	Examples of materials used to produce membranes
MF	Drinking water treatment Clarification Sterile filtration	*Nylaflo* (Pall Corporation) *GVWP* (Millipore) *MCE* (Advantec Toyo Corp.)	Cellulose acetate Poly(vinylidene fluoride) Polyamides Polyolefins Nylon Poly(tetrafluoroethylene)
UF	Concentration Buffer exchange Desalination Sterile Filtration Biomolecule recuperation Clarification	*FSM0.45PP* (Alfa Laval) *3038*, *3065* and *3028* (IRIS) *ES625* (PCI Membrane Systems)	Polyacrylonitrile copolymers Aromatic polyamides Polysulfone Poly(vinylidene fluoride)
NF	Desalination Salt separation Waste water treatment	*MPS-44* (Koch Membrane) *NTR7250* (Nitto-Denko) *NF55* (Dow)	Aromatic polyamides Cellulose acetate
RO	Ultrapure water production Desalination Waste water treatment	*ES20* (Nitto-Denko) *UTC-70* (Toray) *NCM1* (Hydranautics)	Cellulose acetate Polyamide

1.2.3 Membrane Properties

Membrane can be defined as semi-permeable barrier capable of separating substances when applied a driving force across the membrane. The transport through a membrane is affected by a difference in chemical potential between both sides. This difference may be caused by a gradient in temperature, pressure, concentration or electrical potential. The transport is, of course, severely affected by the membrane morphology. Two morphologies are usually distinguished, dense and porous [3, 7].

Dense membranes are permeable to single molecules, being the transport mechanism described by the solution diffusion model [15]. This model explains processes like dialysis, reverse osmosis, gas permeation and pervaporation. According to this model the permeability of a component is directly related to its diffusivity and solubility in the membrane material. With this in mind it is possible to conclude that the transport, in this sort of models, is material dependent, since the diffusivity and solubility of a component depend of its interactions with the membrane material. It is important to retain that the permeability is, in fact, an intrinsic property of the membrane material that shows the membrane transport capacity [3].

The transport in porous membranes is performed through empty spaces (i.e. pores). Hence, the transport, in this case, is primarily governed by membrane morphology, although the interaction with the internal membrane surface may also influence. Membrane morphology comprises the surface and volume porosity, pore size distribution and tortuosity. The tortuosity constitutes a correction for the deviation of the pore shape from perfect cylinders, defined by the ratio of the average path length through the pores and the membrane thickness. Permeability values for porous membranes also indicate the capacity of the membrane [3].

When separation processes are aimed, membranes can be operated in two modes, by dead-end (or direct flow) or tangential flow (or cross-flow) filtration. In dead-end mode the filtration is always done as a batch process, giving that the rejected components by the membrane accumulate on its surface (Figure 3a). On the other hand, tangential flow filtration featuring a feed flow parallel to the membrane, and therefore perpendicular to the filtrate flow, enables retained species to be swept along the membrane surface and out of the device (Figure 3b). When compared to the dead-end mode, the tangential flow enhances the process flux and reduces filter cake formation, and subsequently reduces fouling. Is this processes the stream passing through the membrane is called permeate, while the remaining is named retentate. The pretended product can either be the permeate or the retentate, depending on the desired application [3, 5].

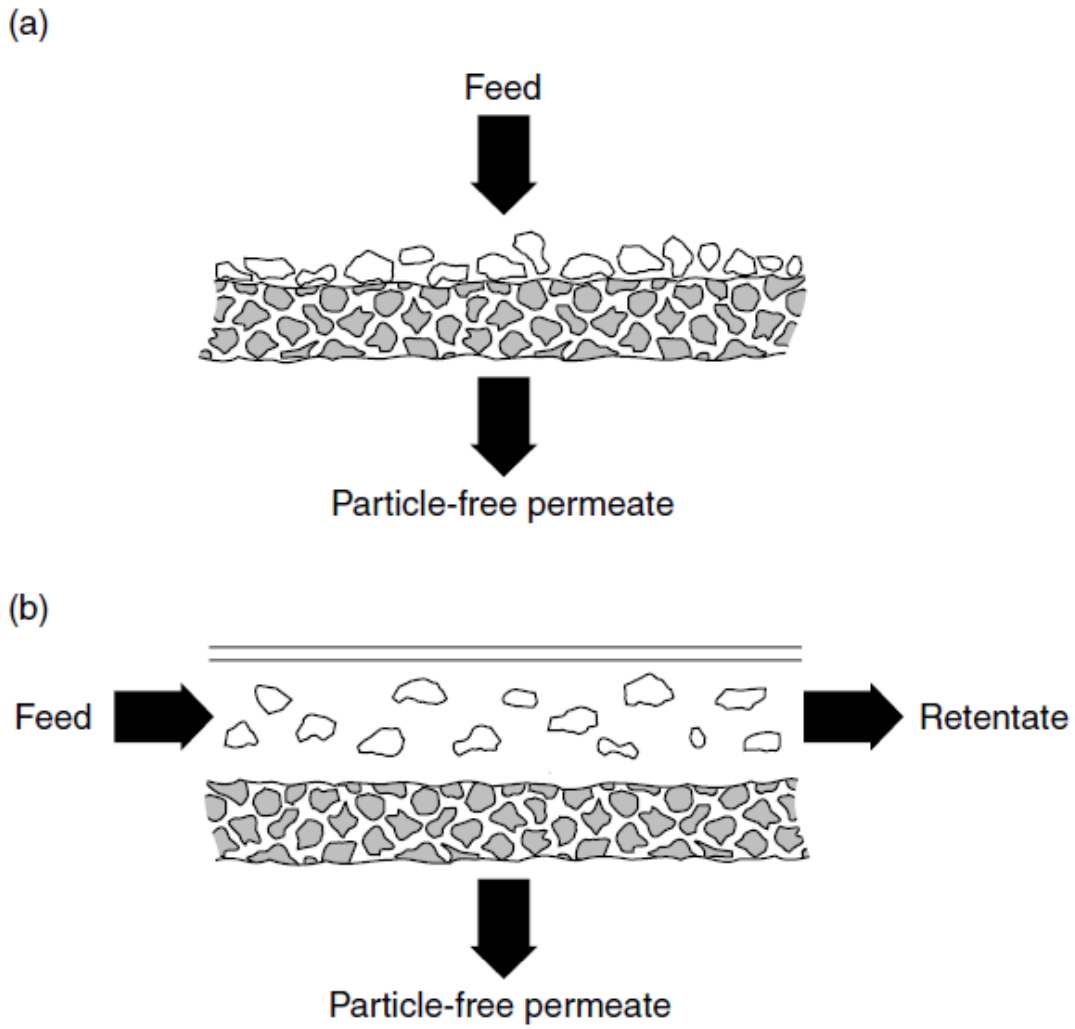

Figure 3 Modes of operation in membrane separation: (a) dead-end mode and (b) tangential flow mode (adapted from [14]).

1.2.4 Parameters affecting membrane processes

When designing a membrane process, there are some key characteristics to take into account, the selectivity, the volumetric flux and the system capacity [11].

The selectivity of the membrane is, of course, determined by the underlying pore size distribution, but is also affected by the membrane surface properties (e.g. electrically charged membranes enhance the retention of biomolecules with the same polarity) [11, 16].

The filtrate flux is affected by two phenomena, fouling and concentration polarization effects, usually resulting in a flux value lower than the predicted from the permeability of a clean membrane. Membrane fouling is generally originated by the adsorption on and within the membrane pores, and/or from the formation of a deposit on the external surface of the membrane (Figure 4). Furthermore, the concentration polarization effect refers to the accumulation of retained solutes, completely or partially, at the membrane surface caused by bulk mass transfer limitations in the membrane system. The latter can be controlled by

adjusting the fluid flow characteristics, providing high local shear rates through tangential flow filtration systems or inducing secondary flow, for instance, through Taylor [17] or Dean [18] vortices [4, 11].

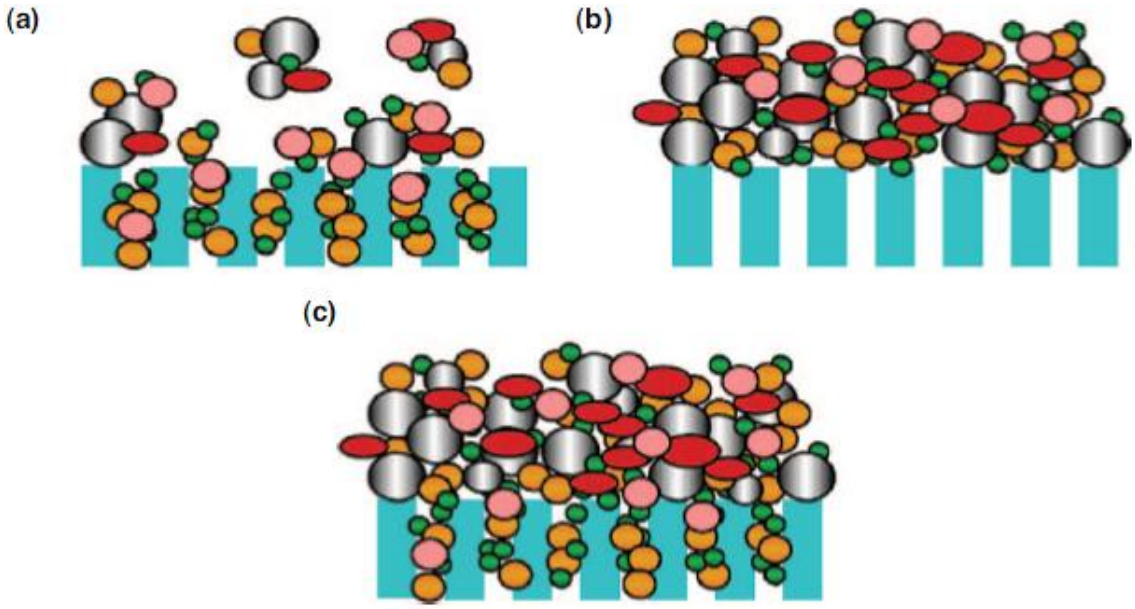

Figure 4 Schematic representation of membrane fouling: clogging of the membrane pores (a), deposition of sludge solids on the membrane (b) and both of them (c) (adapted from [19]).

The last factor affecting membrane processes is the system capacity. This is the volume of feed that can be processed, per unit of membrane area, before the membrane needs to be regenerated or replaced. In pressure-driven membrane systems, functioning at constant transmembrane pressure, the capacity is usually defined as the point at which the filtrate flow rate drops to less than 10% of the initial value (or just below a pre-determined flux limit, required for a determined application). However, operating at constant filtrate flux, the capacity is the maximum pressure drop tolerated by the system [11].

1.3 Plasmid DNA

Plasmid DNA (pDNA) can be used as a vector for gene therapy or vaccination, as several studies have already reported in the past two decades [20-22]. It has been shown that the injection of pDNA containing selected genes from pathogens can elicit a protective immune response [23]. Plasmid DNA vaccines have shown very encouraging results against malaria and AIDS, and its use is also being investigated against other infectious diseases, such as hepatitis B and C, and tuberculosis [24, 25].

Plasmid DNA vaccines are believed to mimic natural intracellular pathogen gene expression pathways, triggering cellular and humoral responses, and this way Overall, DNA-based vaccines are quite safe, due to lack of genetic integration (i.e. the injected foreign genetic material will not be integrated in the host genetic material) and absence of specific immune response to the plasmid itself [24, 25].

1.3.1 Plasmid DNA purification

The ever-increasing use of plasmid DNA as a biopharmaceutical, created a demand for simple, robust and scalable purification processes that can enable the isolation of pDNA from transformed bacteria. There are, in fact, several processes described in the literature for the isolation of small amounts of pure pDNA, although these are mostly useful in a laboratory environment, and considered unsafe (e.g. due to the utilization of harmful chemicals), or impractical, when inserted into large scale operations [12].

The first step of pDNA downstream process, is the release from transformed bacteria by cell lysis [13]. There are some techniques available for cell lysis, such as mechanical [26] and thermal methods [27], as well as alkaline lysis [28]. Alkaline lysis is the most used, as it is the less aggressive process, and therefore the one that offers higher guarantees of obtaining undamaged product. Furthermore, alkaline lysis offers not only cell wall disruption, releasing the pDNA, but also removes a large amount of cell debris, genomic DNA (gDNA) and proteins, which precipitate upon neutralization, leaving RNA (the major contaminant), as well as low amounts of gDNA, proteins and endotoxins [13].

To obtain purified pDNA on a large scale, it is of paramount importance to develop a set of highly efficient processes in terms of yield and absence of harmful chemicals. Conventional laboratory procedures involve the use of chemicals like cesium chloride or ethidium bromide, solvents as isopropanol, phenol or chloroform, enzymes (i.e. RNase A, proteinase K or lysozyme), which allow a selective precipitation of the contaminants, that are subsequently removed by ultracentrifugation [12, 13]. As already addressed, conventional laboratory pDNA purification procedures are quite complex to scale up, as some scalable alternatives were found. Hereupon, purification processes that use membranes were found as

a good solution to purify pDNA at a larger scale, without using potentially harmful chemicals [12, 13].

1.4 Nanofiber production techniques

Lately several processing techniques have been used to produce polymeric nanofibers, such as drawing [29], template synthesis [30], phase separation [31], self-assembly [32] and electrospinning [33], among others. The drawing process is closely related to a dry spinning, used in the fiber industry, making one-by-one single long fibers. This process is, however, limited to viscoelastic materials, the ones that can undergo strong deformations as well as the stresses developed during fibers production through drawing [34]. In the case of template synthesis, a nanoporous membrane is used as a template to produce the nanofibers, making either solid (i.e. fibril) or hollow (i.e. tubule) shaped nanofibers. The best feature of this template synthesis is the variety of raw materials (e.g. electronically conducting polymers, metals, semiconductors, carbons) from which the nanofibers can be made. Nonetheless, this method of fabrication is limited, as it cannot make one-by-one continuous nanofibers. Furthermore, phase separation comprises processes of dissolution, gelation, extraction applying different solvent systems, freezing and drying process to obtain a nanoscale porous foam. The long period that takes to transfer the solid polymer into a nano-porous foam, is a limitation to the process. Finally, concerning the self-assembly process, where individual components organize themselves to achieve desired patterns and functions. The major drawbacks related to this process are, the complexity and excessive time elapsed to process continuous polymer nanofibers.

Hereupon, electrospinning appears as a simple and cheap method to produce one-by-one continuous nanofibers, being able to apply a wide range of polymers, or mixtures of polymers [34, 35]. This method has gained much attention in the past decade, as a versatile technique that offers unique features to make nanofibrous materials with controllable pore structure. The diameter of the fibers produced using electrical forces range from only 2 nanometers to some micrometers, as it is difficult to consistently obtain submicron fibers from standard mechanical fiber-spinning techniques [36-38]. Being a relatively straight-forward method of fiber production, electrospinning was found very helpful in a wide range of applications, including tissue engineering applications, like for instance in bone repair [39], wound healing [40] and drug delivery systems [41], but also in sensors and biosensors [42], electrodes [43] and filtration processes [35].

1.4.1 Electrospinning process

The electrospinning apparatus comprises three basic components (Figure 6), a high voltage supplier, a capillary tube with a needle of small diameter and a grounded collecting plate (e.g. a metal screen). The high voltage power supplier will create an electrically charged jet of polymer solution, which will evaporate or solidify and be collected as an interconnected web of tiny fibers [44]. In the tip of the needle is placed one of the electrodes, being the other attached to the collector, usually just grounded [34]. The polymer solution held by its own surface tension at the end of the needle is subjected to an electric field, so that an electric charge is promoted on the liquid surface. When the intensity of the electric field is increased, the hemispherical surface of the fluid at the tip of the needle elongates, forming a conical shape that is know by Taylor cone [45]. When a critical value is attained, in which the repulsive electrostatic force overcomes the surface tension, the charged jet of polymer is ejected from the tip of the Taylor cone. The ejected polymer is subjected to an instability and elongation process, which enables the discharged to become very long and thin as the solvent evaporates, remaining only a charged polymer fiber [34, 38].

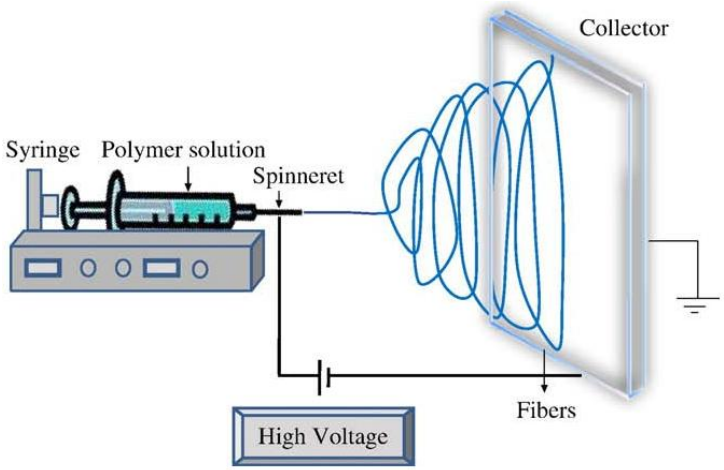

Figure 5 Representation of the electrospinning apparatus (adapted from [38]).

1.4.1.1 Parameters Influencing Nanofiber Production

The production of electrospun nanofibers comprises some key factors: the fibers diameters should be consistent and controllable, the fibers surface should present minimal, or no defects at all, and continuous single nanofibers should be collected [34]. However, the optimization of these three conditions is not easy, as there are several parameters influencing nanofibers production via electrospinning. These parameters include [46]:

- solution properties, such as viscosity, elasticity, conductivity, and surface tension,
- processing variables, such as hydrostatic pressure, electric potential at the needle tip, distance between the collector and the needle tip, the type of collector (e.g. static, rotational) and flow rate,
- ambient related parameters, such as solution temperature, humidity and air velocity inside the electrospinning chamber.

Fiber diameter control is a relevant issue, depending primarily on the jet sizes and polymer contents. The solution viscosity plays an important role, influencing the fiber diameter, when a solution with higher viscosity is used, it results in a larger fiber diameter, regarding that the solution viscosity is proportional to the polymer concentration [34, 47]. Furthermore, fiber diameter is also affected by the applied electrical voltage, being the usual outcome that a higher applied voltage increases solution ejection and, therefore, larger fiber diameter is obtained [48].

These are not the only factors affecting fiber formation though, as interactions between the polymer and the solvent, and the molecular weight (MW) of the polymer do affect the process. Selecting the right solvent, or a combination of solvents, is very important when determining the physical properties of the polymer solution. The dielectric constant (table 4) and the boiling temperature of the solvent are absolutely decisive when selecting the correct one to produce nanofibers. Solvents possessing a low dielectric constant will improve the dissolution of the polymer charged chains by dispersing the ion pairs, enhancing the conductivity and, therefore, reducing the need of applying extreme voltages. Furthermore, solvents with low boiling point will evaporate faster from the polymer surface, upon fiber formation [49].

Table 4 Dielectric constants of the most commonly used solvents to prepare electrospinning solutions (adapted from [50]).

Solvent	Dielectric constant
2-propanol	18.3
Acetic acid	6.15
Acetone	20.7
Acetonitrile	35.92-37.06
Chloroform	4.8
Dichloromethane	8.93
Dimethylformamide	36.71
Ethyl acetate	6.0
Ethanol	24.55
m-Cresol	11.8
Methanol	32.6
Pyridine	12.3
Tetrahydrofuran	7.47
Toluene	2.438
Trifluoroethanol	27.0
Water	80.2

Failing to accomplish the latter factors, it may result in an electrospraying phenomenon, characterized by formation and ejection of macro-drops of polymer solution. Is this cases the repulsive electrostatic force does not overcome the surface tension, as the electric energy created inside the drop solution is higher than the one provided by the electrospinning system. Therefore, the ejected polymer is not subjected to enough instability to produce continuous fibers, as the control of fiber formation becomes harder [49].

As already addressed polymer viscosity is very important to produce fibrous structures, seeing that higher viscosities will lead to large average diameter fibers. On the other hand, excessively low viscosity tends to generate beads, producing defective fibers [51].

According to Li and Xia [52], there are three forces that simultaneously interact and affect fiber formation.

- The surface tension is responsible for converting the liquid jet into one or several spherical droplets through the minimization of the surface area.
- The electrostatic repulsion between different charges on the jet surface is likely to increase the surface area, favoring the formation of a thin jet, a key parameter for the electrospinning process.
- Viscoelastic forces tend to resist sudden changes in the shape, as well as support the formation of fibers with smooth surface.

Hereupon, bead formation can be eliminated if the combined effect of the electrostatic repulsion and viscoeleastic forces is able to overcome the influence of the surface tension.

1.4.1.2 Polymeric Nanofibers

The ability of reducing the diameter of polymer fiber materials from micrometers to nanometers show several remarkable features, such as very large surface area to volume ratio, flexibility in surface functionalities, superior mechanical performance (e.g. stiffness and tensile strength) allowing the production of fiber with a wide variety of sizes and shapes [34]. In addition, the tunable porosity and the ability to control the nanofiber composition and morphology, by using a large variety of polymers, makes electrospun nanofibers potential candidates to be used in different applications (Figure 7), such as: biomedical, biotechnology, defense and security, environmental engineering, filtration, healthcare, optical electronics, pharmaceutical, protective clothing and tissue engineering scaffolds [53, 54].

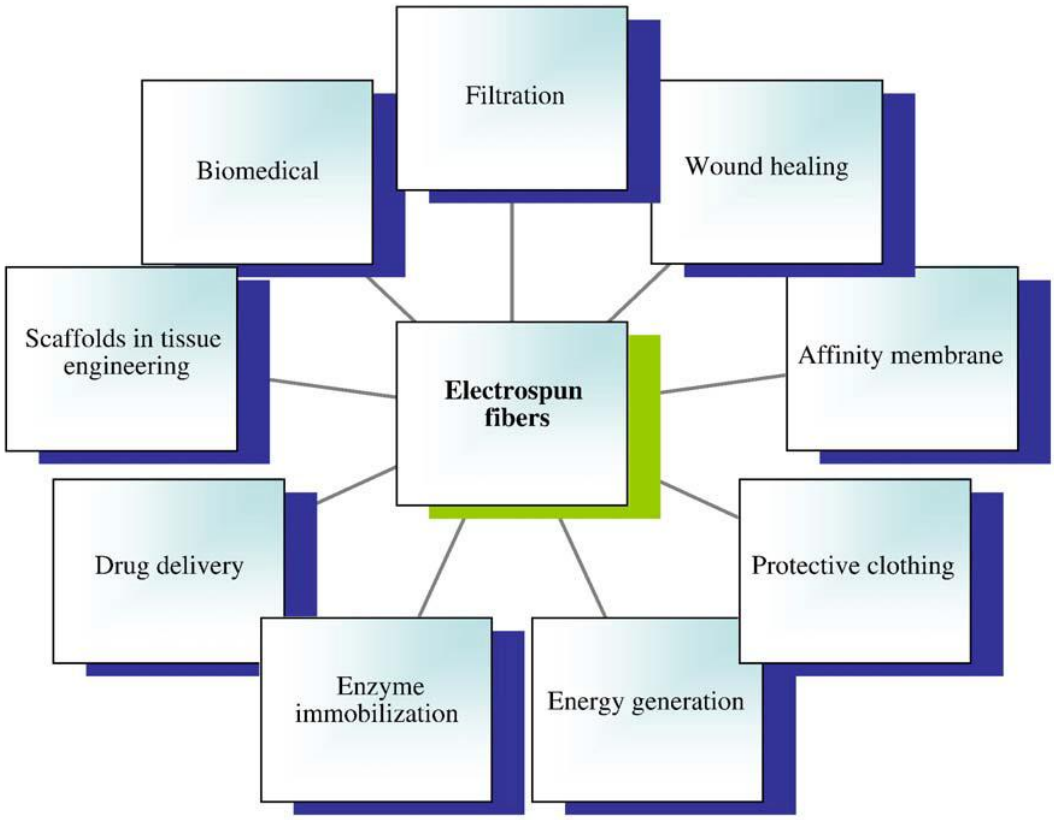

Figure 6 Representation of the areas of application of the polymeric nanofibers (adapted from [38]).

The application of electrospun nanofibers for the production of tissue engineering scaffolds, for wound healing, drug delivery or bone regeneration, has been increasing in the past few years [38]. To engineer living tissue, a biodegradable scaffold is crucial to be applied as a temporary template, enabling cell seeding, invasion, proliferation and differentiation, leading to restore the biological function of the tissue or of the extracellular matrix (ECM) [38]. Electrospinning has been reported to create nanofibrous scaffolds, very useful in tissue engineering, as they have been shown to promote cell-matrix and cell-cell interactions, maintaining the normal phenotypic shape and gene expression of the cells [55, 56]. Furthermore, electrospun fibers show similar diameter magnitude when compared to the ECM fibrils, mimicking the environment in natural tissues, and demonstrated also effectiveness as substrate for cell growth [57].

Nowadays, a wide variety of polymeric nanofibers has been tested as a scaffold for tissue engineering purposes, including in cartilage [58], skin [59], bone [60], arterial blood vessels [61], heart [62] and nerves [63], among others.

In the present thesis three polymers were used to produce an electrospun nanofiber membrane (ENM), poly ε-caprolactone (PCL), poly(ethylene) oxide (PEO) and sodium alginate (SA). PCL was selected as a support, based on the good mechanical properties (e.g. strength

and elasticity) evidenced and low degradability rate (despite being biodegradable) evidenced by its meshes [64], as well as for being environmentally friendly [65]. SA was chosen for the ENMs coating taking into account, its high hidrophilicity, since surface hidrophilicity in separation membranes is very important, relative low cost and its ability of producing small diameter nanofibers. However, SA on its own cannot produce fibers, as it needs to be mixed with a stabilizer. Hereupon, PEO has been widely reported for nanofiber production and for being a stabilizer agent for other polymer, such as SA [66]. The result is an asymmetric arrangement of different two layers (Figure 8), with PCL providing adequate mechanical robustness, whereas separation selectivity is controlled by the ultrathin coating layer of SA/PEO nanofibers.

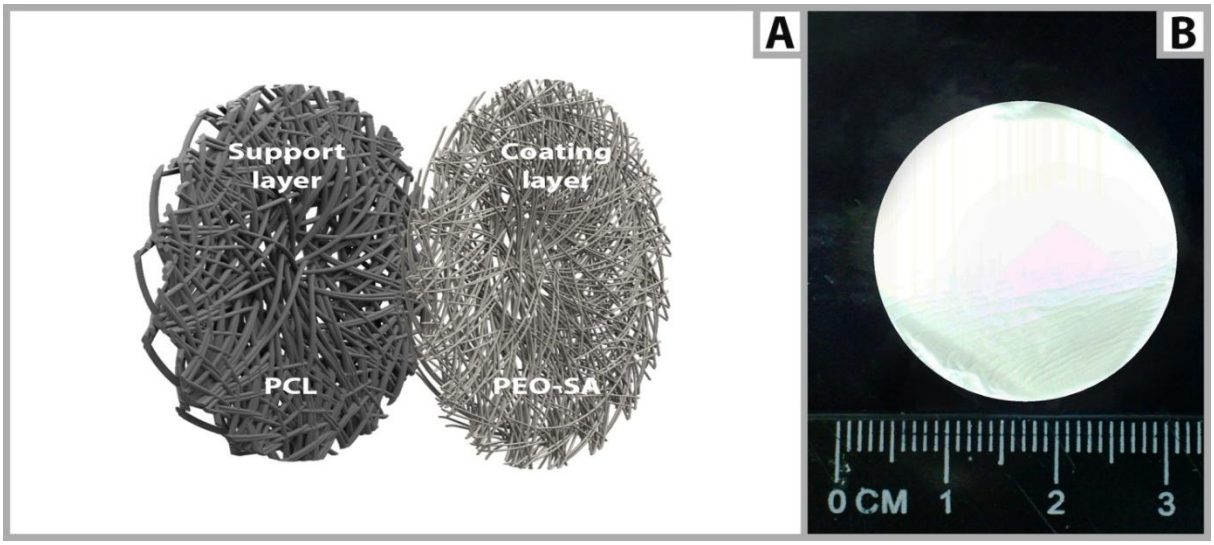

Figure 7 (a) Schematic representation of the bi-layer PCL coated PEO/SA ENM; (b) Macroscopic bi-layer membrane of PCL coated with PEO/SA.

1.4.1.3 Application of nanofiber membranes to separation processes

ENMs have been successfully used to develop air filters. For filtration purposes, the structural elements of a filter must match the scale of solids, obtaining desired selectivity. The electrospun membranes offer a wide set of advantages for filtration application, very high surface area to volume ratio, high surface cohesion, high porosity, lower base weight, continuously interconnected pores and high permeability for gases when compared with common polymers or conventional membranes [38, 67, 68]. High surface area to volume ratio and high surface cohesion will facilitate particle entrapment and, therefore, improving filtration efficiency [38]. The decrease of fiber thickness, generally, results in an increase of filtration efficiency [69]. The consistent production of very small diameter fibers represents a clear advantage of electrospinning, enabling the removal of unwanted particles at the submicron scale [38]. Furthermore, polymer nanofibers can be electrostatically charged with

the purpose of attracting particles without increasing the pressure drop, further enhancing the filtration efficiency [70].

ENMs have been reported for application in separation processes, especially in pressure-driven separations, such as MF, UF or NF [67, 71-73]. The application of ENMs requires a support to provide strength, unlike conventional cast membranes. Therefore, nowadays ENMs used in membrane separation technology are based in hybrid systems. In this kind of systems, electrospun nanofibers are placed over a support, combined in various layers or blended together with micron scale fibers [68].

1.5 Objectives

In the present study an electrospinning technique was used in order to produce a bi-layer nanofiber membrane for recuperation of biotechnology products. The present master thesis work plan had the following aims:

- Electrospun of PCL and PEO-SA nanofibers to produce the ENMs;
- Characterization of the properties of the produced EMNs and commercial membranes by Scanning electron microscopy (SEM), Attenuated total reflectance-fourier transform infrared spectroscopy (ATR-FTIR), determination of the Contact angles and Membrane porosity;
- Evaluation of the filtration performance for both the ENMs and commercial membranes.

Chapter II

Materials & Methods

2. Materials and methods

2.1 Materials

Calcium chloride (Mw=110.99 g/mol), PEO (Mw=300,000 g/mol), PCL (Mw=80,000 g/mol), SA (Mw=120000–190,000g/mol), were purchased from Sigma–Aldrich (Sintra, Portugal) as well as Terrific Broth medium for bacterial culture and kanamycin sulfate. P1 buffer (50mM Tris–HCl, pH=8.00, 10 mM EDTA and 100 µg/mL of RNase A), P2 buffer (200 mM NaOH and 1% SDS (w/v)) and P3 buffer (3M of potassium acetate, pH 5.00) were obtained from a Qiagen Plasmid Maxi Kit and Tris–HCl 10 mM (IZASA, Portugal). Microfiltration membranes, *Nylaflo* (pore diameter of 0.22 µm Pall Corporation and *FSM0.45PP* from Alfa Laval (pore diameter of 0.45 µm).

2.2 Methods

2.2.1 Bacterial growth and cell lysis

The plasmid production procedure was adapted from the literature [13, 74]. The 6050 bp plasmid pVAX1-LacZ was amplified in a cell culture of *Escherichia coli* (*E. coli*) DH5α. The fermentation was carried out at 37 °C in 250 mL of Terrific Broth medium, supplemented with 50 µg/mL of kanamycin. Growth was suspended at the late log phase (OD_{600_nm} ≈ 10–11) and cells were harvested by centrifugation. Afterwards, pDNA extraction was performed by alkaline lysis using three different buffers (P1, P2 and P3, previously specified). For this procedure 120 g/L (wet weight) of cells were resuspended in 4 mL of P1 buffer. Then, 4 mL of P2 were added to promote cell lysis for 5 min, at room temperature. Finally, P3 buffer, at 4 °C, was added to neutralize the alkaline solution. A large quantity of suspended solids was obtained upon neutralization and the suspension was kept on ice for 15 min before membrane filtration.

2.2.2 Electrospinning setup

The system used herein to carry out the electrospinning process was composed by a high power voltage supply (Spellman CZE1000R, 0–30 kV), a syringe pump (KDS-100), a syringe fitted with a stainless steel blunt end needle and an aluminum plate as the conductive collector (10 cm x 12 cm). The needle was positively charged by the power supply and the metal collector was grounded. The charged tip and grounded collector form a static electric field between them, to provide the driving force that enables fiber formation [38].

2.2.3 Preparation of the polymer solutions

PCL was dissolved in acetone to a concentration of 10% (w/v), under constant stirring and heating at 50 ˚C [75]. Meanwhile, a PEO/SA solution was prepared by mixing 6.75% PEO and 0.5% SA aqueous solutions [76].

2.2.4 Electrospun nanofiber membranes production

The PCL polymer solution was used to produce a support ENM, using a constant flow rate and different voltages. Subsequently, the PEO/SA solution was deposited over the PCL ENM by electrospinning, in the same apparatus, at a constant flow rate, with a similar voltage, thereby obtaining a bi-layer ENM. Finally, the membrane was crosslinked in a calcium chloride solution for 24 h [76]. From the obtained films, membranes disks were cut with suitable size to be used in the filtration cell, using a circular blade.

2.2.5 Membrane filtration tests

These assays were performed in a 10mL stirred cell (Amicon/Millipore, model 8010), according to a previously described procedure [13]. The membranes to be tested (*Nylaflo*, *FSM0.45PP* or the ENMs) were initially flushed with 20 mL of Milli-Q water at a constant pressure of 0.07 bar, to ensure the thorough washing of the membranes. Then, the water permeability (hydraulic permeability) of each membrane was determined by measuring the flow rate, at that pressure. Five permeability measurements were performed with each membrane disk and the average value was considered the initial hydraulic permeability of each membrane disk, L_{p0}.

To perform the filtration of the E. coli DH5α lysates the remaining water in the cell was carefully removed and, immediately after that, 10 mL of lysate were introduced in the filtration cell. A continuous diafiltration of the lysate was performed for 1h, using a 10 mM Tris–HCl (pH=8.00) buffer at a constant flow rate of 0.5 mL/min. Two peristaltic pumps were used, one for feeding the diafiltration buffer and the other to perform the filtration (by suction). The experimental setup is shown in Figure 9. Under these conditions, one could estimate that, if no pDNA was adsorbed on the membrane and the membrane rejection was 0, approximately 95% of the pDNA was expected to be recovered in the permeate, while 5% would remain in the cell. It was decided not to try to recover the remaining pDNA to avoid excessive dilution of the whole permeate.

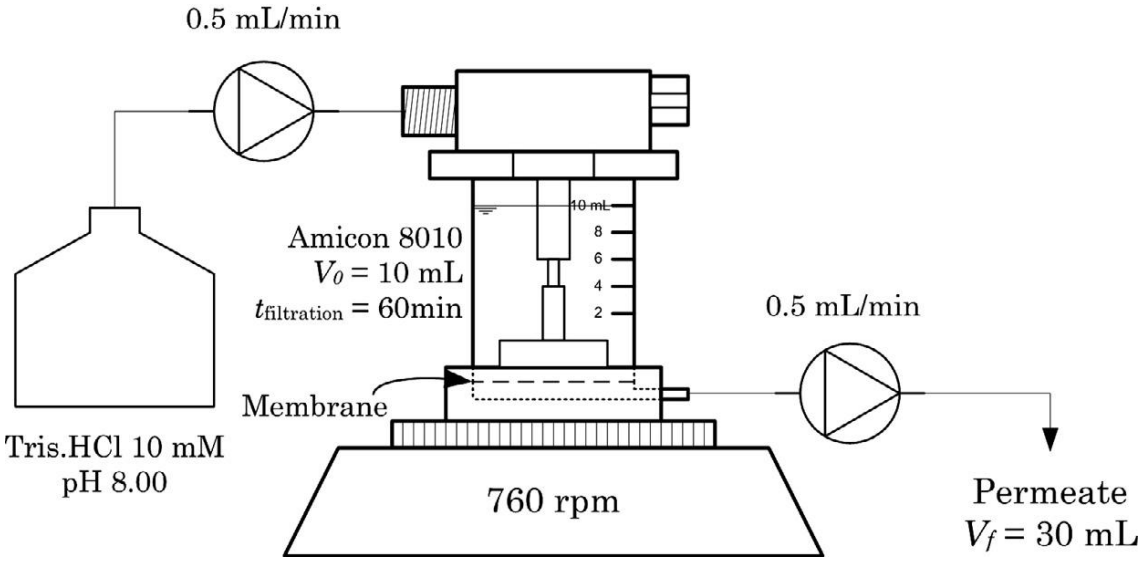

Figure 9 Experimental set-up used for continuous diafiltrations, showing the two peristaltic pumps and the filtration cell (adapted from [35]).

2.2.6 Turbidity measurements

The filtrate was analyzed by UV/Visible Spectroscopy at a wavelength of 600 nm, to determine the amount of suspended solids. A fraction of the alkaline lysate, containing the suspended solids, was transferred to an eppendorf tube and centrifuged at 18,000 g during 30 min, at 4 ˚C (Hettich Zentrifugen, Mikro 200R). Then, the absorbance of the supernatant was measured at a wavelength of 600 nm and the value obtained compared with that of the membrane permeates [35].

2.2.7 Plasmid DNA and RNA quantification

Plasmid DNA and RNA concentrations in lysates, were obtained by hydrophobic interaction chromatography (HIC) [13]. Briefly, a 15 PHE PE column (Amersham Biosciences – GE Healthcare) connected to an AKTA purifier HPLC System was used. The column was initially equilibrated with 1.5 M $(NH_4)_2SO_4$ in a 10 mM Tris–HCl buffer (pH 8.00). Prior to the injection, the suspended solids in lysates were removed by centrifugation, as described in Section 2.2.6.

Samples from the supernatants were directly injected in the column. The injected volume in each run was 20 µL and the samples were eluted at a constant flow rate of 1 mL/min. Two minutes after the injection, the eluent was instantly changed to 10 mM Tris–HCl buffer (pH =8.00), in order to elute bounded species. This concentration was maintained for 5 min before the re-equilibration of the column, which was carried out with 1.5 M $(NH_4)_2SO_4$ in

a 10mM Tris–HCl buffer (pH8.00), in order to prepare the column for the next run. The absorbance of the eluate at 260 nm was monitored. The concentration of pDNA in each sample was calculated from the area of the pDNA peak and a calibration curve, obtained with pure pVAX1-lacZ standard solutions. The filtration yield, in each test, was calculated as the ratio of the amount of pDNA in the whole collected permeate, to the amount of pDNA in the lysate. The RNA removal was calculated as $1-(V_pC_{RNA,p})/(V_{lys}C_{RNA,lys})$ where $C_{RNA,p}$ is the RNA concentration in the whole collected permeate and $C_{RNA,lys}$ is the RNA concentration in the lysate, V_p is the volume of whole the permeate collected and V_{lys} is the volume of lysate processed in each run.

2.2.8 Scanning electron microscopy

The morphology of all the membranes was analyzed by scanning electron microscopy (SEM). Samples were air-dried overnight and then mounted on an aluminum board using a double-side adhesive tape and covered with gold using an Emitech K550 (London, England) sputter coater. The samples were analyzed using a Hitachi S-2700 (Tokyo, Japan) scanning electron microscope operated at an accelerating voltage of 20 kV and at different amplifications [35].

The diameter distribution of the nanofibers in the ENMs was determined from 50 measurements, at least, using *ImageJ* (National Institutes of Health, Bethesda (MD), USA).

2.2.9 Attenuated total reflectance-fourier transform infrared spectroscopy

PEO, SA, PCL and polymer coated ENMs spectra were acquired in the range of 4000–500 cm^{-1}, using a JASCO 4200 FTIR spectrophotometer, operating in ATR mode (MKII GoldenGate™ Single Reflexion ATR System). Data collection was performed with a 4 cm^{-1} spectral resolution and after 64 scans [35].

2.2.10 Contact angle determination

Contact angles of the membranes were determined using a Data Physics Contact Angle System OCAH 200 apparatus, operating in static mode. For each sample, water drops were placed at various locations of the analyzed surface, at room temperature. The reported contact angles are the average of at least three measurements [35].

2.2.11 Membrane porosity determination

The surface porosity of the membranes was estimated from SEM images using the image analysis software, *ImageJ*. The total porosity of the membranes was measured through the determination of the amount of ethanol absorbed by wet membranes, after 1 h of immersion in that solvent, using the following equation [77]:

$$P\% = \frac{W_2 - W_1}{d_{ethanol} V_{membrane}} \times 100 \qquad \textbf{(1)}$$

where W_1 is the weight of the dry membrane and W_2 is the weight of the wet membrane, $d_{ethanol}$ the density of the ethanol at room temperature, and $V_{membrane}$ is the volume of the wet membrane. The latter was determined from the membrane area and by measuring the membrane thickness with a micrometer Adamel Lhomargy M120 acquired from Testing Machines Inc., USA.

Chapter III

Results & Discussion

3. Results and discussion

3.1 ENMs characterization

3.1.1 Morphological characterization

The morphology of the membranes, namely in terms of fiber diameter distribution, fiber average diameter and surface porosity was analyzed through the SEM images.

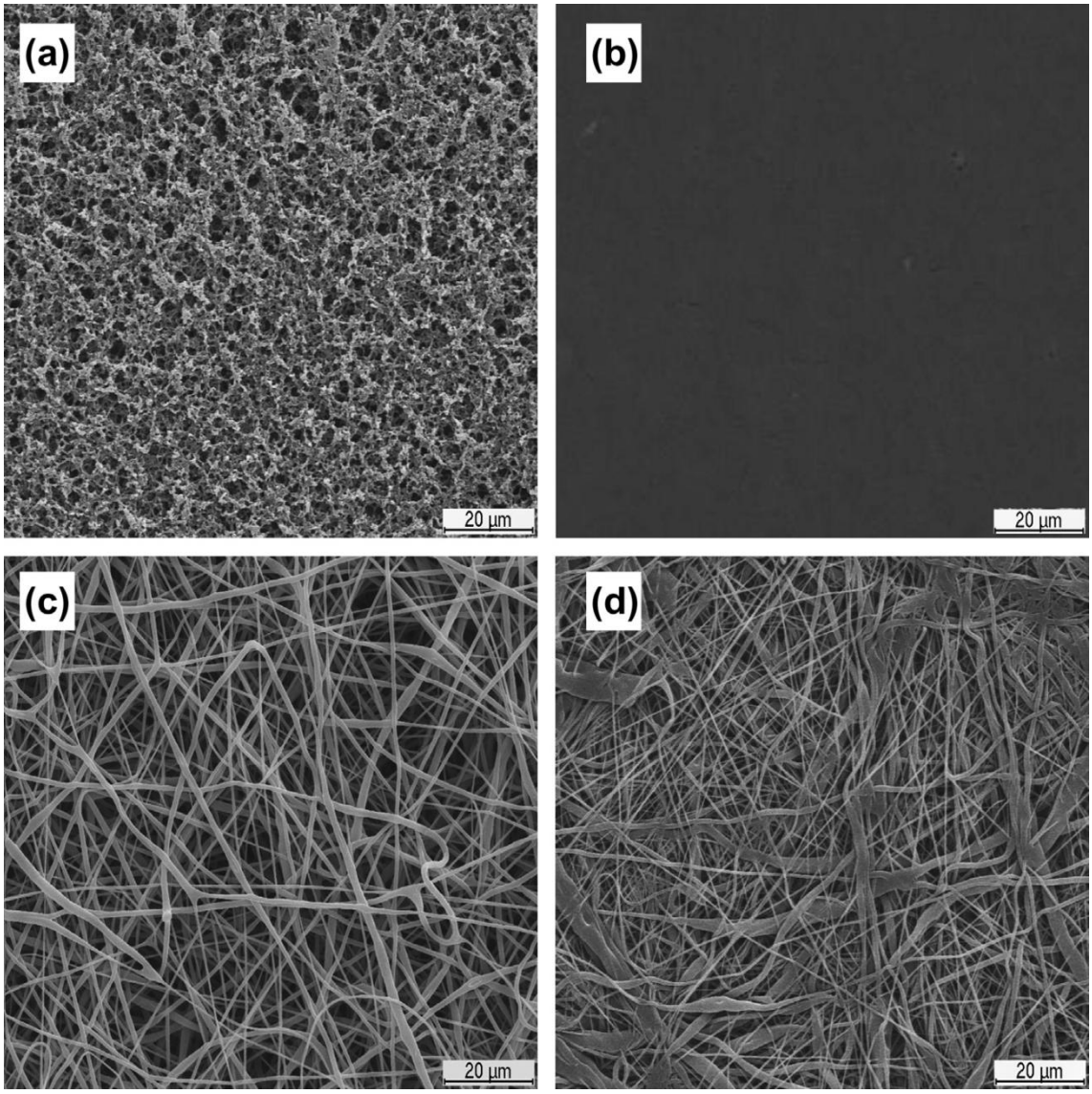

Figure 10 SEM images of (a) Nylaflo 0.22 µm membrane, (b) FSM0.45PP 0.45 µm membrane, (c) PCL ENM and (d) PCL ENMC.

As it can be seen in Figure 10 the ENMs produced present a high density of deposited fibers, in particular after the deposition of the second layer of nanofibers. Fiber diameter distributions are shown in Figure 11. The PCL support has nanofibers with different diameters (200 nm – 2 μm) and this range of fiber diameters is adequate for obtaining a good mechanical support [78]. The polymer-coated ENM (PCL ENMC) presents a higher density of thin fibers (i.e. fibers with 200–300 nm of diameter) than the polymer-uncoated ENM (i.e. the PCL support) which contributes to a decrease in the dimensions of the interstices. The number average fiber diameter of the uncoated ENMs can be estimated to be 720 nm and that of the coated membranes to be 430 nm. The commercial microfiltration membranes have typical values of pore diameter of, 0.22 μm and 0.45 μm for the *Nylaflo* and *FSM0.45PP*, respectively (nominal values given by the manufacturers).

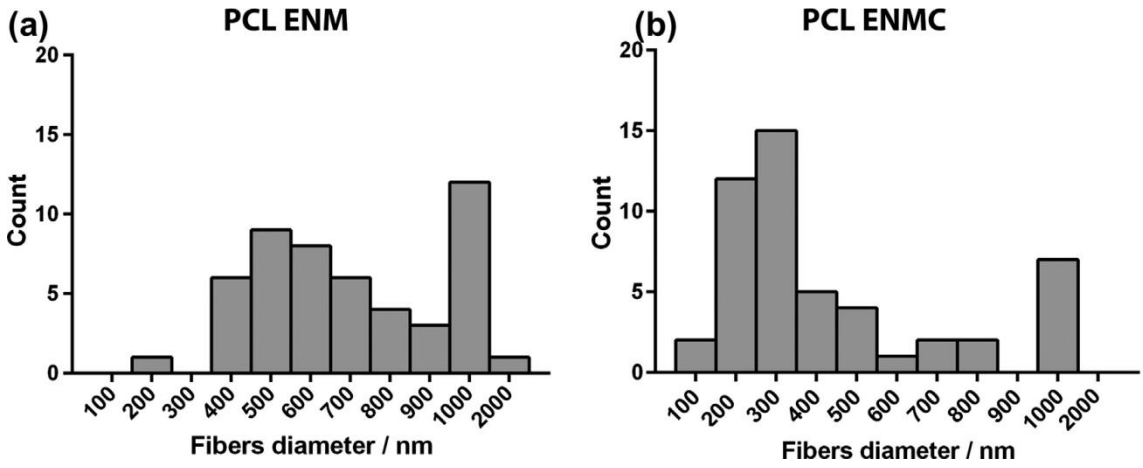

Figure 11 Fiber diameter distribution for the uncoated (a) and coated PCL ENM (b).

The porosity of the membranes is analyzed in Figure 12. As it can be seen, the ENMs have porosities comparable to that of the 0.22 μm *Nylaflo* membranes which have been found to perform very satisfactory in the filtration of lysates from plasmid pVAX1-lacZ fermentation [13]. The porosity of the 0.45 μm membrane used is clearly lower than that of the other membranes studied herein.

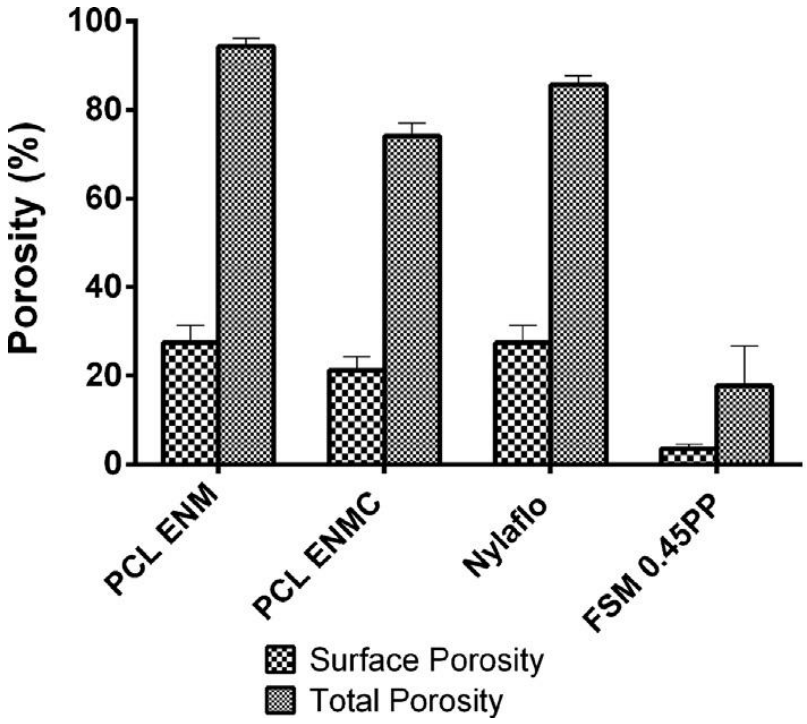

Figure 12 Surface and total porosity of the ENMs and the commercial microfiltration membranes.

3.1.2 Attenuated total reflectance-fourier transform infrared spectroscopy analysis

An ATR-FTIR analysis of the membranes was also carried out to check for the presence of the coating layer. The ATR-FTIR spectra of SA, PEO, PCL and the PCL/SA+PEO ENM (polymer coated ENM) can be seen in Figure 13. The spectrum of SA shows its characteristic absorption band in the region between 1610 cm^{-1} and 1560 cm^{-1}, which is due to COO^- groups [79] (spectrum 1). The spectrum of PEO (spectrum 2) shows the characteristic bands of $-CH_2-$ groups in the region between 2990 cm^{-1} and 2850 cm^{-1} [80]. The third spectrum is that of PCL, which shows an absorption band between 1750 cm^{-1} and 1740 cm^{-1} due to C=O groups [81]. The spectrum of the polymer coated ENM (spectrum 4), shows the characteristic peaks of the functional groups of the polymers used in membrane production, previously mentioned, therefore indicating that a thin layer of PEO/SA was deposited on the PCL support. Moreover, a much higher intensity peak around 3300 cm^{-1} was observed, due to the over-abundance of -OH groups in the coating layer, as previously described in the literature [82, 83].

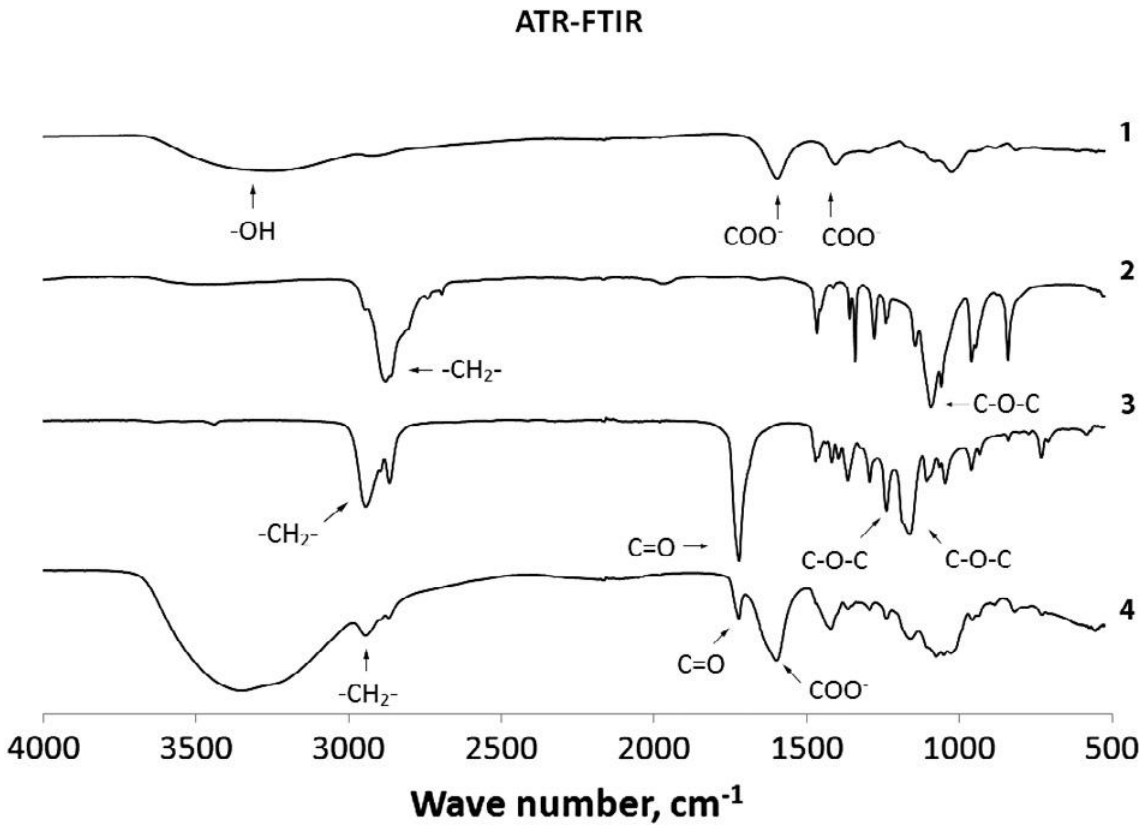

Figure 13 ATR-FTIR spectra of: SA (1), PEO (2), PCL ENM (3) and PCL ENMC (4).

3.1.3 Surface properties characterization

In order to further characterize the surface properties of the membranes, water contact angles were also determined to evaluate the hydrophilicity of the membranes. This is an important property when considering the filtration of suspensions with high organic load; in fact, it is well-known that hydrophilic membranes generally perform better than hydrophobic, due to adsorption phenomena [84]. The obtained contact angles are indicated in Table 5. As it can be seen, the uncoated PCL membrane presented a high contact angle of 104°, which is indicative of a hydrophobic character. After coating it with PEO/SA the contact angle decreased to 16.8°, which is a very similar value to that of the *Nylaflo* membrane. The contact angle of the *FSM0.45PP* membrane is also very high, although lower than that of the uncoated PCL ENM. Herein, the filtration tests performed with this membrane aimed to check the effect of the pore size on the permeate turbidity and permeability recover after filtration.

Table 5 Contact angles of the *FSM0.45PP*, *Nylaflo*, uncoated ENM (PCL support) and PCL coated ENM.

Membranes	Water contact angle
FSM0.45PP – 0.45 μm	85.5° ± 3.5°
Nylaflo – 0.22 μm	18.4° ± 0.1°
PCL ENM	104° ± 7°
PCL ENMC	16.8° ± 2.4°

3.2 Membrane filtration studies

3.2.1 Hydraulic permeability

The results obtained in the permeability tests are summarized in Figure 14. As it can be seen, the coated PCL ENM produced have L_{p0} values near 5000 L/h m^2 bar, which are of the same order of magnitude of those found for the *Nylaflo* membrane. The hydraulic permeability of the *FSM0.45PP* is clearly lower, which is possible due to its lower porosity and also its higher hydrophobicity, as suggested by the results obtained from contact angle measurements.

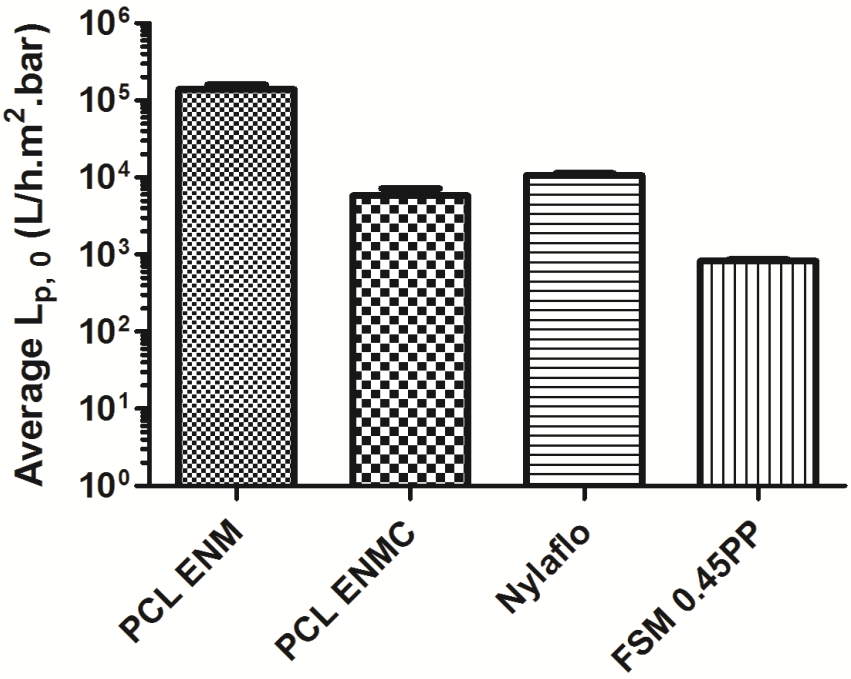

Figure 14 Water permeability (hydraulic permeability) of the different membranes tested, T = 25 °C, before the filtration tests (L_{p0}).

3.2.2 Microfiltration of lysates

After the cell lysis procedure is completed (using the method described in section 2.2.1), a suspension containing a large quantity of precipitates and cell debris is formed, nearly 2.4 g of suspended solids per gram (wet weight) of cells, as described elsewhere [85]. In respect to solids removal, the coated PCL ENMs and the *Nylaflo* membranes gave identical results. Almost, all solids were removed during the filtration, as can be seen by the turbidity measurements (Table 6). This indicates that both membranes have a similar average pore size. The fact that the uncoated ENMs have lower solids retention than the coated is in agreement with their higher average fiber diameter, considering that the dimension of the interstices between fibers becomes smaller as the fiber diameter decreases.

Table 6 Turbidity of the processed lysates.

Centrifugation *	PCL ENM	PCL ENMC	*Nylaflo*	*FSM0.45PP*
0.002 ± 0.001	0.030 ± 0.001	0.0060 ± 0.0009	0.0065 ± 0.0009	0.024 ± 0.008

* As described in section 2.2.6.

In respect to the process yield, in a previous study, where the same lysis method was used the *Nylaflo* membranes presented high yields for the recovery of pVAX1-lacZ from the obtained lysates [13]. Using both coated and uncoated ENMs, high recovery yields were also obtained herein, as indicated in Figure 15. In addition, the results also reveal that a significant RNA removal can be achieved using the ENMs, reaching approximately 30% with the PCL coated ENM. It is possible that the structural differences between ENMs and conventional microfiltration membranes can explain the improved selectivity of the ENMs.

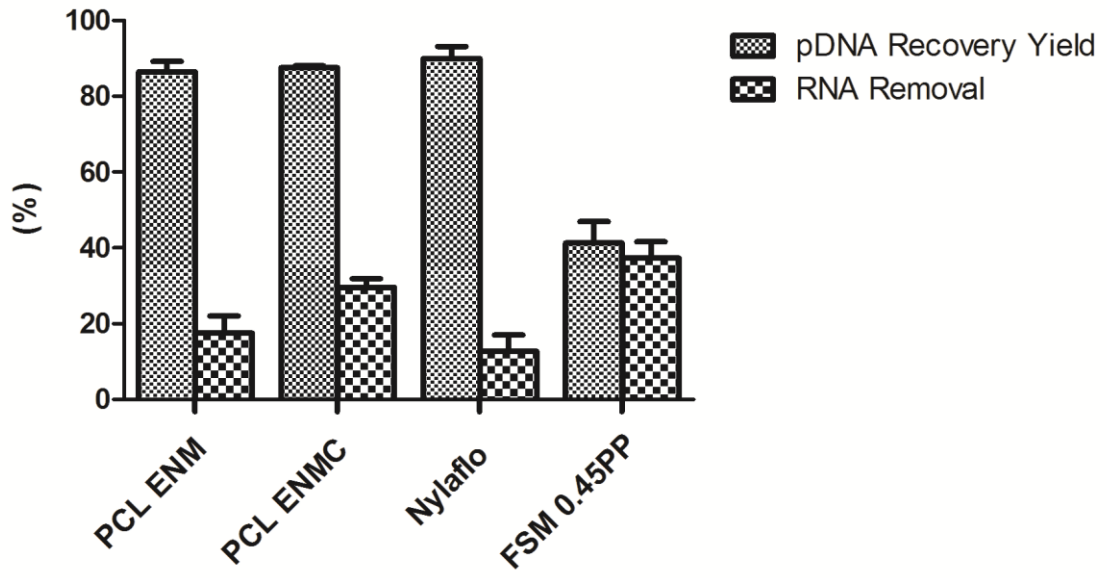

Figure 15 Filtration yield of the different membranes tested in the filtration of lysates.

With the *FSM0.45PP* membrane the highest RNA removal was found, however, much lower yields are also obtained. The occurrence of severe fouling is likely to be the cause of the higher retention of both pDNA and RNA. In fact, after a few minutes of filtration with this membrane, the permeate pump was unable to impose the pre determined flow of 0.5 mL/min (73 L/h m^2), which is indicative of the intense fouling. In order to accomplish the filtration, the stirred cell had to be connected to a pressurized nitrogen reservoir containing the diafiltration buffer. The applied pressure on the feed was adjusted to 0.5 bar and the permeate pump was disconnected. The permeate flux decreased from 140 L/h m^2 to near 20 L/h m^2 by the end of the diafiltration. Fluxes were determined from the volume of permeate collected as a function of time.

The fouling tendency of the different membranes can be better evaluated by comparing the recovery of hydraulic permeability after filtration, i.e., after replacing the lysate suspension inside the cell with water and then, measuring the water permeability (without subjecting the membranes to any cleaning procedure). The ratio L_p/L_{p0}, is a measure of the tendency of the membranes to foul; the obtained values are shown in Figure 16. As it can be seen, the coated PCL ENMs recovered almost completely their initial permeability upon filtration of the lysates. This indicates that the produced membranes are highly resistant to fouling by the cell debris and other suspended solids present in the lysates.

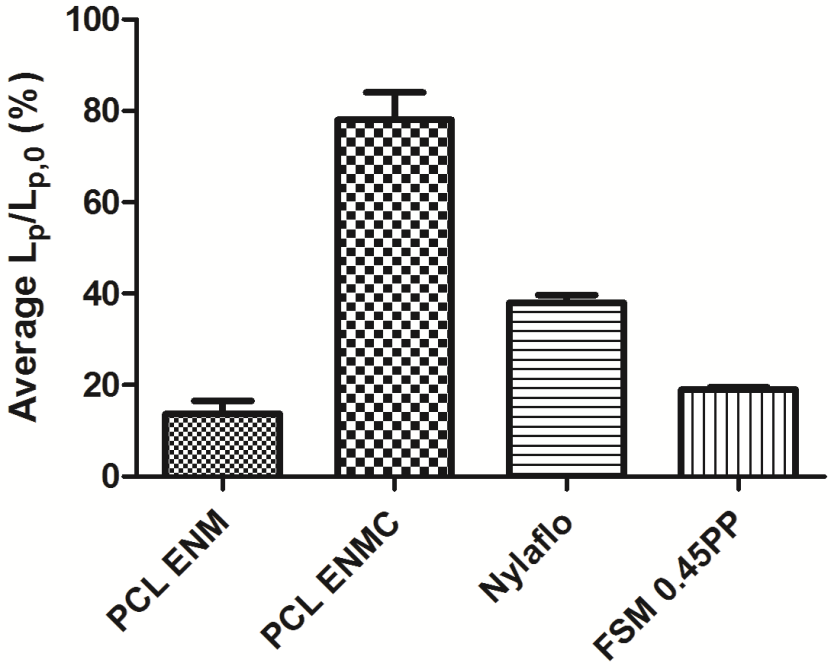

Figure 16 Permeability recovery of the different membranes tested in the filtration of lysates.

The differences between the coated and uncoated ENMs should be also pointed out, with the results clearly showing the importance of the PEO/SA layer in preventing membrane fouling. The decrease in the average fiber diameter may have contributed to a better performance of the coated membranes, by avoiding the accumulation of solids between the fibers, inside the electrospun films. However, the decisive factor affecting membrane performance is more likely to be the increase in hydrophilicity, as it is suggested from the fact that both the uncoated ENMs and the *FSM0.45PP* membranes (that had the highest contact angles) present the lowest L_p/L_{p0} values.

Chapter IV

Conclusion & Future Perspectives

4. Conclusion and future perspectives

In this work a bi-layer membrane was produced, by deposition of a PEO/SA layer on a PCL support. Both layers were produced by electrospinning. Electrospun nanofibers that have been previously used in a practical and cost-effective way for the production of polymer scaffolds are shown here to be also suitable to be used as microfiltration membranes, for processing complex suspensions of solids, with high fouling potential (which is the case of cell lysates). The bi-layer arrangement provided both the selectivity and hydrophilicity required for this application. In fact, the experimental results point out that the bi-layer ENM produced can perform, at least, at the same level as commercial microfiltration membranes, showing a comparable selectivity for retaining the suspended solids while allowing the total permeation of the solute of interest (i.e., the plasmid), with an improved selectivity to retain RNA and an even better resistance to fouling. Moreover, the membranes produced are environmentally friendly due to their known biodegradability.

Despite the potential shown by the obtained results, there are some issues that need to be addressed before considering this work for industrial purposes. The most relevant one is, with no doubt, the reproducibility when producing a membrane. The production process should be optimized so that is obtained a narrow range of fiber diameters, and subsequently an even distribution of the pore size. This would definitely improve the reproducibility of the when using the ENM, as the control of the fiber diameter distribution is very important when defining the correct selectivity of a membrane separation process. Furthermore, plasmid DNA recovery yield and RNA removal could be enhanced, by testing other polymer combinations and working around the membrane surface charge with the purpose of retaining undesired contaminants.

Chapter V

Bibliography

5. Bibliography

1. Kalyanpur, M., *Downstream processing in the biotechnology industry*. Molecular biotechnology, 2002. **22**(1): p. 87-98.
2. Ratledge, C. and B. Kristiansen, *Basic Biotechnology*. 2nd ed. 2001: Cambridge University Press.
3. De Jong, J., R. Lammertink, and M. Wessling, *Membranes and microfluidics: a review*. Lab on a Chip, 2006. **6**(9): p. 1125-1139.
4. Zeman, L.J. and A.L. Zydney, *Microfiltration and ultrafiltration: principles and applications*. 1996: M. Dekker.
5. Charcosset, C., *Membrane processes in biotechnology: An overview*. Biotechnology Advances, 2006. **24**(5): p. 482-492.
6. Hughes, R., *Industrial membrane separation technology*. 1996: Springer.
7. *Membrane Filtration*, 1999, National Drinking Water ClearingHouse.
8. Abels, C., F. Carstensen, and M. Wessling, *Membrane Processes in Biorefinery Applications*. Journal of Membrane Science, 2013 **444**: p. 285-317.
9. Van Der Bruggen, B., C. Vandecasteele, T. Van Gestel, W. Doyen, and R. Leysen, *A review of pressure-driven membrane processes in wastewater treatment and drinking water production*. Environmental progress, 2003. **22**(1): p. 46-56.
10. Van Reis, R. and A. Zydney, *Membrane separations in biotechnology*. Current Opinion in Biotechnology, 2001. **12**(2): p. 208-211.
11. van Reis, R. and A. Zydney, *Bioprocess membrane technology*. Journal of Membrane Science, 2007. **297**(1): p. 16-50.
12. Kahn, D.W., M.D. Butler, D.L. Cohen, M. Gordon, J.W. Kahn, and M.E. Winkler, *Purification of plasmid DNA by tangential flow filtration*. Biotechnology and bioengineering, 2000. **69**(1): p. 101-106.
13. Nunes, J.C., A.M. Morão, C. Nunes, M.T. Pessoa de Amorim, I.C. Escobar, and J.A. Queiroz, *Plasmid DNA recovery from fermentation broths by a combined process of micro-and ultrafiltration: modeling and application*. Journal of Membrane Science, 2012. **415**: p. 24-35.
14. Baker, R., *Membrane technology and applications*. 3rd ed. 2012: Wiley.
15. Wijmans, J. and R. Baker, *The solution-diffusion model: a review*. Journal of membrane science, 1995. **107**(1): p. 1-21.

16. Mehta, A. and A.L. Zydney, *Effect of membrane charge on flow and protein transport during ultrafiltration.* Biotechnology progress, 2006. **22**(2): p. 484-492.

17. Hallström, B. and M. Lopez-Leiva, *Description of a rotating ultrafiltration module.* Desalination, 1977. **24**(1): p. 273-279.

18. Chung, K.Y., R. Bates, and G. Belfort, *Dean vortices with wall flux in a curved channel membrane system. IV: Effect of vortices on permeation fluxes of suspensions in microporous membrane.* Journal of membrane science, 1993. **81**(1-2): p. 139-150.

19. Ni, B.-J., B.E. Rittmann, and H.-Q. Yu, *Soluble microbial products and their implications in mixed culture biotechnology.* Trends in biotechnology, 2011. **29**(9): p. 454-463.

20. Liu, F., Y. Song, and D. Liu, *Hydrodynamics-based transfection in animals by systemic administration of plasmid DNA.* Gene therapy, 1999. **6**(7): p. 1258-1266.

21. Horn, N.A., J.A. Meek, G. Budahazi, and Magda Marquet, *Cancer gene therapy using plasmid DNA: purification of DNA for human clinical trials.* Human Gene Therapy, 1995. **6**(5): p. 565-573.

22. McConkey, S.J., W.H.H. Reece, V.S. Moorthy, D. Webster, S. Dunachie, G. Butcher, J.M. Vuola, T.J. Blanchard, P. Gothard, K. Watkins, C.M. Hannan, S. Everaere, K. Brown, K.E. Kester, J. Cummings, J. Williams, D.G. Heppner, A. Pathan, K. Flanagan, N. Arulanantham, M.T.M. Roberts, M. Roy, G.L. Smith, J. Schneider, T. Peto, R.E. Sinden, S.C. Gilbert, and A.V.S. Hill, *Enhanced T-cell immunogenicity of plasmid DNA vaccines boosted by recombinant modified vaccinia virus Ankara in humans.* Nature medicine, 2003. **9**(6): p. 729-735.

23. Tang, D., M. DeVit, and S.A. Johnston, *Genetic immunization is a simple method for eliciting an immune response.* Nature, 1992. **356**(6365): p. 152-154.

24. Prather, K.J., S. Sagar, J. Murphy, and M. Chartrain, *Industrial scale production of plasmid DNA for vaccine and gene therapy: plasmid design, production, and purification.* Enzyme and microbial technology, 2003. **33**(7): p. 865-883.

25. Donnelly, J.J., B. Wahren, and M.A. Liu, *DNA vaccines: progress and challenges.* The Journal of Immunology, 2005. **175**(2): p. 633-639.

26. Carlson, A., M. Signs, L. Liermann, R. Boor, and K. Jim Jem, *Mechanical disruption of Escherichia coli for plasmid recovery.* Biotechnology and bioengineering, 1995. **48**(4): p. 303-315.

27. Zhu, K., H. Jin, Y. Ma, Z. Ren, C. Xiao, Z. He, F. Zhang, Q. Zhu, and B. Wang, *A continuous thermal lysis procedure for the large-scale preparation of plasmid DNA.* Journal of biotechnology, 2005. **118**(3): p. 257-264.

28. Bimboim, H. and J. Doly, *A rapid alkaline extraction procedure for screening recombinant plasmid DNA*. Nucleic acids research, 1979. **7**(6): p. 1513-1523.

29. Ondarcuhu, T. and C. Joachim, *Drawing a single nanofibre over hundreds of microns*. EPL (Europhysics Letters), 1998. **42**(2): p. 215-220.

30. Feng, L., S. Li, H. Li, J. Zhai, Y. Song, L. Jiang, and D. Zhu, *Super-hydrophobic surface of aligned polyacrylonitrile nanofibers*. Angewandte Chemie, 2002. **114**(7): p. 1269-1271.

31. Liu, X. and P.X. Ma, *Phase separation, pore structure, and properties of nanofibrous gelatin scaffolds*. Biomaterials, 2009. **30**(25): p. 4094.

32. Niece, K.L., J.D. Hartgerink, J.J.J.M. Donners, and S.I. Stupp, *Self-assembly combining two bioactive peptide-amphiphile molecules into nanofibers by electrostatic attraction*. Journal of the American Chemical Society, 2003. **125**(24): p. 7146-7147.

33. Liu, H. and C. Tang, *Electrospinning of cellulose acetate in solvent mixture N, N-dimethylacetamide (DMAc)/acetone*. Polymer Journal, 2006. **39**(1): p. 65-72.

34. Huang, Z.-M., Y.-Z. Zhang, M. Kotaki, and S. Ramakrishna, *A review on polymer nanofibers by electrospinning and their applications in nanocomposites*. Composites science and technology, 2003. **63**(15): p. 2223-2253.

35. Correia, T.R., B.P. Antunes, P.H. Castilho, J.C. Nunes, M.T. Pessoa de Amorim, I.C. Escobar, J.A. Queiroz, I.J. Correia, and A.M. Morão, *A bi-layer electrospun nanofiber membrane for plasmid DNA recovery from fermentation broths*. Separation and Purification Technology, 2013. **112**: p. 20-25.

36. Zussman, E., A. Theron, and A. Yarin, *Formation of nanofiber crossbars in electrospinning*. Applied physics letters, 2003. **82**(6): p. 973-975.

37. He, J.-H., Y.-Q. Wan, and J.-Y. Yu, *Scaling law in electrospinning: relationship between electric current and solution flow rate*. Polymer, 2005. **46**(8): p. 2799-2801.

38. Bhardwaj, N. and S.C. Kundu, *Electrospinning: a fascinating fiber fabrication technique*. Biotechnology Advances, 2010. **28**(3): p. 325-347.

39. Nandakumar, A., H. Fernandes, J. de Boer, L. Moroni, P. Habibovic, C.A. van Blitterswijk, *Fabrication of bioactive composite scaffolds by electrospinning for bone regeneration*. Macromolecular bioscience, 2010. **10**(11): p. 1365-1373.

40. Yang, Y., T. Xia, F. Chen, W. Wei, C. Liu, S. He, and X. Li, *Electrospun fibers with plasmid bFGF polyplex loadings promote skin wound healing in diabetic rats*. Molecular Pharmaceutics, 2011. **9**(1): p. 48-58.

41. Kim, Y.J., M. Ebara, and T. Aoyagi, *A Smart Nanofiber Web That Captures and Releases Cells*. Angewandte Chemie, 2012. **124**(42): p. 10689-10693.

42. Scampicchio, M., A. Bulbarello, A. Arecchi, M.S. Cosio, S. Benedetti, and S. Mannino, *Electrospun Nonwoven Nanofibrous Membranes for Sensors and Biosensors*. Electroanalysis, 2012. **24**(4): p. 719-725.

43. Wu, H., L. Hu, M.W. Rowell, D. Kong, J.J. Cha, J.R. McDonough, J. Zhu, Y. Yang, M.D. McGehee, and Y. Cui, *Electrospun metal nanofiber webs as high-performance transparent electrode*. Nano letters, 2010. **10**(10): p. 4242-4248.

44. Fong, H. and D.H. Reneker, *Electrospinning and the formation of nanofibers*. Vol. 6. 2001: chapter.

45. Taylor, G., *Electrically driven jets*. Proceedings of the Royal Society of London. A. Mathematical and Physical Sciences, 1969. **313**(1515): p. 453-475.

46. Doshi, J. and D.H. Reneker, *Electrospinning process and applications of electrospun fibers*. Journal of electrostatics, 1995. **35**(2): p. 151-160.

47. Fong, H., I. Chun, and D. Reneker, *Beaded nanofibers formed during electrospinning*. Polymer, 1999. **40**(16): p. 4585-4592.

48. Demir, M.M., I. Yilgor, E. Yilgor, and B. Erman, *Electrospinning of polyurethane fibers*. Polymer, 2002. **43**(11): p. 3303-3309.

49. Torres-Giner, S., M. Ocio, and J. Lagaron, *Development of Active Antimicrobial Fiber-Based Chitosan Polysaccharide Nanostructures using Electrospinning*. Engineering in Life Sciences, 2008. **8**(3): p. 303-314.

50. Ramakrishna, S., *An introduction to electrospinning and nanofibers*. 2005: World Scientific Publishing Company.

51. Koski, A., K. Yim, and S. Shivkumar, *Effect of molecular weight on fibrous PVA produced by electrospinning*. Materials Letters, 2004. **58**(3): p. 493-497.

52. Li, D. and Y. Xia, *Electrospinning of nanofibers: reinventing the wheel?* Advanced materials, 2004. **16**(14): p. 1151-1170.

53. Ramakrishna, S., K. Fujihara, W.-E. Teo, T. Yong, Z. Ma, and R. Ramaseshan, *Electrospun nanofibers: solving global issues*. Materials Today, 2006. **9**(3): p. 40-50.

54. Liang, D., B.S. Hsiao, and B. Chu, *Functional electrospun nanofibrous scaffolds for biomedical applications*. Advanced drug delivery reviews, 2007. **59**(14): p. 1392-1412.

55. He, W., S.W. Horn, and M.D. Hussain, *Improved bioavailability of orally administered mifepristone from PLGA nanoparticles*. International journal of pharmaceutics, 2007. **334**(1): p. 173-178.

56. Li, W.-J., C.T. Laurencin, E.J. Caterson, R.S. Tuan, F.K. Ko, *Electrospun nanofibrous structure: a novel scaffold for tissue engineering*. Journal of biomedical materials research, 2002. **60**(4): p. 613-621.

57. Friess, W., *Collagen-biomaterial for drug delivery.* European Journal of Pharmaceutics and Biopharmaceutics, 1998. **45**(2): p. 113-136.

58. Thorvaldsson, A., H. Stenhamre, P. Gatenholm, and P. Walkenström, *Electrospinning of highly porous scaffolds for cartilage regeneration.* Biomacromolecules, 2008. **9**(3): p. 1044-1049.

59. Venugopal, J. and S. Ramakrishna, *Biocompatible nanofiber matrices for the engineering of a dermal substitute for skin regeneration.* Tissue engineering, 2005. **11**(5-6): p. 847-854.

60. Zhang, Y., J.R. Venugopal, A. El-Turki, S. Ramakrishna, B. Su, and C.T. Lim, *Electrospun biomimetic nanocomposite nanofibers of hydroxyapatite/chitosan for bone tissue engineering.* Biomaterials, 2008. **29**(32): p. 4314-4322.

61. Xu, C.Y., R. Inai, M. Kotaki, and S. Ramakrishna, *Aligned biodegradable nanofibrous structure: a potential scaffold for blood vessel engineering.* Biomaterials, 2004. **25**(5): p. 877-886.

62. Zong, X., H. Bien, C.-Y. Chung, L. Yin, D. Fang, B.S. Hsiao, B. Chu, and E. Entcheva, *Electrospun fine-textured scaffolds for heart tissue constructs.* Biomaterials, 2005. **26**(26): p. 5330-5338.

63. Yang, F., R. Murugan, S. Ramakrishna, X. Wang, Y.-X. Ma, and S. Wang, *Fabrication of nano-structured porous PLLA scaffold intended for nerve tissue engineering.* Biomaterials, 2004. **25**(10): p. 1891-1900.

64. Bosworth, L.A. and S. Downes, *Physicochemical characterisation of degrading polycaprolactone scaffolds.* Polymer Degradation and Stability, 2010. **95**(12): p. 2269-2276.

65. Qin, X. and D. Wu, *Effect of different solvents on poly (caprolactone)(PCL) electrospun nonwoven membranes.* Journal of thermal analysis and calorimetry, 2012. **107**(3): p. 1007-1013.

66. Lu, J.-W., Y.-L. Zhu, Z.-X. Guo, P. Hu, and J. Yu, *Electrospinning of sodium alginate with poly (ethylene oxide).* Polymer, 2006. **47**(23): p. 8026-8031.

67. Wang, R., Y. Liu, B. Li, B.S. Hsiao, and B. Chu, *Electrospun nanofibrous membranes for high flux microfiltration.* Journal of Membrane Science, 2012. **392**: p. 167-174.

68. Gopal, R., S. Kaur, Z. Ma, C. Chan, S. Ramakrishna, and T. Matsuura, *Electrospun nanofibrous filtration membrane.* Journal of Membrane Science, 2006. **281**(1): p. 581-586.

69. Subbiah, T., G.S. Bhat, R.W. Tock, S. Parameswaran, and S.S. Ramkumar, *Electrospinning of nanofibers.* Journal of Applied Polymer Science, 2005. **96**(2): p. 557-569.

70. Tsai, P.P., H. Schreuder-Gibson, and P. Gibson, *Different electrostatic methods for making electret filters.* Journal of Electrostatics, 2002. **54**(3): p. 333-341.

71. Liu, Y., R. Wang, H. Ma, B.S. Hsiao, and B. Chu, *High-flux microfiltration filters based on electrospun polyvinylalcohol nanofibrous membranes.* Polymer, 2012. **54**(2): 548-556.

72. Tang, Z., J. Wei, L. Yung, B. Ji, H. Ma, C. Qiu, K. Yoon, F. Wan, D. Fang, B.S. Hsiao, and B. Chu, *UV-cured poly (vinyl alcohol) ultrafiltration nanofibrous membrane based on electrospun nanofiber scaffolds.* Journal of Membrane Science, 2009. **328**(1): p. 1-5.

73. Tang, Z., C. Qiu, J.R. McCutcheon, K. Yoon, H. Ma, D. Fang, E. Lee, C. Kopp, B.S. Hsiao, and B. Chu, *Design and fabrication of electrospun polyethersulfone nanofibrous scaffold for high-flux nanofiltration membranes.* Journal of Polymer Science Part B: Polymer Physics, 2009. **47**(22): p. 2288-2300.

74. Gaspar, V.M., F. Sousa, J.A. Queiroz, and I.J. Correia, *Formulation of chitosan–TPP–pDNA nanocapsules for gene therapy applications.* Nanotechnology, 2011. **22**(1): p. 1-12.

75. Zargarian, S.S. and V. Haddadi-Asl, *A nanofibrous composite scaffold of PCL/hydroxyapatite-chitosan/PVA prepared by electrospinning.* Iranian Polymer Journal, 2010. **19**(6): p. 457-468.

76. Ma, G., D. Fang, Y. Liu, X. Zhu, and J. Nie, *Electrospun sodium alginate/poly (ethylene oxide) core–shell nanofibers scaffolds potential for tissue engineering applications.* Carbohydrate Polymers, 2012. **87**(1): p. 737-743.

77. Nie, H.-L. and L.-M. Zhu, *Adsorption of papain with Cibacron Blue F3GA carrying chitosan-coated nylon affinity membranes.* International journal of biological macromolecules, 2007. **40**(3): p. 261-267.

78. Bazargan, A.M., M. Keyanpour-rad, F.A. Hesari, and M. Esmaeilpour Ganji, *A study on the microfiltration behavior of self-supporting electrospun nanofibrous membrane in water using an optical particle counter.* Desalination, 2011. **265**(1): p. 148-152.

79. Sartori, C., D.S. Finch, and B. Ralph, *Determination of the cation content of alginate thin films by< i> FT</i> ir spectroscopy.* Polymer, 1997. **38**(1): p. 43-51.

80. Ojha, S.S., D.R. Stevens, T.J. Hoffman, K. Stano, R. Klossner, M.C. Scott, W. Krause, L.I. Clarke, and R.E. Gorga, *Fabrication and characterization of electrospun chitosan nanofibers formed via templating with polyethylene oxide.* Biomacromolecules, 2008. **9**(9): p. 2523-2529.

81. Yang, J., S.-B. Park, H.-G. Yoon, Y.-M. Huh, and S. Haam, *Preparation of poly ε-caprolactone nanoparticles containing magnetite for magnetic drug carrier.* International journal of pharmaceutics, 2006. **324**(2): p. 185-190.

82. Tang, C.Y., Y.-N. Kwon, and J.O. Leckie, *Probing the nano-and micro-scales of reverse osmosis membranes—A comprehensive characterization of physiochemical properties of uncoated and coated membranes by XPS, TEM, ATR-FTIR, and streaming potential measurements.* Journal of membrane science, 2007. **287**(1): p. 146-156.

83. Tang, C.Y., Y.-N. Kwon, and J.O. Leckie, *Effect of membrane chemistry and coating layer on physiochemical properties of thin film composite polyamide RO and NF membranes: I. FTIR and XPS characterization of polyamide and coating layer chemistry.* Desalination, 2009. **242**(1): p. 149-167.

84. Chang, I.-S., S.-O. Bag, and C.-H. Lee, *Effects of membrane fouling on solute rejection during membrane filtration of activated sludge.* Process Biochemistry, 2001. **36**(8): p. 855-860.

85. Theodossiou, I., I.J. Collins, J.M. Ward, O.R.T. Thomas, and P. Dunnill, *The processing of a plasmid-based gene from E. coli. Primary recovery by filtration.* Bioprocess Engineering, 1997. **16**(3): p. 175-183.

Chapter VI

Appendix

Polymer 54 (2013) 5–15

Contents lists available at SciVerse ScienceDirect

Polymer

journal homepage: www.elsevier.com/locate/polymer

Microencapsulated chitosan–dextran sulfate nanoparticles for controled delivery of bioactive molecules and cells in bone regeneration

J.F.A. Valente [1], V.M. Gaspar [1], B.P. Antunes, P. Countinho, I.J. Correia*

CICS-UBI – Centro de Investigação em Ciências da Saúde, Universidade da Beira Interior, Av. Infante D. Henrique, 6200-506 Covilhã, Portugal

ARTICLE INFO

Article history:
Received 1 October 2012
Accepted 15 October 2012
Available online 9 November 2012

Keywords:
Alginate microparticles
Chitosan–dextran sulfate nanoparticles
Protein and cell delivery

ABSTRACT

This research work aimed to synthesize and characterize a novel dual delivery system comprised of BSA-loaded in chitosan–dextran sulfate nanoparticulated carriers and mesenchymal stem cells that are encapsulated into alginate microparticles. The physicochemical and biological characteristics of this novel system, such as, morphology, release, swelling, and cytotoxicity were thoroughly characterized. The results obtained from confocal microscopy demonstrate that chitosan–dextran sulfate nanoparticles and cells are fully encapsulated within alginate microparticles, and spatially dispersed in the microparticle matrix. Moreover, scanning electron microscopy images revealed that these micro-sized carriers possess a rough surface, an important parameter that also promoted proper cell migration and adhesion. Notably, the incorporation of BSA in this duplex nano-micro delivery system extended its release profile throughout time, in comparison with microparticles alone, whilst not eliciting any cell damage. Taken together, these findings suggest that this dual carrier is a versatile delivery system with potential for a spatiotemporally controlled release of bioactive molecules and cells.

1. Introduction

The regeneration of bone tissue is preemptively dependent on the establishment of a complex cascade of biological events synergically controlled by numerous bioactive molecules, such as growth factors (GFs) that are responsible for triggering the regenerative signaling cascades at injury sites [1]. These dynamic events further promote bone healing by recruiting progenitor and inflammatory cells that mediate healing processes [2]. In order to enhance its regeneration process several strategies have been assayed, such as scaffolds, micro and nanoparticles have been used for delivery and controlled release molecules [3–5]. Among these delivery systems, several are being currently designed to release cells and growth factors for regenerative medicine applications. Recently, Trouche and coworkers described the use of alginate microspheres and microcapsules for the delivery of mesenchymal stem cells (MSCs) for cell therapy of solid organs [6]. This study revealed that the inclusion of MSCs in alginate microspheres maintained cell viability and cellular function. Furthermore, poly(lactic-co-glycolic acid (PLGA) microspheres have also been described as delivery systems of dexamethasone with sustainable *in vivo* release kinetics that ultimately led to a moderate control of inflammation at a lesion site [7]. Despite the fact that these reports emphasize the versatility of microparticle-based platforms for drug and cell delivery they also underline the urging necessity of developing versatile delivery systems that can mimic, activate and promote regenerative events to a therapeutically relevant scale. Actually, the majority of the delivery systems such as those before mentioned are formulated to release only a single type of biomolecule, a major restriction, since the regeneration process is far from being efficiently promoted with this approach. These restrictive characteristics further demonstrate the need to deliver multiple signals such as GFs and other biomolecules that participate in the healing process and homeostasis [6,7]. Particularly, for the controlled release of GFs, microparticles are quite interesting candidates for delivery, mostly due to their intrinsic benefits such as the ability to provide a larger surface area and also to promote mass transfer of small molecules with precise kinetics from and to the surrounding fluids [8]. Among the polymeric systems currently employed, alginate renders itself as a valuable biomaterial [9–11].

This natural biocompatible polysaccharide contains 1,4-linked beta-D-mannuronic and alpha-L-guluronic acid residues and is able to form water-insoluble gels upon crosslinking with divalent cations (e.g., Ca^{2+}, Zn^{2+}) [12]. This gentle crosslinking behavior is one of the most important advantages of alginate microparticles and enables the establishment of mild conditions for cell or biomolecule encapsulation [13]. The encapsulation of living cells into hydrogel

* Corresponding author. Tel.: +351 275 329 002; fax: +351 275 329 099.
E-mail addresses: icorreia@fcsaude.ubi.pt, icorreia@ubi.pt (I.J. Correia).
[1] Co-first authors.

0032-3861/$ – see front matter © 2012 Elsevier Ltd. All rights reserved.
http://dx.doi.org/10.1016/j.polymer.2012.10.032

microparticles is advantageous since they produce and secrete the bioactive agents continuously to the surrounding medium [17,18]. The semi-permeable membrane of these carriers isolates cells from the host immune system preventing their recognition as a foreign material (e.g., antibodies and cytokines). This structure also plays an important role in the maintenance of cell viability since it also allows the exchange of nutrients, gases and waste products [14–16]. From this stand point the development of a strategy that gathers the advantages of cell therapy in combination with a time-controlled release of GFs might have a profound impact in bone regeneration treatments [19–21]. Taking this into consideration, the inclusion of nanoscale delivery systems within microparticulated carriers arises as a very promising approach to modulate the release profile of drugs [22]. Moreover, this conjugation may allow the release of several GFs from a single drug delivery system [23]. The use of nanoparticles enables the improvement of the serum solubility of the drugs, prolonging systemic circulation lifetime, releasing drugs in a spatio-temporal controlled mode, and concurrently delivering multiple therapeutic agents to the same cells for combined therapy [24,25]. Chitosan and dextran sulfate (CH–Dext) have been employed as materials for nanoparticle synthesis to encapsulate several biomolecules such as peptides [26], insulin [27], among others [28,29]. Chitosan is a non-toxic biodegradable natural polymer with low immunogenicity. This biopolymer has amine functional groups that endow it with a positive charge density in acidic aqueous media. These properties enable its spontaneous interaction with negatively charged macromolecules and polyanions resulting in the formation of nanosized particles. Therefore nanoparticle formulations comprised of chitosan can be synthesized by ionic crosslinking, complex coacervation, or polyelectrolyte complexation [29]. Dextran sulfate is a biodegradable and biocompatible polyanion with negatively charged sulfate groups, and can therefore form electrostatic interactions with the polymeric chitosan backbone, forming polyelectrolyte complexes [27]. The main advantage of these nanoparticles is not only their enhanced stability at different pHs, but also their increased mechanical strength compared with that of chitosan-sodium tripolyphosphate nanoparticles [28,30]. Therefore, the combination of chitosan and dextran sulfate as formulation materials, in an optimal charge ratio, may act synergistically to incorporate, protect, and release the therapeutic molecules [28].

Hence, herein we synthesized and characterized a novel delivery system that is engineered with alginate microencapsulation of CH–Dext–BSA nanoparticles and MSCs in order to simultaneously deliver protein mediators and cells in the same micro carrier for future biomedical applications in the field of regenerative medicine.

2. Materials and methods

2.1. Materials

Alginic acid sodium salt (sodium alginate) (Mw 120,000–190,000 Da), calcium chloride ($CaCl_2$), chitosan (Low molecular weight, Average Mw 120,000 Da) (75–85% deacetylation degree), fluorescein isothiocyanate isomer I (FITC), bovine serum albumin (BSA), Dulbecco's modified Eagle's medium – F12 (DMEM-F12), penicillin G, streptomycin, trypsin, ethylenediaminetetraacetic acid (EDTA) and phosphate-buffered saline (PBS) were all purchased from Sigma–Aldrich. Bicinchoninic acid (BCA) assay was supplied by Thermo Scientific and Dextran sulfate (500,000 Da) was purchased from Amresco. Human osteoblast cells were acquired from Cell Applications, Inc. Fetal bovine serum (FBS) was obtained from Biochrom AG (Berlin, Germany) and L-glutamine, 3-(4,5-dimethylthiazol-2-yl)-5-(3 carboxymethoxyphenyl) 2-(4-sulphofenyl)-2H-tetrazolium, inner salt (MTS) was supplied by Promega. The nuclear fluorescent probe Hoechst 33342® was purchased from Invitrogen (Carlsbad, USA).

2.2. Methods

2.2.1. Nanoparticle synthesis

For nanoparticle synthesis a procedure previously described in the literature was adopted [31]. Briefly, 0.1% wt of chitosan solution (pH = 3.0) was prepared in 0.2% acetic acid, and 0.1% of dextran sulfate solution in distilled water. Then the powder of bovine serum albumin (BSA) was dissolved in the dextran sulfate solution (pH = 7.35). After mixing, the solution of dextran sulfate with BSA and the chitosan solution were irradiated with UV radiation for 30 min (UV Lamp, $\lambda = 253.7$ nm, $P = 100$ μW/cm). Afterwards, the dextran solution with BSA was added to an eppendorf containing the chitosan solution under vigorous stirring in a volume ratio of 1:6, in a sterile environment, and dextran sulfate–chitosan NPs were formed instantaneously. The NPs were then recovered by centrifugation (17,000*g*, for 30 min), at room temperature.

2.2.2. Microparticle synthesis

The microparticles were produced by internal gelation according to a procedure previously described in the literature [32]. For micro-nanoparticle loaded carrier synthesis the nanoparticle pellet was added to a 3% (w/v) sodium alginate solution containing BSA (1% (w/v)). Afterwards, this solution was vortexed and sonicated, in order to obtain a homogeneous dispersion. Briefly, the alginate solution was loaded into a 10 mL plastic syringe attached with a needle and then the solution was extruded into a $CaCl_2$ (5% (w/v)) solution (gelation medium) under stirring, at room temperature. The solution feed rate was controlled through a syringe pump (KdScientific) [33]. Cell encapsulation in the alginate microparticles was performed also by ionic gelation. Following synthesis, the nano and cell-loaded microparticles were filtered with a 0.22 μm filter in order to remove the excess of gelation medium and washed thoroughly with distilled water. All the procedures were performed under sterile atmospheric conditions and with sterile materials.

2.2.3. Nano and microparticle morphology

The morphological appearance of nanoparticles, microparticles and nanoparticles encapsulated in microparticles was examined by scanning electron microscopy (SEM). Prior to SEM analysis, the samples were mounted on aluminum stubs using double-side adhesive tape and sputter coated with gold (Emitech K550 sputter coater, London, UK). Finally the images were acquired with a scanning electron microscope Hitachi S-2700 (Tokyo, Japan), with an acceleration voltage of 20 kV, using appropriate magnifications for particle visualization [34].

2.2.4. Physicochemical characterization of nano and microcarriers

Dynamic light scattering (DLS) was used to analyze nanoparticle size. To determine the diameter by DLS the nanoparticles were produced as previously mentioned in Section 2.2.1, and then incubated for 30 min at room temperature, and finally vortexed. Size measurements were then performed using a Zetasizer Nano ZS instrument (Malvern Instruments, Worcestershire, UK), in automatic mode and with a detection angle of 173°. The measurements were performed in triplicate. The reported particle size was obtained by cumulant analysis performed in the zetasizer software (version 6.34).

In the case of the microparticles, they were produced as previously mentioned in Section 2.2.2. Size measurements were executed in an LS Coulter 2000 laser diffraction particle analyzer, using the Fraunhofer approximation model (Beckman Coulter, Inc, California).

The determination of the electrokinetic potential of the colloidal dispersions was performed in a Zetasier Nano ZS. The experiments were performed in automatic mode at 25 °C, in triplicate.

2.2.5. Study of water uptake ability (swelling)

The swelling properties of microparticles were characterized in Tris–HCL buffer (pH 7.4). These carriers were placed in an eppendorf with 1 mL of swelling solution and allowed to swell at 37 °C. At predetermined intervals, the swollen microparticles were weighed. The wet weight of the swollen scaffolds was determined by blotting them with filter paper to absorb the excess of buffer. Then, they were weighed and re-immersed into the swelling medium [35]. The swelling ratio was evaluated by using Eq. (1):

$$\text{Swelling ratio}\left(\%\right) = \frac{W_t - W_0}{W_0} \times 100 \quad (1)$$

where W_t is the final weight and W_0 is the initial weight of microparticles.

2.2.6. Protein studies

2.2.6.1. Protein loading efficiency. The loading efficiency of micro and nanocarriers was determined using BCA protein assay colorimetric method for protein detection and quantitation. This method combines the reduction of Cu^{+2} to Cu^{+1} by protein with the highly sensitive and selective colorimetric detection of the cuprous cation (Cu^{+1}). The purple-colored reaction product of this assay is formed by the chelation of two molecules of BCA with one cuprous ion [36]. In the nanoparticles case, BSA loading efficiency was determined after nanoparticle recovery by centrifugation (17,000*g*, 30 min, 4 °C) from the aqueous preparation medium that contains the non-associated protein. In the case of microparticles, the loading efficiency was calculated using the gelation medium after microparticle formation and stabilization. The BCA measurements were performed using a microplate reader (Sanofi, Diagnostics Pauster) at 562 nm. A calibration curve with known concentrations of BSA was predetermined, and subsequently, the loading capacity was calculated as follows [37]:

$$\text{Loading efficiency}(\%) = \frac{\text{Actual drug loading}}{\text{Theoretical drug loading}} \times 100 \quad (2)$$

2.2.6.2. In vitro release of BSA. The *in vitro* BSA release from microparticles and microencapsulated nanoparticles was tested in a Tris–HCL buffer solution (pH 7.4). BSA was used as model for water-soluble globular proteins since growth factors also possess these characteristics. To do so, samples were placed in eppendorfs with 500 μL of Tris–HCL buffer and then placed on a shaker bath at 37 °C. At predetermined time intervals, 20 μL of the supernatant was recovered and 20 μL of fresh Tris–HCL were added. The BSA concentration measurements were performed using a BCA protein assay kit in triplicate [37]. The cumulative amount of released protein from the samples was defined by the following equation [38]:

$$\text{Release}\left(\%\right) = \frac{M_t}{M_\infty} \times 100 \quad (3)$$

where M_t is the amount of released protein from the microparticles at time t and M_∞ is the amount of protein pre-loaded in microparticles.

Additionally the release of BSA from de micro-nanocarriers was characterized with the mathematical model proposed by Higuchi [3] that is denoted by the following equation:

$$f_t = k_H \times t^{1/2} \quad (4)$$

where f_t is the fraction of protein released at time t, k_H is the Higuchi release constant.

This model is particularly suitable to describe release of protein as diffusion controlled process based on Fick's law.

The semi-empirical model developed by Korsmeyer–Peppas was also used to illustrate protein release for swellable where M_t/M_∞ is the fractional amount of BSA released, k is a constant that is associated polymeric devices:

$$\frac{M_t}{M_\infty} = k \times t^n \quad (5)$$

with both geometrical and structural characteristics of the delivery system and n is the diffusional exponent that provides insights into the mechanism underlying the release of BSA [4]. To obtain data for the different theoretical models abovementioned, a Matlab routine was designed to simulate a correlation with experimental data by fitting and linear regression calculations (Matlab R2009a, MathWorks Inc., MA, USA).

2.2.7. Biological assays

2.2.7.1. Cell proliferation in the presence of microparticles. Human osteoblast cells were seeded in T-flasks of 25 cm^2 with 6 mL of DMEM-F12 supplemented with FBS (10%, v/v), penicillin G (100 units/cm^3), streptomycin (100 g/cm^3) and amphotericin B (0.25 g/cm^3). When the confluence was achieved, cells were sub-cultivated by a 3–5 min incubation in 0.18% trypsin (1:250) and 5 mM EDTA. Hereafter, the cells were centrifuged, resuspended in culture medium and then seeded in T-flasks of 75 cm^2 and kept in culture at 37 °C, in a 5% CO_2 humidified atmosphere. To evaluate cell behavior in the presence of the scaffolds, they were seeded with materials in 96-well plates, at a density of 1.5×10^4 cells per well. Previously to cell seeding, plates and materials were sterilized by UV irradiation for 30 min [39,40]. Cell growth was monitored using an Olympus CX41 inverted light microscope (Tokyo, Japan) equipped with an Olympus SP-500 UZ digital camera.

2.2.7.2. Characterization of the cytotoxic profile of the carriers. The cytotoxic profiles of the microcarriers were characterized by seeding the human osteoblasts in the presence of the microcarriers with/without encapsulated nanoparticles, in 96-well plates. After an incubation period of 24, 48 and 72 h, the mitochondrial redox activity of the viable cells was assessed through the reduction of MTS into a water-soluble formazan product. First, the medium of each well was removed and replaced with a mixture of fresh culture medium and the MTS/PMS reagent solution. Then cells were incubated for 4 h at 37 °C, under a 5% CO_2 humidified atmosphere. Following incubation, the absorbance of each well was measured at 492 nm using a microplate reader (Sanofi, Diagnostics Pauster). A negative control (K^-) was done using wells containing cells in the culture medium without materials. EtOH (96%) was added to wells that contained cells, to be used as a positive control (K^+) [39–41].

2.2.8. Microencapsulation of MSCs

MSCs from Wistar rats were isolated as previously described in the literature [42]. Then were seeded in T-flasks with DMEM-F12 supplemented with FBS (10%), penicillin G (100 units/cm^3), streptomycin (100 μg/cm^3) and amphotericin B (0.25 μg/cm^3) and kept in culture at 37 °C with a 5% CO_2 humidified atmosphere. Upon confluence these cells were sub-cultivated using in trypsin-based detaching (0.18%) and 5 mM EDTA. The cells were then centrifuged, counted and suspended in 3% (w/v) sodium alginate to a final ratio of 1×10^7 cells/mL. The sodium alginate solution was

previously dissolved in milli-Q water with nanoparticles. This solution was afterwards loaded into a syringe and dropped through a 21 gauge needle into a sterilized $CaCl_2$ (5% (w/v)). The obtained microcarriers were recovered by filtration using a 0.22 μm filter paper and then washed with DMEM-F12 [43,44]. Finally, to characterize cell release from the carriers the microparticles were placed in a 96-well plate. Wells containing cells in the culture medium without materials were used as negative controls (K^-). Ethanol 96% was added to wells containing cells, and they were used as positive controls (K^+). The controls were performed with the same cell number as that used for cell encapsulation in the microparticle carriers.

2.2.9. Confocal laser scanning microscopy (CLSM)

2.2.9.1. Protein labeling. Protein labeling was performed with the FITC fluorescent probe by a protocol previously described with minor modifications [45]. Succinctly, BSA was dissolved in 0.1 M carbonate buffer (pH 9.0) at a concentration of 2 mg/mL. Subsequently, FITC (0.38 mol) was added to the BSA solution and the reaction proceeded for 4 h, in the dark, at room temperature (approximately at 23 °C). The resulting BSA-FITC was then dialyzed for 4 days, at 4 °C, with a Spectra/Por®dialysis membrane (MWC 3500 kDa), against 5 L of distilled water.

2.2.9.2. Cell encapsulation inside microparticles. Analysis of cell encapsulation in alginate microcarriers by fluorescence microscopy was performed by encapsulating cells in order to further provide a proof of concept. Briefly, cells were stained with Hoechst 33342® nuclear probe (10 μM) at room temperature for 15 min. The cells were then centrifuged at 250*g*, for 5 min, and washed twice with PBS to remove the excess of fluorochrome. Labeled cells were subsequently encapsulated in alginate microparticles following the above mentioned procedure.

2.2.9.3. Image acquisition. Prior to image acquisition microencapsulated nanoparticles loaded with BSA-FITC or cell-loaded microparticles were placed on glass bottom μ-dish 35 mm (Ibidi GmbH, Germany). Image acquisition was performed in a Zeiss LSM 710 confocal microscope equipped with a 10x/0.5 dry Fluar objective (Carl Zeiss SMT Inc., USA). All the images were acquired with minimal pinhole aperture and electronic gain to avoid image artifacts. 3D images of microcarriers were obtained after the acquisition of a series of z-stacks with a slice size of 1 μm. Reconstruction of z-stack images into 3D was performed in Zeiss LSM 710 software.

2.2.10. Statistical analysis

The obtained results were expressed as the mean ± the standard error. The one-way analysis of variance (one-way ANOVA) was used to calculate the statistical significance with Dunnets post hoc test ($^*p < 0.001$) [40].

3. Results

3.1. Physicochemical analysis

The morphological characteristics of the developed dual delivery system herein produced were analyzed by SEM. A thorough analysis of Fig. 1 reveals that the surface of the microparticles has some degree of roughness. It is also noticeable that the microparticles contain in their matrix CH–Dext–BSA nanoparticles (Fig. 1B, white arrows). In addition to the morphological features of the synthesized delivery system the size of the different components, namely micro and nanoparticles, was also determined since it plays an important role in delivery of the loaded-bioactive molecules and also in cell release and proliferation [46]. As the

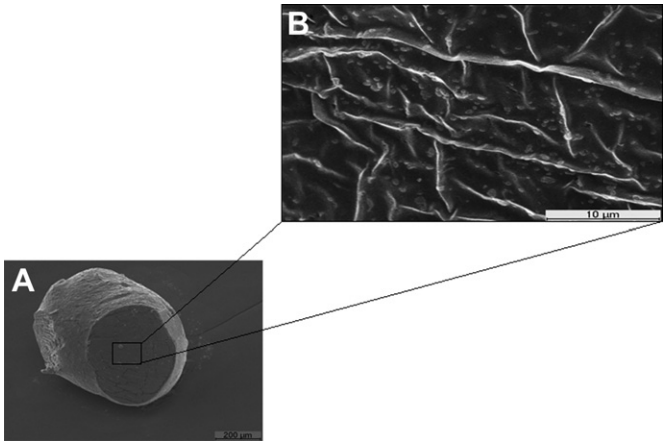

Fig. 1. SEM images of a vertical-section of a microparticle (A); micro-CH–Dext–BSA nanoparticle (B). White arrows indicate nanoparticles.

results in Table 1 demonstrate, CH–Dext–BSA nanoparticles possess sizes in the nanoscale range as determined by SEM and DLS analysis, and also positive zeta potential (+54.7 ± 2.6 mV) above that required for colloidal stability. The final pH of the nanoparticle solution was also determined and an acidic value was obtained (pH = 3.65). This is an important parameter since it influences the protonation of the primary amine residues of the chitosan polymer backbone (pKa = 6.5) and subsequently the overall particle surface charge. Regarding alginate microparticles loaded with the nanocarriers, these show a slightly increased size in light scattering analysis in comparison with SEM, a fact that may be correlated with the dispersion of microparticles in solution.

3.2. Characterization of the water uptake profile of the delivery system

The swelling profile of microparticles and the microencapsulated nanoparticles produced is shown in Fig. 2. Swelling ratio analysis reveals that alginate microcarriers and also CH–Dext–BSA microencapsulated nanocarriers absorb water which is indicative of their hydrophilic character. However, our findings also demonstrate the swelling ratio of microparticles alone is higher when compared with nano-loaded microparticles.

3.3. Release profile of BSA from the microencapsulated CH–Dext nanoparticles

The release profile of the microcarriers was characterized and represented in Fig. 3. In Fig. 3A and B a theoretical scheme of the microencapsulated nanoparticles is presented. Regarding BSA release from the different carriers it is important to emphasize that alginate microparticles alone release the model protein with a burst release profile, whilst, micro-CH–Dext–BSA show a retarded burst release throughout the same initial time frame (Fig. 3). Additionally, Table 2 presents the results obtained with mathematical simulation of BSA release from carriers. These results show a strong correlation

Table 1
Physicochemical characterization of particle size. Values represent the mean ± s.d. ($n = 3$).

Sample	Average size (nm)	
	SEM	DynamicLight scattering
CH–BSA–Dext nanoparticles	200–550	429.3 ± 58.3
Alginate–CH–Dext–BSA	500–750	1371 ± 115

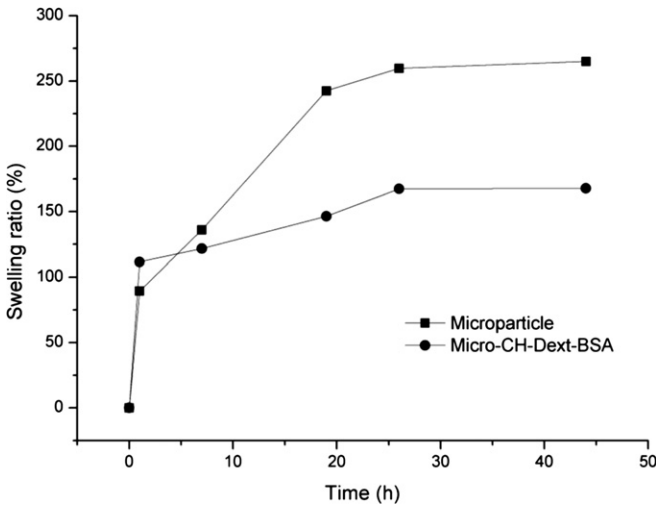

Fig. 2. Swelling profiles of microparticles and microencapsulated nanoparticles; alginate microparticles loaded with BSA; microencapsulated CH–Dext–BSA nanoparticles.

with the diffusion-based models for both systems (i.e., squared correlation coefficients above 95%). Whereas, regarding the swelling-dependent model only protein release from alginate microcarriers shows a significant correlation coefficient with the theoretical data.

3.4. CLSM of microencapsulated CH–Dext–BSA nanoparticles

In order to analyze the spatial distribution of CH–Dext–BSA nanoparticles within the alginate microcarriers, BSA was fluorescently labeled with FITC and the *x-y-z* localization of nanoparticles was investigated through 3D confocal microscopy. As illustrated in Fig. 4 the nanoparticles bearing BSA and are randomly distributed within its 3D volume (Fig. 4D).

Table 2
Characterization of the BSA release from micro and nano-microcarriers based on mathematical modeling.

Sample	R^2	a	b	k	n
Higuchi model					
Alginate microcarriers	0.9594	1.759	4.190	1.733 ($h^{1/2}$)	
Alginate–CH–Dext–BSA	0.9547	1.231	1.1862	1.240 ($h^{1/2}$)	
Korsmeyer–Peppas Model					
Alginate microcarriers	0.945	1.473	5.762	1.310 (h^{-n})	0.508
Alginate–CH–Dext–BSA	0.895	1.029	6.456	0.298 (h^{-n})	0.726

R^2 – the squared correlation coefficient, a – the slope of the linear regression, and b – the linear coefficient.

3.5. Characterization of the cytotoxic profile of the carriers

In vitro studies were performed in order to characterize the cytocompatibility of the microparticles and microencapsulated CH–Dext–BSA nanoparticles. Osteoblast cell adhesion and proliferation was characterized through contrast microscopy (Fig. 5) and finally SEM analysis was performed (Fig. 6) in order to simulate the cellular microenvironment of bone tissue. Both images show that cells adhered and proliferated in contact with the microcarriers as well as in the negative control (Fig. 6). To characterize the physiological response of human osteoblasts in the presence of the microcarriers an MTS assay was performed and the results showed that the cells in contact with the materials had higher viability than that of the positive control. Although cells show slightly higher

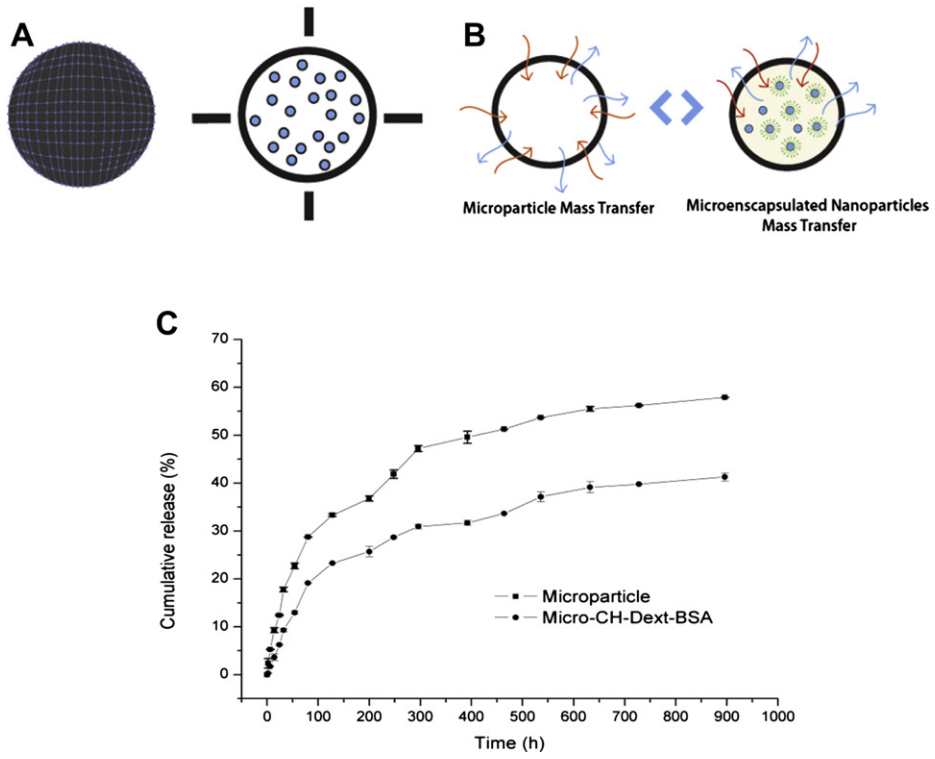

Fig. 3. Design of the synthesized systems and experimental data of its release profile. (A) Theoretical schematics of the micro-nano delivery system; (B) theoretical schematics of transport mechanisms promoted by the devised carrier system; and (C) cumulative release profile of BSA from encapsulated in micro and nanoparticles loaded into microparticles. Each data point represents the mean ± s.e. ($n = 3$).

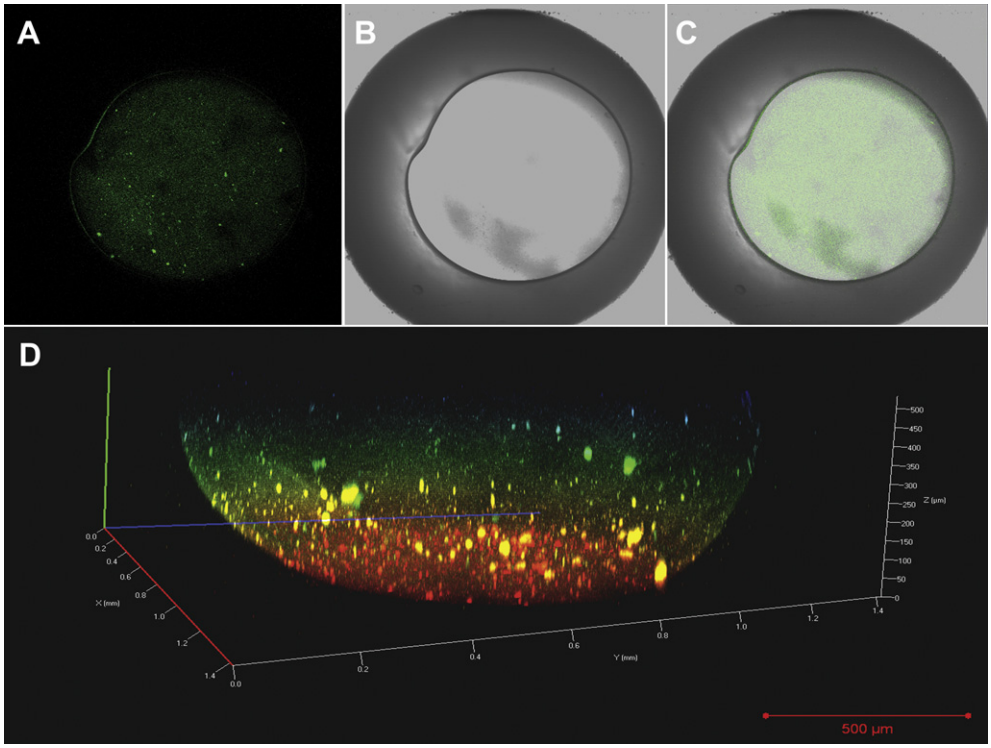

Fig. 4. CLSM micrographs of microencapsulated CH–Dext–BSA nanoparticles. (A) Green channel: FITC labeled BSA within CH–Dext nanoparticles microencapsulated in alginate particles. (B) Differential interference contrast of DIC imaging of an axially-sliced alginate microparticle. (C) Merged image of image A and B; (D) RGB color coded 3D depth coordinate reconstruction of microencapsulated CH–Dext–BSA nanoparticles. Each color represents nanoparticles at different depths within the microparticle (*z*-axis). (For interpretation of the references to colour in this figure legend, the reader is referred to the web version of this article.)

viability in case of microcarriers than in case of microencapsulated nanoparticles, this difference is not statistically significant ($p < 0.001$) (Fig. 7).

3.6. Cell encapsulation and release from microparticles

Apart from the release of BSA or bioactive mediators of interest, the combination with the release of progenitor cells that are able to promote and further improve bone regeneration processes is a highly attractive and effective approach. Therefore, in order to extend the versatility of the synthesized micro-nanoparticulated system MCSs were incorporated in the alginate polymer mesh. As the results presented in Fig. 8 demonstrate that the cell microcarriers possess spherical morphology and are capable of encapsulating a significant number or cells. Furthermore, as shown by the performed time-course experiments the microparticle formulation starts to release the encapsulated cells after 11 days in culture (Figs. 8 and 9).

In order to further characterize cell encapsulation CLSM images of labeled cells incorporated in the microparticle mesh were also acquired. The inclusion of fluorescent probes shows that cells are spatially distributed inside the micro carrier.

4. Discussion

The current challenges associated with the development of drug and cell based therapies for regenerative medicine demand the synthesis of versatile delivery systems that are capable of simultaneously releasing a considerable number of therapeutic mediators that intervene in the regeneration process. To promote this delivery and release in a spatiotemporally controlled manner, several approaches have been developed so far, however too few address the issue of encapsulating multiple bioactive molecules and cells at the same time. Therefore, we devised a novel delivery system that combines the unique features of either nanoscaled or microscaled systems into a single formulation in order to modulate the release of bioactive molecules from nanoparticles. Moreover, in this microparticulated system it is also possible to encapsulate bone progenitor cells that in combination with different GFs further improve the regeneration process [7,11]. These biomimetic and biodegradable microcarriers improve the protection and transport of the cells and GFs into the target injured tissue, promoting their integration and consequently tissue repair or regeneration [14].

The synthesized system is comprised of chitosan–dextran nanoparticles and calcium–alginate microparticles, which have been previously described as being able to be formulated under mild conditions, which assure the stability of the proteins loaded into micro or nanoparticles [31,47]. Nanoparticle formation involves an electrostatic interaction between the positively charged chitosan polymeric structure and the negatively charged dextran sulfate backbone [26]. Whereas, microparticles were synthesized by a gentle gelling/crosslinking process that occur when sodium alginate is drop-wise added to a calcium solution [47]. Due to the alginate polymer geometry, it possesses several exchange points between Na^+ and Ca^{2+} on its surface, which makes the crosslinking process self-driven. In turn, this increase of calcium content in the microcarriers structure has been described as a stimulant for osteoblast proliferation which is a valuable parameter for the biomedical application herein desired [48–50]. The surface of this microparticulated delivery system is an important parameter that needs to be underlined, since surface topology promotes proper cell adhesion and growth [51]. In fact cell–particle contacts are initially promoted due to the establishment of adhesion forces that are modeled by topological characteristics of the surface of the delivery

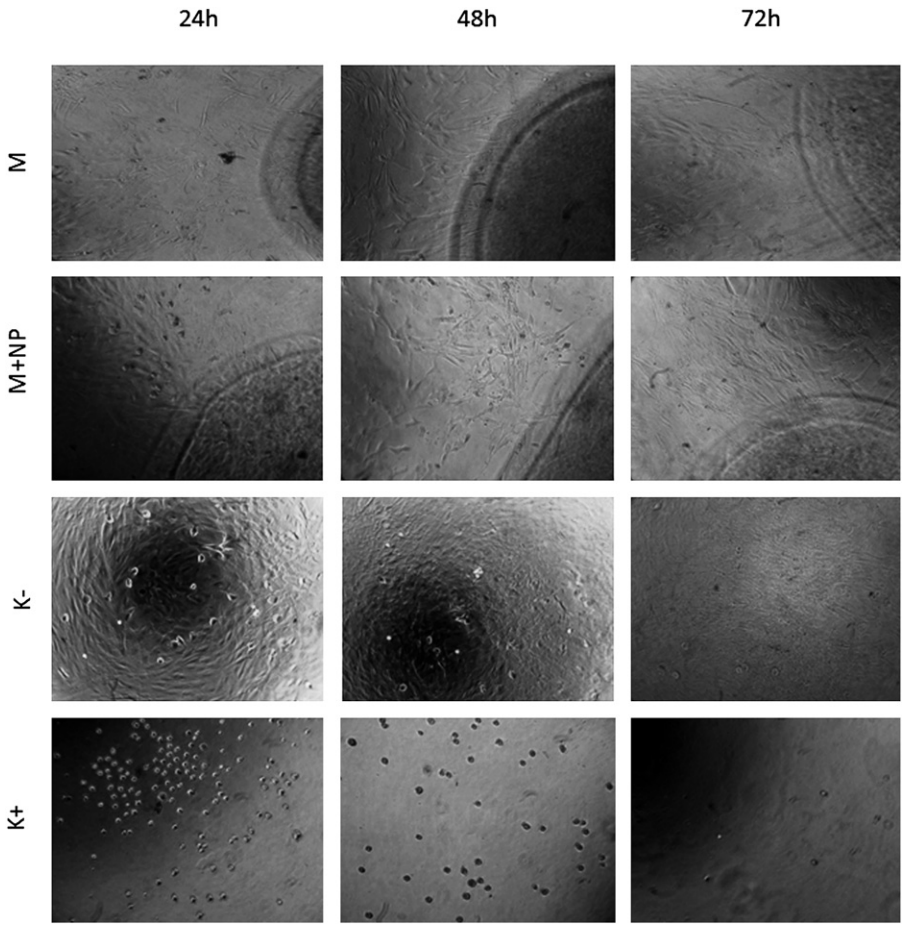

Fig. 5. Micrographs of human osteoblast cells after being seeded in the presence of the microparticle and micro-CH–Dext–BSA (*) during 24, 48 and 72 h; negative control (K^-); positive control (K^+). Magnification 100×.

system [52]. Taking this into account, several groups have focused their research on the effect of the materials surface on cellular response and development, including molecular composition and morphology [53,54]. Among these properties, and for the case of bone-contacting materials, rough surfaces have been shown to promote osteo integration, under *in vivo* conditions, suggesting that osteoblast adhesion and subsequent activity might be promoted [55]. Apart from surface topology particle size and surface charge also largely influence the characteristics of a protein delivery system. Regarding the physicochemical characterization of the CH–Dext–BSA nanoparticles our findings showed that these particles have positive zeta potential with values above those required for colloidal stability. This is a critical parameter for nanoparticle formulations, since particle aggregation may take place when the electrical double layer of particles in solution is too weak to promote particle repulsion [56]. Regarding nanoparticle size these present values within the nanometer scale range as determined by SEM and DLS analysis. It is important to point out however that a small discrepancy in the values obtained by both techniques was observed, namely for SEM in which particle size presented lower range. These results are in accordance with several reports and are correlated with the fact that dynamic light scattering analysis is performed with dispersed nanoparticles in solution, contrariwise to dry samples used for SEM [57,58]. Moreover, the results obtained

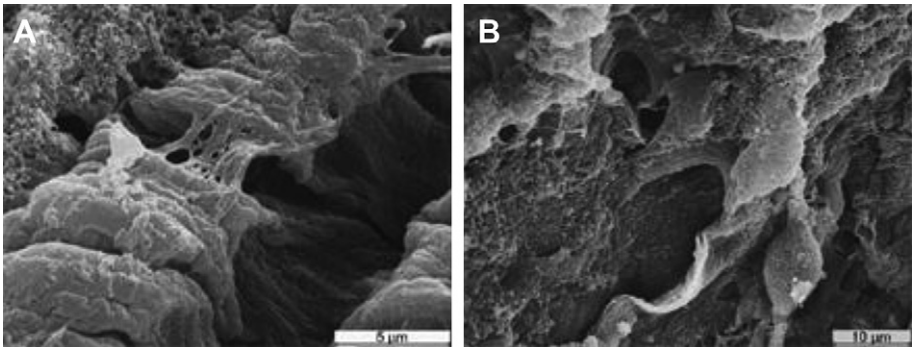

Fig. 6. SEM images of cells adhered on the surface of the microparticle (6000×) (A) And on the surface of the micro-CH–Dext–BSA (2000×) (B).

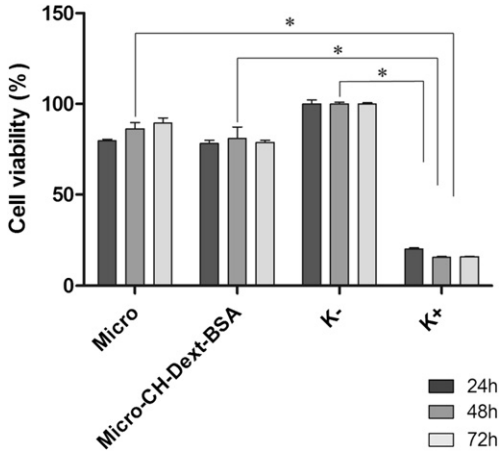

Fig. 7. Evaluation of the cellular activity after 24 h, 48 h and 72 h. Positive control (K^+); negative control (K^-). Each result is the mean ± s.d of at least three independent experiments ($n = 3$). Statistical analysis was performed using one-way ANOVA with Dunnet's post hoc test (*$p < 0.001$).

for the size analysis of alginate microparticles also demonstrate this difference (Table 1).

In addition to physicochemical characteristics, the swelling behavior of the microcarriers loaded with nanoparticles was also investigated. Alginate, the major component of these microcarriers, has a hydrophilic character that is crucial for the controlled release of drugs or proteins from the bead system [59]. This swelling behavior depends on the materials ability to absorb water (free or bulk water) in order to fill the void regions of the polymer network. Microparticles possess a remarkable swelling profile since water uptake takes place until an equilibrium state is attained, due to the osmotic flow that promotes a relaxation of the polymeric network [60]. Interestingly our results showed that alginate microparticles exhibit higher swelling than alginate microencapsulated CH–Dext–BSA nanoparticles. This finding might be a consequence of attractive electrostatic forces that are established between the positively charged CH–Dext–BSA nanoparticles (positive zeta potential) and alginate. Indeed, in the presence of Tris–HCL at pH 7.4, the carboxylic groups of alginate yield negatively charged COO^- groups. Therefore the existence of these electrostatic forces within the microparticle mesh promote a retraction of the alginate polymer chains, hence restraining water influx and consequently originating less swelling and subsequently lowering BSA dissolution to the surrounding medium [61]. On the other hand, the swelling of calcium–alginate microparticles is not hindered by internal forces and is related with the partial disentanglement of the microcarrier mesh which endows the particles with a higher water intake capacity due to the exchange of calcium ions with the solute [62]. This swelling behavior generates an increase in microparticle porosity, contributing for a higher diffusion coefficient of BSA from the alginate microparticles only (Fig. 2) [63].

Controlling the release of proteins from a delivery system with programmed kinetics and in a spatiotemporal mode is another critical parameter for the establishment of accurate and accelerated regeneration in a given tissue. The performed cumulative release studies presented in Fig. 3C highlight that the differences in the BSA release profile in both delivery systems are evident. Such findings illustrate that the production and subsequent microencapsulation of CH–Dext–BSA nanoparticles largely influences the delivery rate of the protein of interest. Actually, BSA is released with sustainable kinetics when encapsulated within nanoparticles and subsequently microparticles, however, to a lower plateau (Fig. 3C). The latter may be correlated with both the net negative charge of BSA, at pH 7.4 [64], that is attracted by the positive spatial charge density of CH–Dext nanoparticles. In comparison with alginate microparticles alone, the micro-nanocarriers are able to release lower protein doses in an extended time frame. Indeed, at 128 h the micro-nano system has released 69.8% less BSA than its microparticulated counterpart, demonstrating that the inclusion of a model protein in delivery systems, with distinct physicochemical characteristics might be an invaluable approach to manipulate the release profile of therapeutic mediators, such as GFs. Moreover, the spatiotemporal protein dose released in the micro-nanoparticulated system is suitable for the establishment of regeneration events if for instance

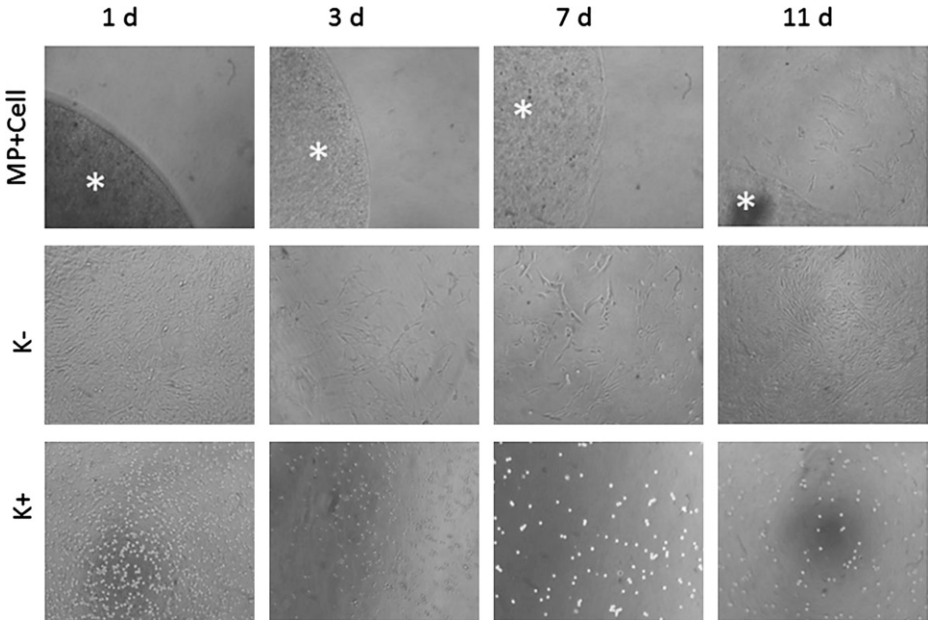

Fig. 8. Micrographs of microencapsulated MSCs during 11 days. *(Microparticle loaded with cells – MP + Cell); negative control (K–); positive control (K^+). Original magnification 100×.

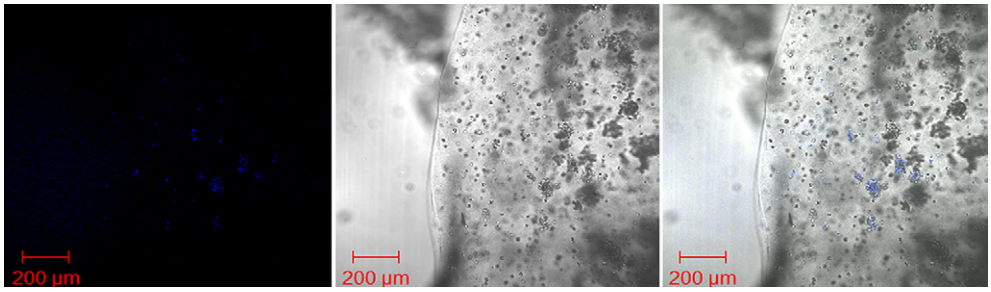

Fig. 9. CLSM images of cell-loaded alginate microparticles. (A) Blue channel: Hoechst 33342® labeled cells. (B) DIC image of alginate microparticles. (C) Merged image of figure A and B. Black arrow indicates cell encapsulation within the microparticle matrix. (For interpretation of the references to colour in this figure legend, the reader is referred to the web version of this article.)

GFs are being delivered. It is also important to emphasize that a significant retardation of the burst release of BSA was observed for the developed microencapsulated CH–Dext–BSA nanoparticles, a relevant finding, since the initial discharge of proteins or drugs with fast kinetics, would increase their body clearance and decrease their effective lifetime [65]. This characteristic is a key parameter in the delivery of GFs for regeneration, since these possess an intrinsic predisposition to be rapidly degraded at the lesion site [3]. Given the latter, these results assume further importance from a pharmacological point of view, since a sustained discharge over time influences the pharmacokinetic/pharmacodynamic profile of bioactive molecules, and consequently their stability and therapeutic concentration [3]. Recently Zuo and coworkers, 2012, reported the development of a strategy to attenuate the intrinsic burst release of BSA from alginate microparticles and increase its residence time by using layer-by-layer deposition of chitosan and dextran on the surface of the microcarriers [71]. However, apart from the fact that burst release is slightly attenuated this study still raises the need for the development of a delivery system capable of enabling the release of several bioactive mediators simultaneously, in order to mimic the complexity of signals involved in tissue regeneration [6,7]. These innovative micro-nanocarriers open up the possibility to encapsulate several GFs in CH–Dext nanoparticles and with the additional flexibility of grafting possible modifications, i.e., layer-by-layer or plasma modification if the modification of the microparticle surface is desired. Moreover, it is important to underline that an ideal delivery carrier of either one or several soluble mediators needs to assure their supply at the injury site for at least three weeks, in order to promote the establishment of signaling cascades that trigger regenerative processes [66,67]. Therefore, the extended release profile attained ($\approx$32%, in 3 weeks) with the simultaneous encapsulation of BSA within nanoparticles and consequently in alginate microparticles possesses suitable characteristics for its envisioned application. Furthermore, as formerly demonstrated by Boerckel et al. (2011), the administration of 1.0 µg of recombinant human Bone morphogenic protein 2 (rhBMP-2) or 5 µg of rhBMP-2 in alginate scaffolds improves regeneration of bone tissue in the affected area, 12 weeks after the treatment [67]. Herein, our findings demonstrate that between 128 h and 200 h the microencapsulated nanoparticle system releases $\approx$ 45.9 µg of protein (15.3 µg/day), a higher amount of delivered protein than that previously reported in the literature [67]. Such result is fundamental to allow the maintenance of drug concentration within the therapeutic window, during several days. Nevertheless, further characterizing and perceiving the mechanisms that may govern release of bioactive molecules is yet a critical requirement in preclinical design of delivery systems for regenerative medicine. Thus, in order to further illustrate the effect of design parameters, such as particle inclusion in the alginate mesh, experimental data was correlated with the mathematical models that describe mass transport and chemical events that are involved in the release process. Analysis of both the diffusion and swelling associated models suggests that protein release is mainly controlled by Fickian diffusion in the case of Alg–CH–Dext–BSA. This fact is corroborated by the high values of the squared correlation coefficient for Higuchi model (HG) and lower values for Korsmeyer–Peppas (KP). Conversely, alginate microparticles present similar correlation values for both models. Actually, the value of the release exponent for the KP model ($n = 0.508$) is above the range of fully diffusional systems ($n < 0.43$), indicating that protein release occurs by anomalous transport mechanisms ($0.43 < n < 0.85$, for spherical devices) that involve both diffusion and polymer relaxation [68]. These findings are in accordance with previous reports that describe the relaxation of Ca^{2+} crosslinked alginate beads through exchange and release of Ca^{2+} ions with the surrounding solvent [69]. Due to this dynamic interchange the polymeric backbone of alginate becomes loosen promoting release. Yet, on the contrary, the re-arrangement of the polymeric chains of CH–Dext into compact nanosized structures with positive surface may delay protein release by restraining relaxation processes through attractive electrostatic interactions that are established between nanoparticles and the alginate backbone [69].

The use of imaging techniques to characterize complex delivery systems, comprised of multi-scaled carriers has become a powerful tool to elucidate particular characteristics such as the spatial distribution of the delivered therapeutics and their nanoparticulated carriers, features that may influence the use of a delivery system, in detriment of other, for a given application. Spatial distribution plays an important role not only in colloidal stability and protection of the therapeutic cargo, but also in the directional release of the therapeutic biomolecules. In fact spatially dispersing bioactive molecules improves the topological cues that cells need to recognize, in order to promptly migrate and infiltrate onto damaged tissues [3].

Hence, in order to elucidate the distribution of the CH–Dext-BSA systems in their alginate carriers the x-y-z localization of BSA-loaded nanoparticles was investigated using confocal microscopy. Our findings reveal that after 3D image reconstruction of the sliced particle nanoparticles loaded with BSA, are noticeably localized within the microparticle mesh (Fig. 4A, C and D). This parameter has a crucial influence in the spatiotemporal release of the model protein and consequently on its bioactivity and half-life at the injury site. In addition, as demonstrated in Fig. 4D, the formulated nanoparticles are widely distributed within the 3D matrix of the alginate microsphere, suggesting that upon release in a complex biological environment BSA might diffuse in all spatial directions.

The microcarriers cytotoxicity was also evaluated trough contrast microscopy (Fig. 5) being possible to observe cell growth and proliferation in contact with the materials after 3 days of incubation. In Fig. 6 cell *filopodium* were also observed, indicating that human osteoblast cells were attached and spread on the carriers surface after 72 h, showing that it has suitable morphological and chemical properties for tissue renewal [53,70].

The MTS assay further evidences the biocompatibility of the delivery systems since it is possible to observe that for both kind of microparticles cell viability values were similar to that of the negative control. These results may be explained by the presence of Ca^{2+} in the alginate structure, which has been described as an osteoblast proliferation inducer [51].

After the biocompatibility of these microcarriers be confirmed, MSCs were also encapsulated in the alginate mesh. The results presented in Fig. 8 show that cells had a characteristic spherical shape within the microparticles until day 7. At day 11 the microcarriers started to release the encapsulated cells that immediately adhered to the culture plate. These results demonstrate that during the period that the cells remained internalized in the microparticles, nutrients, waste and gases were being actively diffused from and to the surrounding medium avoiding cell starvation or cytotoxicity. Further characterization of cell internalization in the microparticulated carriers reveal that cells are randomly dispersed in the spherical-shaped particle, emphasizing that cell release can then take place in all the directions surrounding the delivery system, similarly to what happens for BSA.

5. Conclusions

In the present work, microencapsulated CH–Dext-BSA nanoparticles were produced in order to obtain a dual drug delivery system to be applied in bone regeneration. These microcarrier systems were characterized in terms of size, morphology, swelling, and encapsulation efficiency for a model protein (BSA) and also the cytotoxic profile was studied in order to evaluate their application for the biomedical application herein proposed. The results obtained showed that this low cost delivery system, based in the encapsulation of CH–Dext-BSA into an alginate microparticle in conjugation with cell encapsulation, can be used as dual carrier. These novel microcarriers will improve the protection and transport of the biomolecules and cells into the target injured tissue, thus enabling their integration and consequently bone tissue repair. Due to their versatility the mico-nanocarriers may also be used in a near future to encapsulate other autologous patient cells that further deposit extracellular matrix and accelerate regenerative processes of different tissues.

Acknowledgments

The authors would like to thank to Fradique, R for the help with the design of the BSA release simulation in Matlab. This work was supported by the Portuguese Foundation for Science and Technology (FCT) (PTDC/EME-TME/103375/2008). Gaspar V.M. also acknowledges a PhD fellowship from FCT (SFRH/BD/80402/2011).

References

[1] Berner A, Boerckel J, Saifzadeh S, Steck R, Ren J, Vaquette C, et al. Biomimetic tubular nanofiber mesh and platelet rich plasma-mediated delivery of BMP-7 for large bone defect regeneration. Cell and Tissue Research 2012;347(3):603–12.
[2] Liu J, Xu L, Li Y, Ma J. Temporally controlled multiple-gene delivery in scaffolds: A promising strategy to enhance bone regeneration. Medical Hypotheses 2011;76(2):173–5.
[3] Vo TN, Kasper FK, Mikos AG. Strategies for controlled delivery of growth factors and cells for bone regeneration. Advanced Drug Delivery Reviews 2012;64(12):1292–309.
[4] Bae SE, Choi J, Joung YK, Park K, Han DK. Controlled release of bone morphogenetic protein (BMP)-2 from nanocomplex incorporated on hydroxyapatite-formed titanium surface. Journal of Controlled Release 2012;160(3):676–84.
[5] Kim S, Kang Y, Krueger CA, Sen M, Holcomb JB, Chen D, et al. Sequential delivery of BMP-2 and IGF-1 using a chitosan gel with gelatin microspheres enhances early osteoblastic differentiation. Acta Biomaterialia 2012;8(5):1768–77.
[6] Trouche E, Girod Fullana S, Mias C, Ceccaldi C, Tortosa F, Seguelas MH, et al. Evaluation of alginate microspheres for mesenchymal stem cell engraftment on solid organ. Cell transplantation 2010;19(12):1623–33.
[7] Zolnik BS, Burgess DJ. Evaluation of in vivo in vitro release of dexamethasone from PLGA microspheres. Journal of controlled release 2008;127(2):137–45.
[8] Richardson TP, Peters MC, Ennett AB, Mooney DJ. Polymeric system for dual growth factor delivery. Nature biotechnology 2001;19(11):1029–34.
[9] Simmons CA, Alsberg E, Hsiong S, Kim WJ, Mooney DJ. Dual growth factor delivery and controlled scaffold degradation enhance in vivo bone formation by transplanted bone marrow stromal cells. Bone 2004;35(2):562–9.
[10] Kumar S, Reddy J. A Review on Microsphere for Novel drug delivery System. Journal of Pharmacy Research 2012;5(1).
[11] Lee M, Li W, Siu RK, Whang J, Zhang X, Soo C, et al. Biomimetic apatite-coated alginate/chitosan microparticles as osteogenic protein carriers. Biomaterials 2009;30(30):6094–101.
[12] Oliva-Rodríguez R, Pérez-Urizar J, Dibildox-Alvarado E, Martínez-Saldaña MC, Avelar-González FJ, Flores-Reyes H, et al. Design of a controlled release system of OP-1 and TGF-β1 based in microparticles of sodium alginate and release characterization by HPLC-UV. Vitro Cellular & Developmental Biology-Animal 2011;47(10):1–8.
[13] Lin Y, Tang W, Wu L, Jing W, Li X, Wu Y, et al. Bone regeneration by BMP-2 enhanced adipose stem cells loading on alginate gel. Histochemistry and cell biology 2008;129(2):203–10.
[14] Möbus K, Siepmann J, Bodmeier R. Zinc–alginate microparticles for controlled pulmonary delivery of proteins prepared by spray-drying. European Journal of Pharmaceutics and Biopharmaceutics 2012;81(1):121–30.
[15] Grellier M, Granja PL, Fricain J-C, Bidarra SJ, Renard M, Bareille R, et al. The effect of the co-immobilization of human osteoprogenitors and endothelial cells within alginate microspheres on mineralization in a bone defect. Biomaterials 2009;30(19):3271–8.
[16] Hernández RM, Orive G, Murua A, Pedraz JL. Microcapsules and microcarriers for in situ cell delivery. Advanced drug delivery reviews 2010;62(7-8):711–30.
[17] Baruch L, Benny O, Gilert A, Ukobnik M, Ben Itzhak O, Machluf M. Alginate-PLL cell encapsulation system Co-entrapping PLGA-microspheres for the continuous release of anti-inflammatory drugs. Biomedical microdevices 2009;11(5):1103–13.
[18] Murua A, Portero A, Orive G, Hernández RM, de Castro M, Pedraz JL. Cell microencapsulation technology: towards clinical application. Journal of Controlled Release 2008;132(2):76–83.
[19] Kanczler JM, Ginty PJ, White L, Clarke NMP, Howdle SM, Shakesheff KM, et al. The effect of the delivery of vascular endothelial growth factor and bone morphogenic protein-2 to osteoprogenitor cell populations on bone formation. Biomaterials 2010;31(6):1242–50.
[20] Shah NJ, Macdonald ML, Beben YM, Padera RF, Samuel RE, Hammond PT. Tunable dual growth factor delivery from polyelectrolyte multilayer films. Biomaterials 2011;32(26):6183–93.
[21] Grenha A, Remuñán-López C, Carvalho ELS, Seijo B. Microspheres containing lipid/chitosan nanoparticles complexes for pulmonary delivery of therapeutic proteins. European journal of pharmaceutics and biopharmaceutics 2008;69(1):83–93.
[22] Park JS, Yang HN, Woo DG, Jeon SY, Park K-H. The promotion of chondrogenesis, osteogenesis, and adipogenesis of human mesenchymal stem cells by multiple growth factors incorporated into nanosphere-coated microspheres. Biomaterials 2011;32(1):28–38.
[23] Mohanraj EK, K., S., Rajkumar N. Study on concrete using waste materials by partial replacement of aggregates to reduce global warming gases. Indian Journal of Science Technology 2011;4(3):159–264.
[24] Zhao D, Zhao X, Zu Y, Li J, Zhang Y, Jiang R, et al. Preparation, characterization, and in vitro targeted delivery of folate-decorated paclitaxel-loaded bovine serum albumin nanoparticles. International journal of nanomedicine 2010;5:669–77.
[25] Chen Y, Mohanraj VJ, Parkin JE. Chitosan-dextran sulfate nanoparticles for delivery of an anti-angiogenesis peptide. International Journal of Peptide Research and Therapeutics 2003;10(5):621–9.
[26] Sarmento B, Ribeiro A, Veiga F, Ferreira D. Development and characterization of new insulin containing polysaccharide nanoparticles. Colloids and Surfaces B: Biointerfaces 2006;53(2):193–202.
[27] Chen Y, Mohanraj VJ, Wang F, Benson HAE. Designing chitosan-dextran sulfate nanoparticles using charge ratios. AAPS Pharmscitech 2007;8(4):131–9.
[28] Sharma S, Mukkur TK, Benson H, Chen Y. Enhanced immune response against pertussis toxoid by IgA-loaded chitosan–dextran sulfate nanoparticles. Journal of Pharmaceutical Sciences 2012;101(1):233–44.

[29] Pan Y, Li Y, Zhao H, Zheng J, Xu H, Wei G, et al. Bioadhesive polysaccharide in protein delivery system: chitosan nanoparticles improve the intestinal absorption of insulin in vivo. International journal of pharmaceutics 2002; 249(1):139–47.
[30] Anitha A, Deepagan V, Rani V, Menon D, Nair S, Jayakumar R. Preparation characterization in vitro drug release and biological studies of curcumin loaded dextran sulfate-chitosan nanoparticles. Carbohydrate Polymers 2011; 84(3):1158–64.
[31] Li Z, Chen X, Xu X, Ye, Wang J. Preparation of chitosan–sodium alginate microcapsules containing ZnS nanoparticles and its effect on the drug release. Materials Science and Engineering: C 2009;29(7):2250–3.
[32] Xu Y, Hanna MA. Electrosprayed bovine serum albumin-loaded tripolyphosphate cross-linked chitosan capsules: Synthesis and characterization. Journal of microencapsulation 2007;24(2):143–51.
[33] Gaspar V, Sousa F, Queiroz J, Correia I. Formulation of chitosan–TPP–pDNA nanocapsules for gene therapy applications. Nanotechnology 2011;22. 015101.
[34] Zhang L, Guo J, Peng X, Jin Y. Preparation and release behavior of carboxymethylated chitosan/alginate microspheres encapsulating bovine serum albumin. Journal of applied polymer science 2004;92(2):878–82.
[35] Scientific, T., BCA-based Protein Assays. Thermo Scientific Pierce Protein Assay Technical Handbook: 15.
[36] Han Y, Tian H, He, Chen X, Jing X. Insulin nanoparticle preparation and encapsulation into poly (lactic-co-glycolic acid) microspheres by using an anhydrous system. International journal of pharmaceutics 2009;378(1-2): 159–66.
[37] Yu CY, Zhang XC, Zhou FZ, Zhang XZ, Cheng SX, Zhuo RX. Sustained release of antineoplastic drugs from chitosan-reinforced alginate microparticle drug delivery systems. International journal of pharmaceutics 2008;357(1):15–21.
[38] Higuchi T. Mechanism of sustained-action medication. Theoretical analysis of rate of release of solid drugs dispersed in solid matrices. Journal of pharmaceutical sciences 1963;52(12):1145–9.
[39] Costa, Sousa Lobo JM. Modeling and comparison of dissolution profiles. European journal of pharmaceutical sciences 2001;13(2):123–33.
[40] Ribeiro MP, Espiga A, Silva D, Baptista J, Henriques, Ferreira C, et al. Development of a new chitosan hydrogel for wound dressing. Wound Repair and Regeneration 2009;17(6):817–24.
[41] Coimbra P, Ferreira H, de Sousa, Batista M, Rodrigues, Correia I, et al. Sodium hyaluronate/chitosan polyelectrolyte complex scaffolds for dental pulp regeneration: Synthesis and characterization. International Journal of Biological Macromolecules 2011;49(4):573–9.
[42] da Silva MS, Viveiros R, Morgado PI, Aguiar-Ricardo A, Correia IJ, Casimiro T. Development of 2-(dimethylamino) ethyl methacrylate-based molecular recognition devices for controlled drug delivery using supercritical fluid technology. International journal of pharmaceutics 2011;416(1):61–8.
[43] Xu S, De Becker A, Van Camp B, Vanderkerken K, Van Riet I. An improved harvest and in vitro expansion protocol for murine bone marrow-derived mesenchymal stem cells. Journal of Biomedicine and Biotechnology 2010; 2010:10.
[44] Hunt N, Smith AM, Gbureck U, Shelton R, Grover L. Encapsulation of fibroblasts causes accelerated alginate hydrogel degradation. Acta Biomaterialia 2010;6(9):3649–56.
[45] Gonçalves A, Costa MT, Rodrigues IR, Dias RL, Reis, Gomes ME. Effect of flow perfusion conditions in the chondrogenic differentiation of bone marrow stromal cells cultured onto starch based biodegradable scaffolds. Acta Biomaterialia 2011;7(4):1644–52.
[46] Hungerford G, Benesch J, Mano JF, Reis RL. Effect of the labelling ratio on the photophysics of fluorescein isothiocyanate (FITC) conjugated to bovine serum albumin. Photochem. Photobiol. Sci. 2007;6(2):152–8.
[47] Causa F, Netti PA, Ambrosio L. A multi-functional scaffold for tissue regeneration: The need to engineer a tissue analogue. Biomaterials 2007;28(34): 5093–9.
[48] Gombotz WR, Wee SF. Protein release from alginate matrices. Advanced Drug Delivery Reviews 1998;31(3):267–85.
[49] Tu J, Bolla S, Barr J, Miedema J, Li X, Jasti B. Alginate microparticles prepared by spray–coagulation method: Preparation, drug loading and release characterization. International journal of pharmaceutics 2005;303(1):171–81.
[50] Iijima M, Hatakeyama T, Nakamura K, Hatakeyama H. Thermomechanical analysis of calcium alginate hydrogels in water. Journal of thermal analysis and calorimetry 2002;70(3):807–14.
[51] Moudgil S, Ying JY. Calcium-Doped Organosilicate Nanoparticles as Gene Delivery Vehicles for Bone Cells. Advanced Materials 2007;19(20):3130–5.
[52] Hatano K, Inoue H, Kojo T, Matsunaga T, Tsujisawa T, Uchiyama C, et al. Effect of surface roughness on proliferation and alkaline phosphatase expression of rat calvarial cells cultured on polystyrene. Bone 1999;25(4):439–45.
[53] Huang S, Fu X. Cell behavior on microparticles with different surface morphology. Journal of Alloys and Compounds 2010;493(1):246–51.
[54] Chu PK, Chen J, Wang L, Huang N. Plasma-surface modification of biomaterials. Materials Science and Engineering: R: Reports 2002;36(5-6):143–206.
[55] Price RL, Ellison K, Haberstroh KM, Webster TJ. Nanometer surface roughness increases select osteoblast adhesion on carbon nanofiber compacts. Journal of Biomedical Materials Research Part A 2004;70(1):129–38.
[56] Roach P, Parker T, Gadegaard N, Alexander M. Surface strategies for control of neuronal cell adhesion: A review. Surface Science Reports 2010;65(6):145–73.
[57] Richardi J. One-dimensional assemblies of charged nanoparticles in water: A simulation study. The Journal of chemical physics 2009;130. 044701.
[58] Bessa PC, Machado R, Nürnberger S, Dopler D, Banerjee A, Cunha AM, et al. Thermoresponsive self-assembled elastin-based nanoparticles for delivery of BMPs. Journal of Controlled Release 2010;142(3):312–8.
[59] Mahl D, Diendorf J, Meyer-Zaika W, Epple M. Possibilities and limitations of different analytical methods for the size determination of a bimodal dispersion of metallic nanoparticles. Colloids and Surfaces A: Physicochemical and Engineering Aspects 2011;377(1–3):386–92.
[60] Al-Kassas RS, Al-Gohary O, Al-Faadhel MM. Controlling of systemic absorption of gliclazide through incorporation into alginate beads. International journal of pharmaceutics 2007;341(1-2):230–7.
[61] Pasparakis G, Bouropoulos N. Swelling studies and in vitro release of verapamil from calcium alginate and calcium alginate–chitosan beads. International journal of pharmaceutics 2006;323(1):34–42.
[62] Bajpai S, Tankhiwale R. Investigation of water uptake behavior and stability of calcium alginate/chitosan bi-polymeric beads: Part-1. Reactive and Functional Polymers 2006;66(6):645–58.
[63] Gao C, Liu M, Chen J, Zhang X. Preparation and controlled degradation of oxidized sodium alginate hydrogel. Polymer Degradation and Stability 2009; 94(9):1405–10.
[64] Chretien C, Chaumeil J. Release of a macromolecular drug from alginate-impregnated microspheres. International journal of pharmaceutics 2005; 304(1):18–28.
[65] Huang X, Brazel CS. On the importance and mechanisms of burst release in matrix-controlled drug delivery systems. Journal of Controlled Release 2001; 73(2):121–36.
[66] Dimitriou R, Tsiridis E, Giannoudis PV. Current concepts of molecular aspects of bone healing. Injury 2005;36(12):1392–404.
[67] Boerckel JD, Kolambkar YM, Dupont KM, Uhrig BA, Phelps EA, Stevens HY, et al. Effects of protein dose and delivery system on BMP-mediated bone regeneration. Biomaterials 2011;32(22):5241–5251.
[68] Arifin DY, Lee LY, Wang CH. Mathematical modeling and simulation of drug release from microspheres: Implications to drug delivery systems. Advanced drug delivery reviews 2006;58(12):1274–325.
[69] Bajpai SK, Sharma S. Investigation of swelling/degradation behaviour of alginate beads crosslinked with Ca2+ and Ba2+ ions. Reactive and Functional Polymers 2004;59(2):129–40.
[70] Zhou H, Xu HHK. The fast release of stem cells from alginate-fibrin microbeads in injectable scaffolds for bone tissue engineering. Biomaterials 2011;32(30): 7503–13.
[71] Zuo Q, Lu J, Hong A, Zhong D, Xie S, Liu Q, et al. Preparation and characterization of PEM-coated alginate microgels for controlled release of protein. Biomedical Materials 2012;(3):7. 035012.

Separation and Purification Technology 112 (2013) 20–25

Contents lists available at SciVerse ScienceDirect

Separation and Purification Technology

journal homepage: www.elsevier.com/locate/seppur

A bi-layer electrospun nanofiber membrane for plasmid DNA recovery from fermentation broths

Tiago R. Correia [a], Bernardo P. Antunes [a], Pedro H. Castilho [a], José C. Nunes [a], Maria T. Pessoa de Amorim [b], Isabel C. Escobar [c], João A. Queiroz [a], Ilídio J. Correia [a,*], António M. Morão [a]

[a] CICS-UBI – Health Sciences Research Center, Faculty of Health Sciences, University of Beira Interior, Covilhã, Portugal
[b] Department of Textile Engineering, University of Minho, 4800-058 Guimarães, Portugal
[c] Department of Chemical and Environmental Engineering, University of Toledo, Toledo, OH 43606, United States

ARTICLE INFO

Article history:
Received 2 February 2013
Received in revised form 28 March 2013
Accepted 29 March 2013
Available online 6 April 2013

Keywords:
Microfiltration
Electrospinning
Bi-layer membrane
Lysate
Plasmid DNA

ABSTRACT

The demanding ever-increasing quantities of highly purified biomolecules by bio-industries, has triggered the development of new, more efficient, purification techniques. The application of membrane-based technologies has become very attractive in this field, for their high throughput capability, simplicity of operation and scale-up.

Herein we report the production of a bi-layer membrane by electrospinning (ES), in which a support of poly ε-caprolactone nanofibers was coated with a polyethylene oxide/sodium alginate layer, and subsequently cross-linked with calcium chloride. The membranes were characterized by SEM, ATR-FTIR, contact angle measurements, and were applied in the recovery process of a plasmid. The results show that membranes retained the suspended solids while allowing the permeation of plasmid DNA, with high recovery yields and improved RNA retention. Moreover, they also showed a very low fouling tendency. To the best of our knowledge it is the first time that ES membranes are applied in this type of bioprocess.

1. Introduction

The development of new separation technologies suitable for the large-scale production of highly purified plasmid DNA (pDNA) for gene therapy applications and the production of DNA vaccines has found increasing interest in the recent years [1–4]. The use of microfiltration and ultrafiltration membranes for pDNA recovery and purification from fermentation broths has been demonstrated as a promising alternative to conventional separation methods, namely those involving precipitation with solvents and centrifugation [5].

Electrospinning is an easy and cheap method of producing nanofibrous materials. These can be obtained from a wide variety of polymers by controlling the solution properties and the processing conditions [6]. The simplicity of this procedure and the wide range of applications found in recent years, including tissue engineering applications, such as bone repair, wound healing and drug delivery carriers [7–9], in sensors and biosensors [10], in electrodes [11] and that of filtration [12–14] are important factors that lead to an increasing interest in developing new types of electrospun nanofiber membranes (ENMs) [15]. Commonly, nanofibers are electrospun into a support or produced in layer by layer arrangements [16,17]. In either case fiber deposition should be always carried out on a support which provides the required mechanical strength to the films produced [16].

In the present study, a poly ε-caprolactone (PCL) support was prepared by a conventional electrospinning process. This polymer was selected based on the good mechanical properties that PCL meshes present [18] and also for being environmentally friendly [19]. A coating based on an electrospun mixture of two polymers, sodium alginate (SA) combined with poly(ethylene) oxide (PEO) was deposited on the support. SA was selected for ENMs coating due to its high hydrophilicity, relatively low cost and the ability of producing small diameter fibers by electrospinning, when mixed with PEO [20]. This asymmetric arrangement of two different layers provides the membrane with adequate mechanical robustness whereas separation selectiveness is regulated predominantly by the ultrathin layer of nanofibers.

The bi-layer membranes produced were characterized in terms of their morphology, hydrophilicity and hydraulic permeability prior to the filtration tests. The performance of the ENMs on the filtration of cell lysates, obtained immediately after the cell lysis step, was evaluated and compared with that of commercial microfiltration membranes. From the best of our knowledge, this is the first time that ENMs are tested in the recovery process of biomolecules from fermentation broths.

* Corresponding author. Address: Av. Infante D. Henrique, 6200-506 Covilhã, Portugal. Tel.: +351 275 329 002; fax: +351 275 329 099.
E-mail address: icorreia@ubi.pt (I.J. Correia).

1383-5866/$ - see front matter © 2013 Elsevier B.V. All rights reserved.
http://dx.doi.org/10.1016/j.seppur.2013.03.049

2. Materials and methods

2.1. Materials

PEO (Mw = 300,000 g/mol), SA (Mw = 120000–190,000 g/mol), PCL (Mw = 80,000 g/mol), calcium chloride (Mw = 110.99 g/mol) were purchased from Sigma–Aldrich (Sin tra, Portugal) as well as Terrific Broth medium for bacterial culture and kanamycin sulfate. P1 buffer (50 mM Tris–HCl, pH = 8.00, 10 mM EDTA and 100 μg/mL of RNase A), P2 buffer (200 mM NaOH and 1% SDS (w/v)) and P3 buffer (3 M of potassium acetate, pH 5.00) were from a Qiagen Plasmid Maxi Kit and Tris–HCl 10 mM (*IZASA*, Portugal). Microfiltration membranes, *Nylaflo* (pore diameter of 0.22 μm *Pall Corporation* and *FSM0.45PP* from *Alfa Laval* (pore diameter of 0.45 μm).

2.2. Methods

2.2.1. Bacterial growth and cell lysis

The plasmid production procedure was adapted from the literature [5,21]. The 6050 bp plasmid pVAX1-LacZ was amplified in a cell culture of *Escherichia coli* DH5α. The fermentation was carried out at 37 °C in 250 mL of Terrific Broth medium, supplemented with 50 μg/mL of kanamycin. Growth was suspended at the late log phase ($OD_{600\_nm} \approx 10–11$) and cells were harvested by centrifugation. Afterwards, pDNA extraction was performed by alkaline lysis using three different buffers (P1, P2 and P3, previously specified). For this procedure 120 g/L (wet weight) of cells were resuspended in 4 mL of P1 buffer. Then, 4 mL of P2 were added to promote cell lysis for 5 min, at room temperature. Finally, P3 buffer at 4 °C was added to neutralize the alkaline solution. A large quantity of suspended solids was obtained upon neutralization and the suspension was kept on ice for 15 min before membrane filtration.

2.2.2. ENMs production process

A conventional electrospinning apparatus was used for ENMs production. The system setup consisted in a high voltage source (*Spellman CZE1000R*, 0–30 kV), a syringe pump (*KDS-100*), a plastic syringe with a stainless steel needle and an aluminum disk connected to a copper collector. PCL was dissolved in acetone (10% w/v), at 50 °C, under constant stirring [22]. Meanwhile, a PEO/SA solution was prepared by mixing 6.75% PEO and 0.5% SA aqueous solutions [23]. The PCL polymer solution was used to produce a support ENM, using a constant flow rate of 3 mL/h and an applied voltage of 15 kV. The distance between needle tip and collector was set at 10 cm [22]. Subsequently, the PEO/SA solution was deposited over the PCL ENM by electrospinning, in the same apparatus, at a constant flow rate of 0.6 mL/h and an applied voltage of 18 kV, thereby obtaining a bi-layer ENM. Finally, the membrane was crosslinked in a calcium chloride solution for 24 h [23]. From the obtained films, membranes disks were cut with suitable size to be used in the filtration cell, using a circular blade.

2.2.3. Membrane filtration tests

These assays were performed in a 10 mL stirred cell (*Amicon/Millipore*, model *8010*), according to a procedure previously described in the literature [19]. The membranes to be tested (*Nylaflo*, *FSM0.45PP* or the ENMs) were initially flushed with 20 mL of *Milli-Q* water at a constant pressure of 0.07 bar, to ensure the thorough washing of the membranes. Then, the water permeability (hydraulic permeability) of each membrane was determined by measuring the flow rate, at that pressure. Five permeability measurements were performed with each membrane disk and the average value was considered the initial hydraulic permeability of each membrane disk, L_{p0}.

To perform the filtration of the *E. coli* DH5α lysates the remaining water in the cell was carefully removed and, immediately after that, 10 mL of lysate were introduced in the filtration cell. A continuous diafiltration of the lysate was performed for 1 h, using a 10 mM Tris–HCl (pH = 8.00) buffer at a constant flow rate of 0.5 mL/min. Two peristaltic pumps were used, one for feeding the diafiltration buffer and the other to perform the filtration (by suction). The experimental setup is shown in Fig. 1. Under these conditions, one could estimate that, if no pDNA was adsorbed on the membrane and the membrane rejection was 0, approximately 95% of the pDNA was expected to be recovered in the permeate, while 5% would remain in the cell. It was decided to not try to recover the remaining pDNA to avoid excessive dilution of the whole permeate.

2.2.4. Turbidity measurements

The filtrate was analyzed by UV/Visible Spectroscopy at a wavelength of 600 nm, to determine the amount of suspended solids. A fraction of the alkaline lysate, containing the suspended solids, was transferred to an eppendorf tube and centrifuged at 18,000*g* during 30 min at 4 °C (*Hettich Zentrifugen*, *Mikro 200R*). Then, the absorbance of the supernatant was measured at a wavelength of 600 nm and the value obtained compared with that of the membrane permeates.

2.2.5. Plasmid DNA and RNA quantification

Plasmid DNA and RNA concentrations in lysates, were obtained by hydrophobic interaction chromatography (HIC) [5]. Briefly, a 15 PHE PE column (*Amersham Biosciences – GE Healthcare*) connected to an *AKTA* purifier HPLC System was used. The column was initially equilibrated with 1.5 M $(NH_4)_2SO_4$ in a 10 mM Tris–HCl buffer (pH 8.00). Prior to the injection, the suspended solids in lysates were removed by centrifugation, as described in Section 2.2.4.

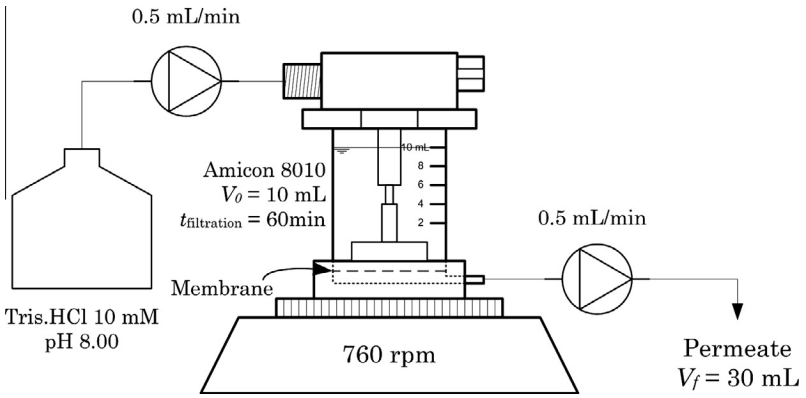

Fig. 1. Experimental set-up used for continuous diafiltrations, showing the two peristaltic pumps and the filtration cell.

Samples from the supernatants were directly injected in the column. The injected volume in each run was 20 μL and the samples were eluted at a constant flow rate of 1 mL/min. Two minutes after the injection, the eluent was instantly changed to 10 mM Tris–HCl buffer (pH = 8.00), in order to elute bounded species. This concentration was maintained for 5 min before the re-equilibration of the column, which was carried out with 1.5 M $(NH_4)_2SO_4$ in a 10 mM Tris–HCl buffer (pH 8.00), in order to prepare the column for the next run. The absorbance of the eluate at 260 nm was monitored. The concentration of pDNA in each sample was calculated from the area of the pDNA peak and a calibration curve, obtained with pure pVAX1-lacZ standard solutions.

The filtration yield, in each test, was calculated as the ratio of the amount of pDNA in the whole collected permeate to the amount of pDNA in the lysate. The RNA removal was calculated as $1 - (V_p C_{RNA,p})/(V_{lys} C_{RNA,lys})$ where $C_{RNA,p}$ is the RNA concentration in the whole collected permeate and $C_{RNA,lys}$ is the RNA concentration in the lysate, V_p is the whole volume of permeate collected and V_{lys} is the volume of lysate processed in each run.

2.2.6. Scanning electron microscopy

The morphology of the membranes was analyzed by scanning electron microscopy (SEM). Samples were air-dried overnight and then mounted on an aluminum board using a double-side adhesive tape and covered with gold using an *Emitech* K550 (London, England) sputter coater. The samples were analyzed using a *Hitachi* S-2700 (Tokyo, Japan) scanning electron microscope operated at an accelerating voltage of 20 kV and at different amplifications [21].

The diameter distribution of the nanofibers in the ENMs was determined from 50 measurements, at least, using *ImageJ* (National Institutes of Health, Bethesda (MD), USA).

2.2.7. Attenuated total reflectance-fourier transform infrared spectroscopy

PEO, SA, PCL and polymer coated ENMs spectra were acquired in the range of 4000–500 cm^{-1}, using a *JASCO* 4200 FTIR spectrophotometer, operating in ATR mode (MKII *GoldenGate*™ Single Reflexion ATR System). Data collection was performed with a 4 cm^{-1} spectral resolution and after 64 scans [24].

2.2.8. Contact angle

Contact angles of the membranes were determined using a *Data Physics Contact Angle System OCAH 200* apparatus, operating in static mode. For each sample, water drops were placed at various locations of the analyzed surface, at room temperature. The reported contact angles are the average of at least three measurements.

2.2.9. Membrane porosity

The surface porosity of the membranes was estimated from SEM images using the image analysis software, *ImageJ*. The total porosity of the membranes was measured through the determination of the amount of ethanol absorbed by wet membranes, after 1 h of immersion in that solvent, using the following equation [25]:

$$P(\%) = \frac{W_2 - W_1}{d_{\text{ethanol}} V_{\text{membrane}}} \times 100 \quad (1)$$

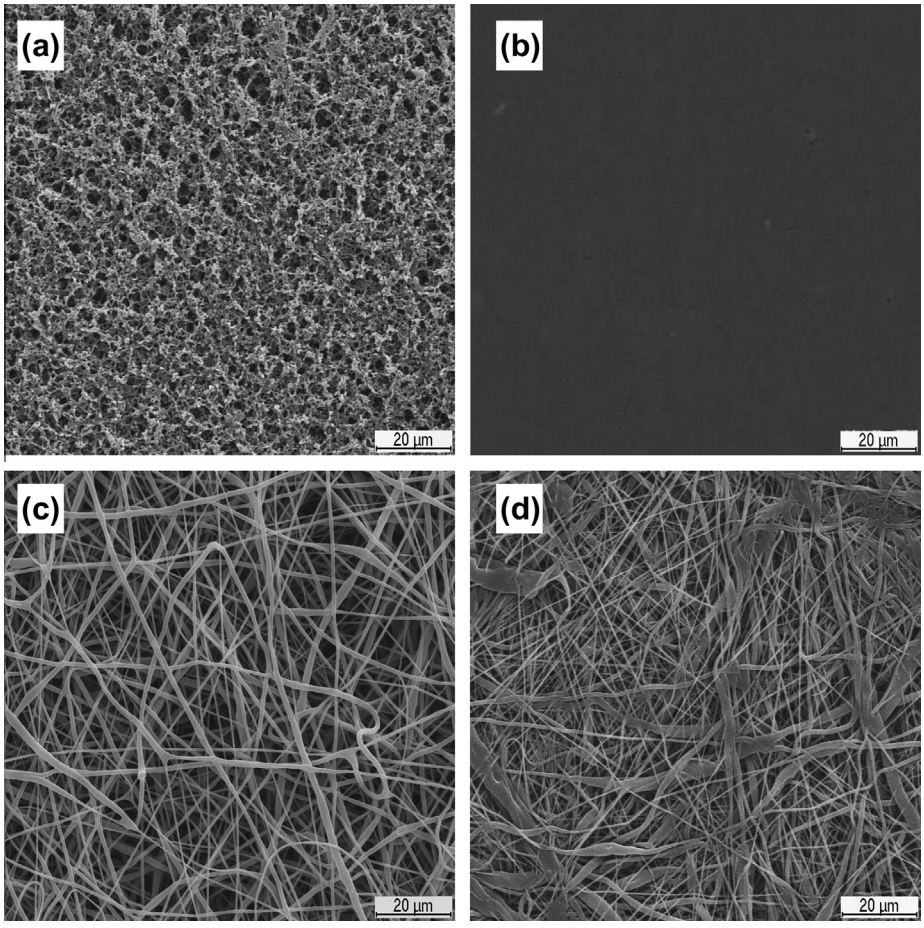

Fig. 2. SEM images. (a) *Nylaflo* 0.22 μm membrane; (b) *FSM0.45PP* 0.45 μm membrane; (c) PCL ENM; and (d) PCL ENMC.

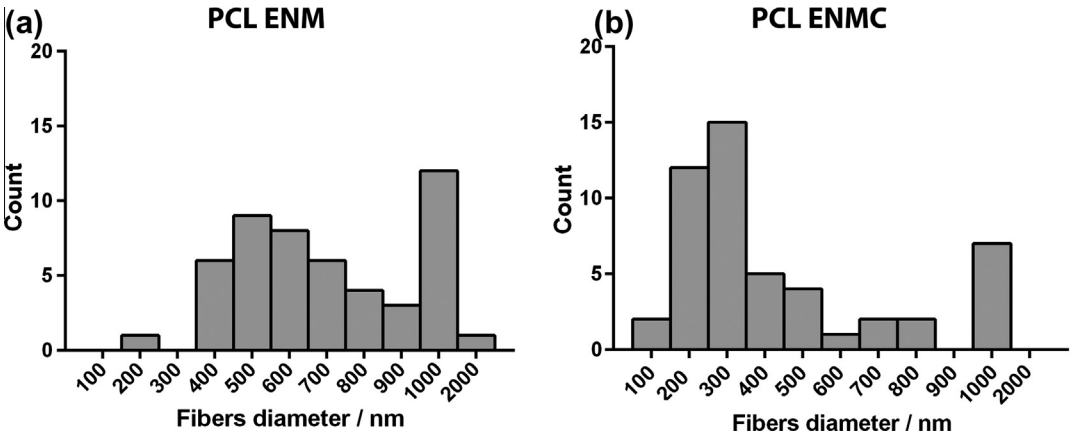

Fig. 3. Fiber diameter distribution for the uncoated and coated PCL ENM.

where W_1 is the weight of the dry membrane and W_2 is the weight of the wet membrane, $d_{ethanol}$ the density of the ethanol at room temperature, and $V_{membrane}$ is the volume of the wet membrane. The latter was determined from the membrane area and by measuring the membrane thickness with a micrometer *Adamel Lhomargy M120* acquired from *Testing Machines Inc*., USA.

3. Results and discussion

3.1. ENMs characterization

The morphology of the membranes, namely in terms of fiber diameter distribution, fiber average diameter and surface porosity was analyzed from SEM images. As can be seen in Fig. 2 the ENMs produced present a high density of deposited fibers, in particular after deposition of the second layer of nanofibers.

Fiber diameter distributions are shown in Fig. 3. The PCL support has nanofibers with different diameters (200 nm – 2 μm) and this range of fiber diameters is adequate for obtaining a good mechanical support [26]. The polymer-coated ENM presents a higher density of thin fibers (i.e., fibers with 200–300 nm of diameter) than the polymer-uncoated ENM (i.e., the PCL support) which contributes to a decrease in the dimensions of the interstices. The number average fiber diameter of the uncoated ENMs can be estimated to be 720 nm and that of the coated membranes to be 430 nm. The commercial microfiltration membranes have typical values of pore diameter for this type of membranes, 0.22 μm and 0.45 μm for the *Nylaflo* and *FSM0.45PP*, respectively (nominal values given by the manufacturers).

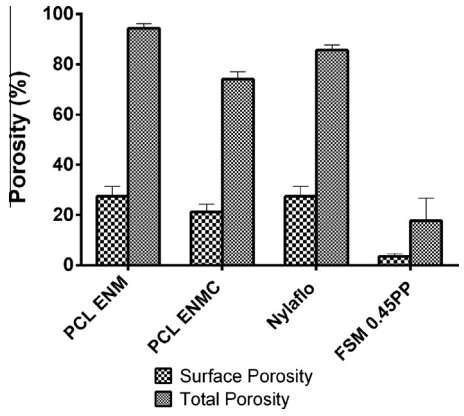

Fig. 4. Surface and total porosity of the ENMs and the commercial microfiltration membranes.

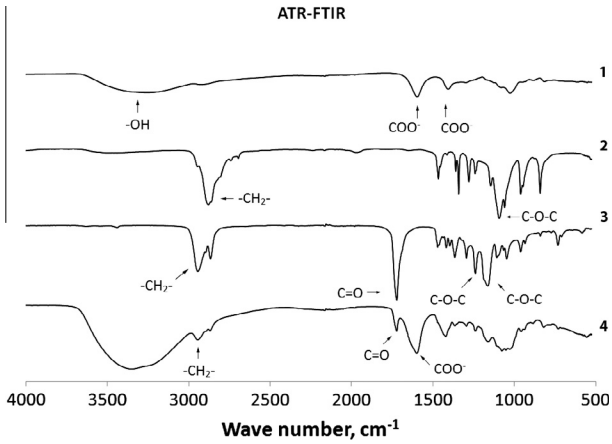

Fig. 5. ATR-FTIR spectra of: (1) SA; (2) PEO; (3) PCL ENM; and (4) PCL ENMC.

The porosity of the membranes is analyzed in Fig. 4. As can be seen, the ENMs have porosities comparable to that of the 0.22 μm *Nylaflo* membranes which have been found to perform very satisfactory in the filtration of lysates from plasmid pVAX1-lacZ fermentation [5]. The porosity of the 0.45 μm membrane used is clearly lower than that of the other membranes studied herein.

An ATR-FTIR analysis of the membranes was also carried out to check for the presence of the coating layer. The ATR-FTIR spectra of SA, PEO, PCL and the PCL/SA ENM (polymer coated ENM) can be seen in Fig. 5. The spectrum of SA shows its characteristic absorption band in the region between 1610 cm^{-1} and 1560 cm^{-1}, which is due to COO^- groups [27] (spectrum 1). The spectrum of PEO (spectrum 2) shows the characteristic bands of —CH2— groups in the region between 2990 cm^{-1} and 2850 cm^{-1} [28]. The third spectrum is that of PCL, which shows an absorption band between 1750 cm^{-1} and 1740 cm^{-1} due to C=O groups [29]. The spectrum of the polymer coated ENM (spectrum 4), shows the characteristic peaks of the functional groups of the polymers used in membrane production, previously mentioned, therefore indicating that a thin layer of PEO/SA was deposited on the PCL support. Moreover, a

Table 1
Contact angles from the FSM, Nylon, uncoated ENM (PCL support) and PCL coated ENM.

Membranes	Water contact angle
FSM0.45PP – 0.45 μm	85.5° ± 3.5°
Nylaflo – 0.22 μm	18.4° ± 0.1°
PCL ENM	104° ± 7°
PCL ENMC	16.8° ± 2.4°

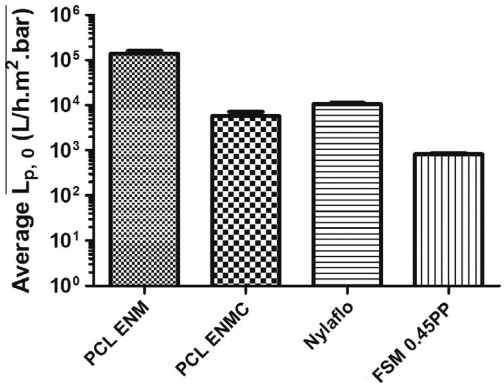

Fig. 6. Water permeability (hydraulic permeability) of the different membranes tested, $T = 25$ °C, before the filtration tests (L_{p0}).

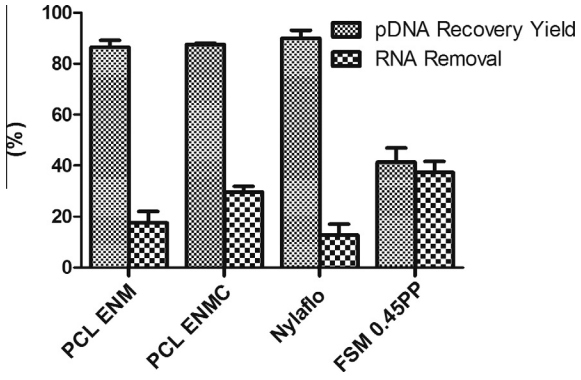

Fig. 7. Filtration yield of the different membranes tested in the filtration of lysates.

much higher intensity peak around 3300 cm^{-1} was observed, due to the over-abundance of —OH groups in the coating layer, as previously described in the literature [30,31].

In order to further characterize the surface properties of the membranes, water contact angles were also determined to evaluate the hydrophilicity of the membranes. This is an important property when considering the filtration of suspensions with high organic load; in fact, it is well-known that hydrophilic membranes generally perform better than hydrophobic due to adsorption phenomena [32]. The obtained contact angles are indicated in Table 1. As can be seen, the uncoated PCL membrane presented a high contact angle of 104°, which is indicative of a hydrophobic character. After coating it with PEO/SA the contact angle decreased to 16.8°, which is a very similar value to that of the *Nylaflo* membrane. The contact angle of the *FSM0.45PP* membrane is also very high, although lower than that of the uncoated PCL ENM. Herein, the filtration tests performed with this membrane aimed to check the effect of the pore size on the permeate turbidity and permeability recover after filtration.

3.2. Membrane filtration studies

3.2.1. Hydraulic permeability

The results obtained in the permeability tests are summarized in Fig. 6. As can be seen, the coated PCL ENM produced have L_{p0} values near 5000 L/h m^2 bar, which are of the same order of magnitude of those found for the *Nylaflo* membrane. The hydraulic permeability of the *FSM0.45PP* is clearly lower, which is possibly due to its lower porosity and also its higher hydrophobicity, as suggested by the results obtained from contact angle measurements.

3.2.2. Microfiltration of lysates

After the cell lysis procedure is completed, using the previously described method, a suspension containing a large quantity of precipitates and cell debris is formed, nearly 2.4 g of suspended solids per gram (wet weight) of cells, as described elsewhere [33]. In respect to solids removal, the coated PCL ENMs and the *Nylaflo* membranes gave identical results. Practically, all solids were removed during the filtration, as can be seen by the turbidity measurements (Table 2). This indicates that both membranes have a similar average pore size. The fact that the uncoated ENMs have a lower solids retention than the coated is in agreement with their higher average fiber diameter, considering that the dimensions of the interstices between fibers becomes smaller as the fiber diameter decreases.

In respect to the process yield, in a previous study, where the same lysis method was used the *Nylaflo* membranes presented high yields for the recovery of pVAX1-lacZ from the obtained lysates [5]. Using both coated and uncoated ENMs, high recovery yields were also obtained herein, as indicated in Fig. 7. In addition, the results also reveal that a significant RNA removal can be achieved using the ENMs, reaching approximately 30% with the PCL coated ENM. It is possible that the structural differences between ENMs and conventional microfiltration membranes can explain the improved selectivity of the ENMs.

With the *FSM0.45PP* membrane the highest RNA removal was found, however, much lower yields are also obtained. The occurrence of severe fouling is likely to be the cause of the higher retention of both pDNA and RNA. In fact, after a few minutes of filtration with this membrane, the permeate pump was unable to impose the predetermined flow of 0.5 mL/min (73 L/h m^2), which is indicative of the intense fouling. In order to accomplish the filtration, the stirred cell had to be connected to a pressurized nitrogen reservoir containing the diafiltration buffer; the applied pressure on the feed was adjusted to 0.5 bar and the permeate pump was disconnected. The permeate flux decreased from 140 L/h m^2 to near 20 L/h m^2 by the end of the diafiltration. Fluxes were determined from the volume of permeate collected as a function of time.

The fouling tendency of the different membranes can be better evaluated by comparing the recovery of hydraulic permeability after filtration, i.e., after replacing the lysate suspension inside the cell with water and then, measuring the water permeability (without subjecting the membranes to any cleaning procedure). The ratio L_p/L_{p0}, is a measure of the tendency of the membranes to foul; the obtained values are shown in Fig. 8. As can be seen, the coated PCL ENMs recovered almost completely their initial permeability upon filtration of the lysates. This indicates that the produced membranes are highly resistant to fouling by the cell debris and other suspended solids present in the lysates.

The differences between the coated and uncoated ENMs should be also pointed out, with the results clearly showing the importance of the PEO/SA layer in preventing membrane fouling. The decrease in the average fiber size may have contributed to a better performance of the coated membranes, by avoiding the accumulation of solids between the fibers, inside the electrospun films. However, the decisive factor affecting membrane performance is more likely to be the increase in hydrophilicity, as it is suggested

Table 2
Turbidity of processed lysates (by centrifugation or microfiltration).

Centrifugation[a]	PCL ENM	PCL ENMC	*Nylaflo*	*FSM0.45PP*
0.002 ± 0.001	0.030 ± 0.001	0.0060 ± 0.0009	0.0065 ± 0.0009	0.024 ± 0.008

[a] As described in Section 2.2.4.

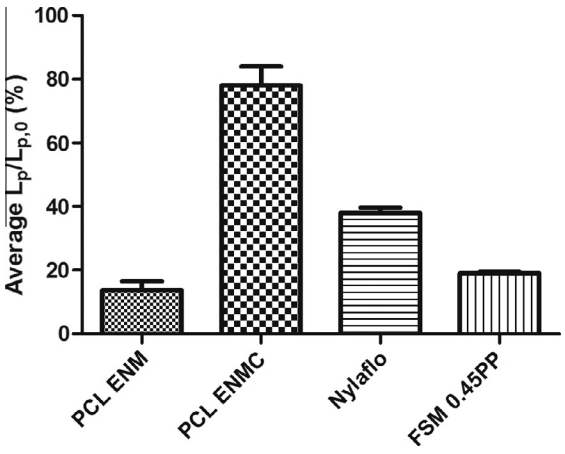

Fig. 8. Permeability recovery of the different membranes tested in the filtration of lysates.

from the fact that both the uncoated ENMs and the *FSM0.45PP* membranes (that had the highest contact angles) present the lowest L_p/L_{p0} values.

4. Conclusion

In this work a bi-layer membrane was produced, by deposition of a PEO/SA layer on a PCL support. Both layers were produced by electrospinning. Electrospun nanofibers that have been previously used in a practical and cost-effective way for the production of polymer scaffolds, are shown here to be also suitable to be used as microfiltration membranes, for processing complex suspensions of solids, with high fouling potential (which is the case of cell lysates). The bi-layer arrangement provided both the selectivity and hydrophilicity required for this application. In fact, the experimental results point out that the bi-layer ENM produced can perform, at least, at the same level as commercial microfiltration membranes, showing a comparable selectivity for retaining the suspended solids while allowing the total permeation of the solute of interest (i.e., the plasmid), with an improved selectivity to retain RNA and an even better resistance to fouling. Moreover, the membranes produced are environmentally friendly due to their known biodegradability.

Acknowledgments

This work was supported by the Portuguese Foundation for Science and Technology (FCT), (PTDC/EME-TME/103375/2008 and PTDC/EBB-BIO/114320/2009). To Ricardo Fradique for helping in the production of the graphical abstract.

References

[1] G.N.M. Ferreira, Chromatographic approaches in the purification of plasmid DNA for therapy and vaccination, Chemical Engineering & Technology 28 (2005) 1285–1294.
[2] M.A. Liu, DNA vaccines: an historical perspective and view to the future, Immunological Reviews 239 (2011) 62–84.
[3] A. Mountain, Gene therapy: the first decade, Trends in Biotechnology 18 (2000) 119–128.
[4] K.J. Prather, S. Sagar, J. Murphy, M. Chartrain, Industrial scale production of plasmid DNA for vaccine and gene therapy: plasmid design, production, and purification, Enzyme and Microbial Technology 33 (2003) 865–883.
[5] J.C. Nunes, A.M. Morão, C. Nunes, M.T. Pessoa de Amorim, I.C. Escobar, J.A. Queiroz, Plasmid DNA recovery from fermentation broths by a combined process of micro- and ultrafiltration: modeling and application, Journal of Membrane Science 415–416 (2012) 24–35.
[6] N. Ashammakhi, A. Ndreu, Y. Yang, H. Ylikauppila, L. Nikkola, Nanofiber-based scaffolds for tissue engineering, European Journal of Plastic Surgery 35 (2012) 135–149.
[7] Y.J. Kim, M. Ebara, T. Aoyagi, A smart nanofiber web that captures and releases cells, Angewandte Chemie International Edition 51 (2012) 10537–10541.
[8] M. Sumitha, K. Shalumon, V. Sreeja, R. Jayakumar, S.V. Nair, D. Menon, Biocompatible and antibacterial nanofibrous poly (ε-caprolactone)–nanosilver composite scaffolds for tissue engineering applications, Journal of Macromolecular Science, Part A 49 (2012) 131–138.
[9] Y. Yang, T. Xia, F. Chen, W. Wei, C. Liu, S. He, X. Li, Electrospun fibers with plasmid bFGF polyplex loadings promote skin wound healing in diabetic rats, Molecular Pharmaceutics 9 (2011) 48–58.
[10] M. Scampicchio, A. Bulbarello, A. Arecchi, M.S. Cosio, S. Benedetti, S. Mannino, Electrospun nonwoven nanofibrous membranes for sensors and biosensors, Electroanalysis 24 (2012) 719–725.
[11] H. Wu, L. Hu, M.W. Rowell, D. Kong, J.J. Cha, J.R. McDonough, J. Zhu, Y. Yang, M.D. McGehee, Y. Cui, Electrospun metal nanofiber webs as high-performance transparent electrode, Nano Letters 10 (2010) 4242–4248.
[12] R. Barhate, S. Ramakrishna, Nanofibrous filtering media: filtration problems and solutions from tiny materials, Journal of Membrane Science 296 (2007) 1–8.
[13] A. Cooper, R. Oldinski, H. Ma, J.D. Bryers, M. Zhang, Chitosan-based nanofibrous membranes for antibacterial filter applications (CARBPOL-D-12-01692-R1, August 26, Carbohydrate Polymers 92 (2012) (2012) 254–259.
[14] K. Yoon, K. Kim, X. Wang, D. Fang, B.S. Hsiao, B. Chu, High flux ultrafiltration membranes based on electrospun nanofibrous PAN scaffolds and chitosan coating, Polymer 47 (2006) 2434–2441.
[15] N. Bhardwaj, S.C. Kundu, Electrospinning: a fascinating fiber fabrication technique, Biotechnology Advances 28 (2010) 325–347.
[16] R. Gopal, S. Kaur, Z. Ma, C. Chan, S. Ramakrishna, T. Matsuura, Electrospun nanofibrous filtration membrane, Journal of Membrane Science 281 (2006) 581–586.
[17] K.C. Krogman, J.L. Lowery, N.S. Zacharia, G.C. Rutledge, P.T. Hammond, Spraying asymmetry into functional membranes layer-by-layer, Nature Materials 8 (2009) 512–518.
[18] L.A. Bosworth, S. Downes, Physicochemical characterisation of degrading polycaprolactone scaffolds, Polymer Degradation and Stability 95 (2010) 2269–2276.
[19] X. Qin, D. Wu, Effect of different solvents on poly(caprolactone) (PCL) electrospun nonwoven membranes, Journal of Thermal Analysis and Calorimetry 107 (2012) 1007–1013.
[20] J.W. Lu, Y.L. Zhu, Z.X. Guo, P. Hu, J. Yu, Electrospinning of sodium alginate with poly (ethylene oxide), Polymer 47 (2006) 8026–8031.
[21] V. Gaspar, F. Sousa, J. Queiroz, I. Correia, Formulation of chitosan–TPP–pDNA nanocapsules for gene therapy applications, Nanotechnology 22 (2010) 015101.
[22] S.S. Zargarian, V. Haddadi-Asl, A nanofibrous composite scaffold of PCL/hydroxyapatite-chitosan/PVA prepared by electrospinning, Iran Polymer Journal 19 (2010) 457–468.
[23] G. Ma, D. Fang, Y. Liu, X. Zhu, J. Nie, Electrospun sodium alginate/poly (ethylene oxide) core–shell nanofibers scaffolds potential for tissue engineering applications, Carbohydrate Polymers 87 (2012) 737–743.
[24] P. Coimbra, P. Alves, T. Valente, R. Santos, I. Correia, P. Ferreira, Sodium hyaluronate/chitosan polyelectrolyte complex scaffolds for dental pulp regeneration: synthesis and characterization, International Journal of Biological Macromolecules 49 (2011) 573–579.
[25] H.L. Nie, L.M. Zhu, Adsorption of papain with Cibacron Blue F3GA carrying chitosan-coated nylon affinity membranes, International Journal of Biological Macromolecules 40 (2007) 261–267.
[26] A. Bazargan, M. Keyanpour-rad, F. Hesari, M.E. Ganji, A study on the microfiltration behavior of self-supporting electrospun nanofibrous membrane in water using an optical particle counter, Desalination 265 (2011) 148–152.
[27] C. Sartori, D.S. Finch, B. Ralph, K. Gilding, Determination of the cation content of alginate thin films by FTIR spectroscopy, Polymer 38 (1997) 43–51.
[28] S.S. Ojha, D.R. Stevens, T.J. Hoffman, K. Stano, R. Klossner, M.C. Scott, W. Krause, L.I. Clarke, R.E. Gorga, Fabrication and characterization of electrospun chitosan nanofibers formed via templating with polyethylene oxide, Biomacromolecules 9 (2008) 2523–2529.
[29] J. Yang, S.B. Park, H.G. Yoon, Y.M. Huh, S. Haam, Preparation of poly ε-caprolactone nanoparticles containing magnetite for magnetic drug carrier, International Journal of Pharmaceutics 324 (2006) 185–190.
[30] C.Y. Tang, Y.N. Kwon, J.O. Leckie, Probing the nano-and micro-scales of reverse osmosis membranes—a comprehensive characterization of physiochemical properties of uncoated and coated membranes by XPS, TEM, ATR-FTIR, and streaming potential measurements, Journal of Membrane Science 287 (2007) 146–156.
[31] C.Y. Tang, Y.N. Kwon, J.O. Leckie, Effect of membrane chemistry and coating layer on physiochemical properties of thin film composite polyamide RO and NF membranes: I. FTIR and XPS characterization of polyamide and coating layer chemistry, Desalination 242 (2009) 149–167.
[32] I.S. Chang, S.O. Bag, C.H. Lee, Effects of membrane fouling on solute rejection during membrane filtration of activated sludge, Process Biochemistry 36 (2001) 855–860.
[33] I. Theodossiou, I. Collins, J. Ward, O. Thomas, P. Dunnill, The processing of a plasmid-based gene from E. coli. Primary recovery by filtration, Bioprocess and Biosystems Engineering 16 (1997) 175–183.